이학박사학위논문

애기장대 세포분열조절에 필요한 NDC80 동원체 복합체의 SPC24 상동유전자 MUN의 기능 연구

MERISTEM UNSTRUCTURED (MUN),
a SPC24 Homolog of the NDC80 Kinetochore Complex,
Is Required for Cell Division Control in Arabidopsis

2018년 2월

서울대학교 대학원

생명과학부

신 진 우

애기장대 세포분열조절에 필요한 NDC80 동원체 복합체의 SPC24 상동유전자 MUN의 기능 연구

MERISTEM UNSTRUCTURED (MUN),
a SPC24 Homolog of the NDC80 Kinetochore Complex,
Is Required for Cell Division Control in Arabidopsis

지도 교수 이 일 하

이 논문을 이학박사 학위논문으로 제출함

2017년 12월

서울대학교 대학원

생명과학부

신 진 우

신 진 우의 이학박사 학위논문을 인준함

2017년 12월

위 원 장 최 연 희 (인)

부위원장 이 일 하 (인)

위 원 조 형 택 (인)

위 원 이 지 영 (인)

위 원 이 호 림 (인)

MERISTEM UNSTRUCTURED (MUN),

a SPC24 Homolog of the NDC80 Kinetochore Complex,

Is Required for Cell Division Control in Arabidopsis

A dissertation submitted in partial fulfillment of

the requirement for the degree of

DOCTOR OF PHILOSOPHY

to the faculties of

School of Biological Sciences

at

Seoul National University

by

Jinwoo Shin

Date Approved	**Dissertation Committee**	
2017.12.05	Chair	Yeonhee Choi (Seal)
	Supervisor	Ilha Lee (Seal)
	Examiner	Hyung-Taeg Cho (Seal)
	Examiner	Ji-Young Lee (Seal)
	Examiner	Horim Lee (Seal)

Abstract

MERISTEM UNSTRUCTURED (MUN),

a SPC24 Homolog of the NDC80 Kinetochore Complex,

Is Required for Cell Division Control in Arabidopsis

Jinwoo Shin

School of Biological Sciences

The Graduate School

Seoul National University

Kinetochore, a protein super-complex on the centromere of chromosomes, mediates chromosome segregation during cell division by providing attachment sites for spindle microtubules. The NDC80 complex, composed of four proteins, NDC80, NUF2, SPC24, and SPC25, is localized at the outer kinetochore and connects spindle fibers to the kinetochore. Until date, loss-of-function analyses of the components have been limited because of the severe defects in the growth and development of the mutants, although the complex is conserved across species. In addition, SPC24 homolog in plants

has not been disclosed yet, the functional studies are rare in *Arabidopsis thaliana*.

Here, I characterize a recessive mutant, *meristem unstructured-1* (*mun-1)*, at organismal level in *Arabidopsis thaliana*. The mutant *mun-1* exhibits an abnormal phenotype with unstructured shoot apical meristem caused by ectopic expression of the *WUSCHEL* and meristem identity genes in unexpected tissues. The mutant *mun-1* is a weak allele and shows incomplete penetrance because of the insertion of T-DNA in the promoter region of the *SPC24* homolog, which is a component of NDC80 complex. The *mun-1* mutant exhibits stunted growth, embryo arrest, DNA aneuploidy, and defects in chromosome segregation, with a low cell division rate. Null mutants of *MUN* from transcription activator-like effector nuclease (TALEN) and clustered regularly interspaced short palindromic repeats/CRISPR associated protein 9 (CRISPR/Cas9)-mediated mutagenesis showed zygotic embryonic lethality similar to that in *nuf2-1*, which is another mutant of NDC80 complex. However, the null mutations were fully transmissible via pollen and ovules. Interactions among the components of the NDC80 complex were confirmed in a yeast two-hybrid assay and *in planta* co-immunoprecipitation. MUN is expressed in actively dividing tissues in whole plants and co-localized at the centromere with HTR12/CENH3, which is a centromere-specific histone variant. However, MUN is not required to recruit HTR12/CENH3 to the kinetochore, indicating that MUN is assembled into kinetochore after the

loading of inner kinetochore components, as typical of the outer kinetochore components.

My results support that MUN is a functional homolog of SPC24 in *Arabidopsis thaliana*, which is required for cell division. In contrast to animals, NDC80 complex in *Arabidopsis thaliana* localizes constitutively to the kinetochore throughout the cell cycles. In addition, I report the novel interaction between MUN and RBR, the well-known cell cycle regulator. Thus, I suggest the MUN is a dual-function protein, which is not only a structural component of kinetochore, but also a regulator of cell cycle in plants. In addition, I report the novel case of ectopic generations of stem cell niches by the malfunction of kinetochore components. This study provides cornerstones of studying the differences between plant and animal kinetochores related cell division.

Keywords: SPC24, NDC80 complex, kinetochore, centromere, chromosome segregation, cell division, *Arabidopsis thaliana*

Student Number: 2008-20360

Table of Contents

Abstract ..... **i**

Table of Contents ..... **iv**

List of Figures ..... **viii**

List of Tables ..... **xi**

Abbreviations ..... **xii**

I. Background 1

1.1. Cell cycle 1

1.2. Kinetochore 2

II. Introduction 5

III. Materials and methods 8

3.1. Plant materials and growth conditions 8

3.2. Constructs design 8

3.3. Thermal asymmetric interlaced polymerase chain reaction and molecular marker-assisted mapping 9

3.4. Gene expression analysis 9

3.5. Confocal laser scanning microscopic analysis 10

3.6. Imaging scanning electron microscopy 11

3.7. Targeted gene knockout by TALEN and CRISPR/Cas9 11

3.8. Flow cytometry analysis 12

3.9. Edu cell proliferation assay 13

3.10. Seed-set analysis, whole-mount clearing, and pollen viability analysis 13

3.11. GUS staining 14

3.12. Multiple alignment and phylogenetic analyses 14

3.13. Yeast two-hybrid assay 15

3.14. Co-immunoprecipitation (Co-IP) assays 15

3.15. Measurement of hormones by liquid chromatography/time-of-flight/mass spectrometry (LC/TOF-MS) Analysis .. 16

3.16. Accession Numbers 17

IV. Results 19

4.1. A weak allele, *mun-1*, shows unstructured SAM, growth retardation, defects in embryo development, and spontaneous *de novo* shoot organogenesis 19

4.2. Spontaneous *de novo* shoot organogenesis (DNSO) in *mun-1* occurs without hormone treatment 31

4.3. Abnormal regulations of hormones in *mun-1* 35

4.4. Defects in cell division and chromosome segregation, and aneuploidy, in *mun-1* plants 38

4.5. *MUN* encodes a SPC24 homolog, a member of the NDC80 kinetochore complex 45

4.6. *MUN* is predominantly expressed in actively dividing tissues and the protein is co-localized at the centromere with HTR12/CENH3 54

4.7. MUN interacts with components of the NDC80 complex.... 61

4.8. Null mutation in *MUN* causes zygotic embryonic lethal phenotype 69

4.9. K/O alleles of *MUN* and *NUF2* shows same zygotic embryo lethal phenotype 70

4.10. *mun-2T* and *nuf2-1* did not show the phenotypes in gamete development 70

4.11. MUN might have a role in cell cycle regulation with RBR 78

V. Discussion 83

5.1. MUN is an ortholog of SPC24, a component of the NDC80 kinetochore complex 83

5.2. Divergence of the plant NDC80 complex..... 85

5.3. Null mutations of the NDC80 complex are fully transmissible via pollen and ovules: 'Concentration' or 'Meitosis' theory 87

5.4. Spontaneous *de novo* shoot organogenesis in *mun-1* 88

5.5. MUN might have dual functions as a cell cycle regulator. .. 90

VI. References 93

VII. Abstract in Korean 국문초록..... 103

VIII. Appendix 종자분주기 등록특허공보 및 특허증 105

감사의 글 116

List of Figures

Figure 1. Morphology of *mun-1* compared to Col-0 (WT). 21

Figure 2. Images of SAM of WT and *mun-1* from a scanning electron microscope (SEM). 23

Figure 3. Defects of embryo development in *mun-1*. 27

Figure 4. Cloning of *MUN*. 28

Figure 5. Ectopic expression of *WUS* in *mun-1*. 33

Figure 6. Expression of the genes regulating SAM and embryogenesis markers by RT-qPCR. 34

Figure 7. Abnormal regulations of hormones in *mun-1* plants. 37

Figure 8. The *mun-1* plants show a short root phenotype. 39

Figure 9. Reduced cell division rate in *mun-1* plants. 40

Figure 10. Cells of WT and *mun-1* have similar sizes. 41

Figure 11. DNA aneuploidy in *mun-1*. 43

Figure 12. Defects in chromosome segregation of *mun-1*. 44

Figure 13. MUN, which has a coiled-coils domain, shows the similarity to SPC24 superfamily. 48

Figure 14. MUN is evolutionarily conserved SPC24 ortholog in *Arabidopsis thaliana*. 50

Figure 15. MUN/AtSPC24 cannot complement the yeast SPC24. 51

Figure 16. Predicted protein structure of MUN, a SPC24 homolog. . 53

Figure 17. Expression of *MUN*. 57

Figure 18. Cellular localization of *MUN*. 58

Figure 19. Co-localization of MUN and HTR12 at centromeres in root cells. 59

Figure 20. Localization of HTR12/CENH3-GFP in root of WT and *mun-1*. 60

Figure 21. Subcellular localizations of the components of the NDC80 complex. 63

Figure 22. *In vitro* interactions of the components of the NDC80 complex

with MUN. 64

Figure 23. *In vivo* interactions of the components of the NDC80 complex with MUN. 66

Figure 24. Expression profiles of the four components of the NDC80 complex obtained from the analysis of RNA-Seq expression data for 113 different samples in Araport DB. 68

Figure 25. Generation of null alleles of *MUN* by targeted gene knockout techniques. 73

Figure 26. Null allele, *mun-2t,* and *nuf2-1* show similar zygotic lethal phenotype. 75

Figure 27. Normal pollen development in *mun-1* plants. 76

Figure 28. MUN interacts with RBR. 79

Figure 29. Expression of the genes of RBR targets. 80

Figure 30. Expression of the cell cycle-related genes in *mun-1*. 81

List of Tables

Table 1. Segregation ratio of seeds obtained from the self-cross of *mun-1*/+ for antibiotic resistance. 24

Table 2. Phenotypic segregation of seeds from the siliques of *mun-1*/+, *mun-2t*/+, and *nuf2-1*/+. 30

Table 3. Aborted seeds in siliques of *nuf2-1* (+/-). 77

Table 4. List of primers used in this study. 82

Abbreviations

aa	Amino acid
ABA	Abscisic acid
ABRC	Arabidopsis biological resource center
AD	Activation domain
BAC	Bacterial artificial chromosome
BD	Binding domain
CaMV	Cauliflower mosaic virus
CENP-A/C/T	Histone H3-like centromeric protein A/C/T
CH	Calponin-homology
CLSM	Confocal laser scanning microscopic
Co-IP	Co-immunoprecipitation
CRISPR/Cas9	Clustered regularly interspaced short palindromic repeats /CRISPR associated protein 9
CV	Coefficient of variation
DAG	Days after germination
DAPI	4',6-diamidino-2-phenylindole
DIC	Differential interference contrast
DNSO	*de novo* shoot organogenesis
Edu	5-ethynyl-2′-deoxyuridine
EGTA	Ethylene glycol-bis(β-aminoethyl ether)-N,N,N',N'-tetraacetic acid
eGFP	enhanced green fluorescent protein

GUS	*β-glucuronidase*
HPLC	High-performance liquid chromatography
HTR12/CENH3	Histone three related 12/Centromeric histone H3
IAA	Indole-3-acetic acid
JA	Jasmonic acid
kDa	kilodalton
KMN	KNL-1/MIS12complex/NDC80
KNL-2	Kinetochore null protein 2
LC/TOF-MS	Liquid chromatography/time-of-flight/mass spectrometry
LRI	Lateral root initiation
MTSB	Microtubule stabilizing buffer
MUN	MERISTEM UNSTRUCTURED
NDC80/HEC1	Nuclear division cycle 80/Highly expressed in cancer1
NUF2	Nuclear filament-containing protein 2
PBS	Phosphate-buffered saline
PDB	Protein data bank
PI	Propidium iodide
PIPES	Piperazine-N,N'-bis(2-ethanesulfonic acid)
PRC2	Polycomb repressive complex 2
RAM	Root apical meristem
RT-PCR	Reverse transcription-polymerase chain reaction
RT-qPCR	Quantitative real-time polymerase chain reaction
RWD	RING finger, WD repeat, DEAD-like helicases

RZZ	Rod/Zwilch/Zw10
SAC	Spindle assembly checkpoint
SAM	Shoot apical metistem
SA	Salicylic acid
SDS-PAGE	Sodium dodecyl sulfate polyacrylamide gel electrophoresis
SD	Standard deviation
SD medium	Synthetic defined medium
SEM	Scanning electron microscope
sgRNA	single guide RNA
SPC24	Spindle pole body component 24
SPC25	Spindle pole body component 25
TAIL-PCR	Thermal asymmetric interlaced PCR
TAIR10	The arabidopsis information resource 10
TALEN	Transcription activator-like effector nuclease
TUA6	Tubulin alpha-6 chain
UPLC-ESI-MicrOTOF	ultra performance liquid chromatography-electrospray ionization-MicrOTOF
UTR	Untranslated region
WT	Wild-type
XTCs	*Xenopus* tissue culture cells
Y2H	Yeast two hybrid-assay
YPD	Yeast extract-peptone-dextrose

I. Background

1.1. Cell cycle

Apical meristems define plant architecture by providing new cells with proper control of cell division; thus, mutants with defects in cell division have abnormal meristem structures and unusual morphology in plants (Jager *et al.*, 2005; Nieuwland *et al.*, 2009). Misregulations in some phases of the cell cycle may lead to morphological defects in plants. Mitotic cell cycle consists of four phases, gap phase 1 (G1), synthesis phase (S), gap phase 2 (G2), and mitotic phase (M). During the cell cycle, proper condensation and segregation of chromosomes are particularly critical for successful cell division and maintenance of genome stability.

1.2. Kinetochore

Kinetochore, a protein super-complex providing a site for the attachment of spindle fibers with the centromere of chromosomes, has important roles in cell division. plays critical roles in the cohesion of sister chromatids, proper segregation of chromosomes, and management of the spindle assembly checkpoint (SAC) (Janke *et al.*, 2001). Given that it is an essential complex for the maintenance of genome integrity and survival of all eukaryotes, many components of kinetochores are evolutionarily well-conserved from yeast to humans (Meraldi *et al.*, 2006; Lermontova *et al.*, 2014). Up to 100 proteins were estimated to constitute the whole kinetochore complex in vertebrates (Samejima *et al.*, 2015). As kinetochore is an enormous protein complex, the components are mainly separated into two groups, inner and outer kinetochores (Chan *et al.*, 2005).

The inner kinetochore complex also consists of several protein factors, including a centromere specific histone H3 variant, CENH3 (CENP-A in humans, HTR12 in *A. thaliana*), which acts as a foundation protein that recruits additional kinetochore proteins (Earnshaw and Rothfield, 1985; Palmer *et al.*, 1987; Talbert *et al.*, 2002; Zhong *et al.*, 2002; Lermontova *et al.*, 2006; Lermontova *et al.*, 2011), MIS18 complex, composed of Mis18a, Mis18b and Mis18BP1/KNL-2, recruiting and loading CENH3 into kinetochore (De Rop *et al.*, 2012; Lermontova *et al.*, 2013; Sandmann *et al.*,

2017), a structural platform protein, CENP-C (Saitoh *et al.*, 1992; Ogura *et al.*, 2004), and a nucleosome-like CENP-T-W-S-X complex (Schleiffer *et al.*, 2012; Takeuchi *et al.*, 2014), capturing the NDC80 complex that is a component of outer kinetochore, are components of inner kinetochore complex.

The functions of the outer kinetochore complex include binding of microtubule and control of SAC. KMN protein network, consisting of KNL-1/MIS12 complex/NDC80 complex, is a major component of outer kinetochore and enables microtubule binding (Sato *et al.*, 2005; Cheeseman *et al.*, 2006; Li and Dawe, 2009; Petrovic, 2010; Lermontova *et al.*, 2015). The Dam1 ring complex consisting of ten-proteins, is also a critical component for microtubule binding (Westermann, 2006). In addition, the other components of the outer kinetochore, e.g., Rod/Zwilch/Zw10 (RZZ) complex, controls SAC activation (Gassmann *et al.*, 2008).

Among the components of the outer kinetochore complex, the four-proteins in the NDC80 complex, including Nuclear division cycle 80 [NDC80; also known as highly expressed in cancer1 (Hec1) in humans], Nuclear filament-containing protein 2 (NUF2), Spindle pole body component 24 (SPC24), and Spindle pole body component (SPC25), play critical roles in connecting spindle fibers to chromosomes. These proteins are assembled into a 170–190 kDa complex in diverse species (Kline-Smith *et al.*, 2005; Ciferri *et al.*, 2007). In vertebrates, the C-terminal ends of the NUF2-NDC80

heterodimer associate with the N-terminal coiled-coil domains of the SPC24-SPC25 heterodimer (Ciferri *et al.*, 2005; Wei *et al.*, 2005). All four subunits contain a long coiled-coil domain, providing a long rod-shaped structure, and a globular domain. The globular domains of each component of NDC80 complex are functionally important. Each of the N-terminal globular heads of the NDC80-NUF2 heterodimer contains calponin-homology (CH) domains that directly bind to the acidic tails of the α- and β-tubulin dimers in microtubules (Ciferri *et al.*, 2008). In addition, globular dimeric heads, containing the RING finger, WD repeat, DEAD-like helicases (RWD) domain of the SPC24-SPC25 dimer, bind to the inner kinetochore components, the KNL1-Mis12 complex (Rago *et al.*, 2015) to generate the so-called KMN protein network (Petrovic *et al.*, 2014). In addition, the SPC24-SPC25 heterodimer can bind to the N-terminal tail of CENP-T in humans (Schleiffer *et al.*, 2012; Nishino *et al.*, 2013). CENP-T (Cnn1 in yeast) has been reported as a histone-fold protein acting as a centromere receptor for microtubule-binding NDC80 complex. Therefore, the NDC80 complex serves as a central "hub" connecting the kinetochore complexes, which provides the "bridges" between the inner kinetochore complexes and the microtubule spindles (Samejima *et al.*, 2015).

II. Introduction

Loss-of-function studies of the components of the NDC80 outer kinetochore complex have been performed in several organisms; however, the phenotypic characterization of the mutants in the NDC80 complex has been limited because of the severe defects in the growth and development of the mutants. Knockdown of *HEC1*, the human *NDC80*, in T24 bladder carcinoma cells caused abnormal chromatid segregation (Chen *et al.*, 1997). Knockdown of *Nuf2* in HeLa cells also caused similar phenotypes (DeLuca *et al.*, 2002). In yeast, all the mutants of the NDC80 complex exhibited abnormal segregation of chromosomes and defects in cell division (Wigge *et al.*, 1998; Janke *et al.*, 2001; Wigge and Kilmartin, 2001). Similar phenotypes of loss-of-function in the components of the NDC80 complex were observed in *Xenopus* tissue culture cells (XTCs), chicken DT40 cells, and mouse oocytes (Hori *et al.*, 2003; McCleland, 2003; Sun *et al.*, 2010). However, none of these studies described mutant phenotypes at the organismal level.

In plants, several protein components of the kinetochore have been reported (Lermontova *et al.*, 2015). CENH3 (CENP-A in humans, HTR12 in *Arabidopsis thaliana*), a centromere specific histone H3 variant, acts as a foundation protein for recruiting additional kinetochore proteins (Talbert *et al.*, 2002; Zhong *et al.*, 2002; Lermontova *et al.*, 2006; Lermontova *et al.*,

2011). CENP-C functions as a structural platform for kinetochore assembly by interacting with CENH3 (Ogura *et al.*, 2004). As an upstream component of CENH3 deposition at centromeres, KNL-2/Mis18BP1 recruits and loads the CENH3 into the kinetochore (Lermontova *et al.*, 2013; Sandmann *et al.*, 2017). Among the components of the NDC80 complex, only NDC80 was characterized in maize (Du and Dawe, 2007). ZmNDC80 is localized on the outer surface of the inner kinetochore complex including CENP-C protein. It rapidly associates with DNA following replication and is stably maintained at centromeres throughout the cell cycle. In contrast, NDC80 protein in humans is detected only at the M phase (Chen *et al.*, 1997), indicating that the function of NDC80 complex is subtly different in animals and plants. However, the study was limited to the localization analysis at the cellular level and phenotypic characterization of mutations in the components of the NDC80 complex has not been reported.

In the present study, I report the SPC24 homolog in *Arabidopsis thaliana*. I characterize a recessive T-DNA insertion mutant, *meristem unstructured-1 (mun-1)*, which exhibits unstructured shoot apical meristem (SAM) and ectopic development of the SAM caused by ectopic expression of meristem identity genes. In addition, I observed the null mutant phenotypes of *MERISTEM UNSTRUCTURED (MUN)* by using transcription activator-like effector nuclease (TALEN) and CRISPR/Cas9. *MUN* has been annotated as an “unknown gene”; however, my analyses strongly suggest that *MUN* is

an *Arabidopsis thaliana* ortholog of SPC24, a member of the NDC80 complex. *MUN* is involved in proper chromosome segregation and normal cell division as a component of the kinetochore complex at the centromere. In addition to its role in cell division, I observed interesting phenotypes in *mun-1*, a weak knockdown allele of *MUN/AtSPC24*. For example, it generates ectopic stem cell niches from somatic cells without any hormone treatment. I postulate that the constitutively expressed core kinetochore hub-protein MUN is involved not only in the attachment of spindle fibers to chromosomes, but also in inducing *de novo* shoot organogenesis directly or indirectly. Together, I propose that MUN is required for chromosome segregation to ensure proper cell division and the maintenance of plant architecture.

III. Materials and methods

3.1. Plant materials and growth conditions

All *Arabidopsis thaliana* plants used in the present study had Col-0 background. The mutant, *mun-1,* was generated by transforming Col-0 with the pSKI015 vector used for activation tagging mutagenesis. The seeds of *nuf2-1* (SALK_087432) were obtained from the Arabidopsis Biological Resource Center (ABRC). The seeds were surface sterilized twice with 75% ethanol with 0.05% Triton X-100 for 10 min using gentle rotation, rinsed once using absolute ethanol, and dried. They were sown on 1% plant agar (Duchefa) containing 1% sucrose and 0.5× Murashige & Skoog medium, including B5 vitamins (Duchefa), and seed stratification was performed for 3 days at 4°C. The plants were then transferred and grown under 16 h/8 h light/dark cycle (22°C/20°C) in a controlled growth room illuminated with cool white fluorescent lights (125 μmol m^{-2} s^{-1}).

3.2. Constructs design

All constructs were created using genomic sequences covering promoters and the complete coding sequences fused with reporter genes or tag proteins. A 1.7 kb sequence upstream from the start codon ATG was used as the promoter for *WUS*, and a 2 kb sequence upstream from the start codon ATG was used

as the promoter for *NDC80*, *NUF2*, *SPC25*, and *MUN*. The constructs *pWUS::WUS-GUS* and *pMUN::MUN-GUS* were prepared using the pDW137 vector, which contains the *GUS* coding sequence (Blazquez *et al.*, 1997). The constructs *pNDC80::NDC80-eGFP*, *pNUF2::NUF2-eGFP*, *pSPC25::SPC25-eGFP*, and *pMUN::MUN-eGFP* were prepared by fusing the *eGFP* coding sequence at the C-terminus of each genomic sequence in the pCAMBIA1300-NOS vector (Cho and Cosgrove, 2002; Lee *et al.*, 2010). The *pMUN::MUN-mRFP1* construct was prepared using the pBI-mRFP vector (Park *et al.*, 2014b). The construct pJW20 (*pMUN::MUN*) was constructed using the pPZP211 vector (Hajdukiewicz *et al.*, 1994). The construct *pMUN::MUN-FLAG* was prepared using the pPZP211 vector by fusing the 3X-FLAG peptides at the C-terminus of the *MUN* genomic sequences.

3.3. Thermal asymmetric interlaced polymerase chain reaction and molecular marker-assisted mapping

Thermal asymmetric interlaced polymerase chain reaction (TAIL-PCR) and Hi-TAIL-PCR used to find the T-DNA insertion site were performed as previously described (Liu *et al.*, 1995; Liu and Chen, 2007). Molecular marker-assisted mapping was followed using the method previously described (Choi *et al.*, 2005).

3.4. Gene expression analysis

Total RNA was extracted using RNeasy Plant Mini Kit (Qiagen) following the manufacturer's instructions. Quantitative real-time polymerase chain reaction (RT-qPCR) analysis was repeated at least three times using independently harvested plant samples. The primers used for RT-qPCR have been listed in **Table 4**. RT-qPCR analysis was performed using CFX96™ Real-Time PCR Detection System and iQ SYBR Green supermix (Bio-Rad). Eight microliters of diluted (1/20) cDNA from 4 μg of total RNA was used in a 20 μL reaction. Reaction conditions were as follows: 3 min at 95°C, 40 cycles of 15 s at 95°C, 20 s at 60°C, and 20 sec at 72°C, and a dissociation step from 55–95°C. Data was collected at 72°C in each cycle, and *TUB2* was used as a reference gene.

3.5. Confocal laser scanning microscopic analysis

The samples were pre-stained with propidium iodide (PI) or DAPI, and mounted on glass slides and observed using confocal microscopy (LSM700, Zeiss or TCS SP8, Leica) following the manufacturer's instructions. To observe the M phase cells in the *pUBQ14::GFP-TUA6* transgenic line, the samples were fixed as previously described, but with a few modifications (Park *et al.*, 2014a). The samples were immersed in 1 mL 4% paraformaldehyde in microtubule stabilizing buffer (MTSB) (50 mM piperazine-N,N'-bis(2-ethanesulfonic acid) (PIPES), 2 mM ethylene glycol-bis(β-aminoethyl ether)-N,N,N',N'-tetraacetic acid (EGTA), and 2 mM

$MgSO_4$) solution and subjected to vacuum suction for 20 min, and left in a hood for 40 min. The solution was changed into MTSB prior to observation.

3.6. Imaging scanning electron microscopy

For use with a scanning electron microscope (SUPRA 55VP, Zeiss), the samples were primarily fixed with Karnovsky's fixative for 2 h, and washed three times with 0.05 M sodium cacodylate buffer for 10 min. Thereafter, the samples were post-fixed with 2% osmium tetroxide and 0.1 M cacodylate buffer for 2 h, and washed three times with 0.05 M sodium cacodylate buffer in 10 min. After dehydration with serial ethanol washes, the samples were dried with a critical point dryer (CPD-030, Bal-Tec). The samples were mounted on the carbon tape of a metal stub and coated with gold particles using a sputter coater (SCD 005, Bal-Tec).

3.7. Targeted gene knockout by TALEN and CRISPR/Cas9

TALEN modules to target the first exon sequence of *MUN* were designed and cloned by ToolGen Inc., Seoul, South Korea. The *TALEN-L* and *TALEN-R* modules were subcloned into the plant binary vectors pSOL1 and pCGN18, both of them harboring the CaMV 35S promoter (Jack *et al.*, 1994). The constructs were transformed into Col-0 using the floral dip method (Clough and Bent, 1998). Selected T1 plants for each *TALEN-L* and *TALEN-R* module under the proper antibiotic selection were crossed. The null mutants were

selected from the seedlings of the F2 generation and confirmed by T7E1 assay and sequencing of target sequences in the progenies. For the generation of mutants using CRISPR/Cas9, I followed a previously described method with a few modifications (Hyun *et al.*, 2015). The five candidate target sequences in the *MUN* exon were selected using Cas-OFFinder software (http://www.rgenome.net/cas-offinder/) (Bae *et al.*, 2014). These constructs were transformed into Col-0 using the floral dip method, and the null mutants were isolated from the seedlings of the T2 generation. The mutants were confirmed by T7E1 assay and sequencing of the target sequence in the progenies.

3.8. Flow cytometry analysis

Flow cytometric analysis to measure DNA content was performed as previously described with some modifications (Galbraith, 2009). Twenty milligrams of tissues from aerial parts were sampled and sliced with a razor blade in Tris-$MgCl_2$ buffer with PI and RNase. Thereafter, the solution was filtered using a 40 μm cell strainer and run in FACSCanto™ II (BD Biosciences), following the manufacturer's instructions. The samples were gated for singlet events using a FSC-A by FSC-H plot and subsequently gated using a PE-A by PerCP-A plot. Histograms were created using BD FACSDiva™. Values for coefficient of variation (CV, %) were obtained from the equation below.

$$CV = 100 \times (\sigma \div \mu)$$

where, σ is the standard deviation and μ is the mean.

3.9. Edu cell proliferation assay

5-ethynyl-2′-deoxyuridine (Edu) staining to detect S-phase cells was performed using an Invitrogen Edu Kit (C10350) following the manufacturer's instructions. Seedlings were sampled in liquid MS solution containing 1 μM Edu and incubated in a culture room at 22°C for 30 min. The samples were fixed in 4% (w/v) formaldehyde solution in phosphate-buffered saline (PBS) with 0.1% Triton X-100 for 30 min, and washed three times with PBS for 5 min. Thereafter, the samples were incubated in Edu detection cocktail solution for 30 min in the dark, and washed once with Click-iT® rinse buffer and thrice with PBS solution. The samples were counterstained with PI solution and stored in PBS solution until observation under a confocal microscope.

3.10. Seed-set analysis, whole-mount clearing, and pollen viability analysis

Siliques were dissected under a stereoscope, and the numbers of normal seeds, aborted seeds and underdeveloped ovules were counted. Whole-mount clearing and pollen viability analysis were performed as described in a previous study (Park *et al.*, 2014b). For analysis of pollen viability, stamens

from floral buds were placed on a microscopic slide. A few drops of Alexander stain buffer [95% ethanol, 10 mL; Malachite green (1% in 95% ethanol), 1 mL; Fuchsin acid (1% in water), 5 mL; Orange G (1% in water), 0.5 mL; phenol, 5 g; chloral hydrate, 5 g; glacial acetic acid, 2 mL; glycerol, 25 mL; distilled water, 50 mL] was added. The stained pollen grains were observed with a Zeiss Axio Imager A1 microscope equipped with differential contrast interference microscopy optics. Viable pollens were stained purple, whereas dead pollens were stained green.

3.11. GUS staining

GUS staining and histological analysis were performed following standard methods described in a previous study (Choi *et al.*, 2007). Photographs were taken with a USB digital-microscope Dimis-M (Siwon Optical Technology, South Korea).

3.12. Multiple alignment and phylogenetic analyses

Multiple alignments of protein sequences were performed with CLC Main Workbench. The phylogenetic tree was generated with MEGA7 (Kumar *et al.*, 2016) using the maximum likelihood method based on the JTT matrix-based model (Jones *et al.*, 1992). All the positions with <90% site coverage were eliminated. The analysis was performed using 18 protein sequences (PF08286

family) obtained from the database of UniProt, NCBI, and Phytozome (see accession number in section 3.16).

3.13. Yeast two-hybrid assay

Full-length cDNAs of *NDC80*, *NUF2*, *SPC25*, and *MUN* were individually cloned into the pGADT7 prey vector and pGBKT7 bait vector, and transformed into AH109 yeast cells. The vectors and yeast strains (Matchmaker GAL4 Two-Hybrid System 3, Clontech). The yeast two two-hybrid assay was performed according to the manufacturer's instructions (Matchmaker GAL4 Two-Hybrid System 3, Clontech). After 3 days of incubation at 30°C, the yeast cells were spotted on the selection plates containing SD medium lacking Leu and Trp and another SD medium lacking Leu, Trp, His, and Ade. These plates were further incubated at 30°C until the yeast cells formed colonies.

3.14. Co-immunoprecipitation (Co-IP) assays

Co-immunoprecipitation experiments among the components of NDC80 complex in seedlings of *Arabidopsis thaliana* were performed as previously described, with a few modifications, as described in a previous study (Lee and Seo, 2016). Constructs of *pNDC80::NDC80-eGFP*, *pNUF2::NUF2-eGFP*, and *pSPC25::SPC25-eGFP* were transformed into Col-0 ecotype or *pMUN::MUN-FLAG* plants separately by floral dip method. T2 seedlings

after antibiotic selection were used for Co-IP assays. Up to 1 g of seedlings was homogenized in a mortar with grinding buffer [50 mM Tris-HCl (pH 7.5), 150 mM NaCl, 10 mM $MgCl_2$, 0.1% Nonidet P-40, 1 mM phenylmethylsulfonylfluoride, and 1× complete cocktail of protease inhibitors]. Total protein extracts were immunoprecipitated with GFP-Trap®_A beads (gta-20, Chromotek) for 1 h at 4°C with gentle rotation. The precipitated samples and beads were washed three times (5 min per wash) with the grinding buffer, and then eluted by incubation with 2× sodium dodecyl sulfate –polyacrylamide gel electrophoresis (SDS-PAGE) loading buffer for 10 min at 95°C. The elutants were subsequently used for western blot analysis with anti-GFP (1:2000 dilution; JL-8, Clontech) or anti-FLAG antibodies (1:2000 dilution; F3165, Sigma). Signals of western blots were detected by a chemiluminescent CCD imager (ImageQuant™ LAS 4000, GE Healthcare Life Sciences) with ECL solution (WesternBright™ Sirius, Advansta).

3.15. Measurement of hormones by liquid chromatography/time-of-flight/mass spectrometry (LC/TOF-MS) Analysis

One-hundred and fifty milligrams of rosette leaves from plants (33 DAG) were frozen and ground in 2 mL screw-cap tubes, by adding two steel balls and 1 mL ethyl acetate. The samples were ground by genogrinder at 4500 rpm for 1 min and centrifuged. The supernatants were transferred to 2 mL e-tubes

and evaporated using a vacuum concentrator. The dried samples were dissolved in 70% methanol and transferred into a high-performance liquid chromatography (HPLC) vial containing the insert. The samples were injected into ultra performance liquid chromatography-electrospray ionization-MicrOTOF (UPLC-ESI-MicrOTOF) and analyzed.

3.16. Accession Numbers

Sequence information cited in this dissertation can be found in the Arabidopsis Genome Initiative, or GenBank/EMBL data libraries under the following accession numbers: *MUN* (AT3G08880), *NDC80* (AT3G54630), *NUF2* (AT1G61000), *SPC25* (AT3G48210), *WUS* (AT2G17950), *CLV3* (AT2G27250), *STM* (AT1G62360), *MP* (AT1G19850), *WOX2* (AT5G59340), *KNAT2* (AT1G70510), *ABI3* (AT3G24650), *FUS3* (AT3G26790), *TUB2* (AT5G62690), *ABI5* (AT2G36270), *CCS52A1* (AT4G22910), *CCS52A2* (AT4G11920), *VIN3* (AT5G57380), *SEP3* (AT1G24260), *FLC* (AT5G10140), *MET1* (AT5G49160), *RBR* (AT3G12280), *CYCB1;1* (AT4G37490), *CYCB1;2* (AT5G06150), *FBL17* (AT3G54650), *BRCA1* (AT4G21070), *WEE1* (AT1G02970), *ATR* (AT5G40820); and UniProt ID for the protein sequence of SPC24 (Pfam accession PF08286) homologues in various species: *Xenopus tropicalis* (Q6P8A1), *Homo sapiens* (Q8NBT2), *Saccharomyces cerevisiae* (Q04477), *Schizosaccharomyces pombe* (Q9UST6), *Mus musculus* (Q9D083), *Bos taurus* (Q24JY3), *Danio rerio* (Q503N2), *Arabidopsis lyrata*

(D7L7N7), *Arabidopsis thaliana* (Q67XT3), *Capsella rubella* (R0I4I6), *Glycine max* (K7MTM7), *Sorghum bicolor* (A0A1B6PL61), and NCBI Reference Sequence for the protein sequence of SPC24 homologues: *Gallus gallus* (XP_015129502.1), *Zea mays* (NP_001142463.1); and Gene information of Phytozome for the protein sequence of SPC24 homologues: *Brassica rapa* FPsc (Brara.A03558.1), *Boechera stricta* (Bostr.22252s0186.1), *Brachypodium distachyon* (Bradi5g11082.1), and *Capsella grandiflora* (Cagra.2991s0006.1). UniProt ID for the protein sequence of yeast CTF19 and human KNL1 are Q02732 and Q8NG31, respectively. The IDs of the chicken CENP-T-Spc24/25 complex in Protein Data Bank (PDB) is 3vza.

IV. Results

4.1. A weak allele, *mun-1*, shows unstructured SAM, growth retardation, defects in embryo development, and spontaneous *de novo* shoot organogenesis

From the pools of activation tagging mutants generated in the lab (Hyun *et al.*, 2008), a mutant showing defects in the development of shoot apex and leaf morphology was isolated. The mutant showed unstructured SAM morphology, as well as severe growth retardation; therefore, I named it *meristem unstructured-1* (*mun-1*) (**Figure 1**, **Figure 2**). The mutant, *mun-1*, was recessive because it segregated into 678 normal vs. 89 mutants in the F2 population (**Table 1**), which indicates that it was not a gain-of-function mutant. The *mun-1* mutants produced small and shrunken leaves with rough surface margins (**Figure 1**). In addition, it failed to produce regular dome-shaped SAM structure, and occasionally produced ectopic protrusions of cell masses at random locations, unlike Col-0 (wild-type, WT) (**Figure 2**C vs. D). Thus, it often produced multiple shoots with irregular phyllotaxy before flowering (red arrows in **Figure 1**G, H, **Figure 2**E, F). Occasionally, stomata were observed near the ectopic protrusions, which indicated that the ectopic protrusions may have developed from differentiated tissues, such as fully developed leaf epidermis (**Figure 2**G, H, yellow arrows).

Figure 1

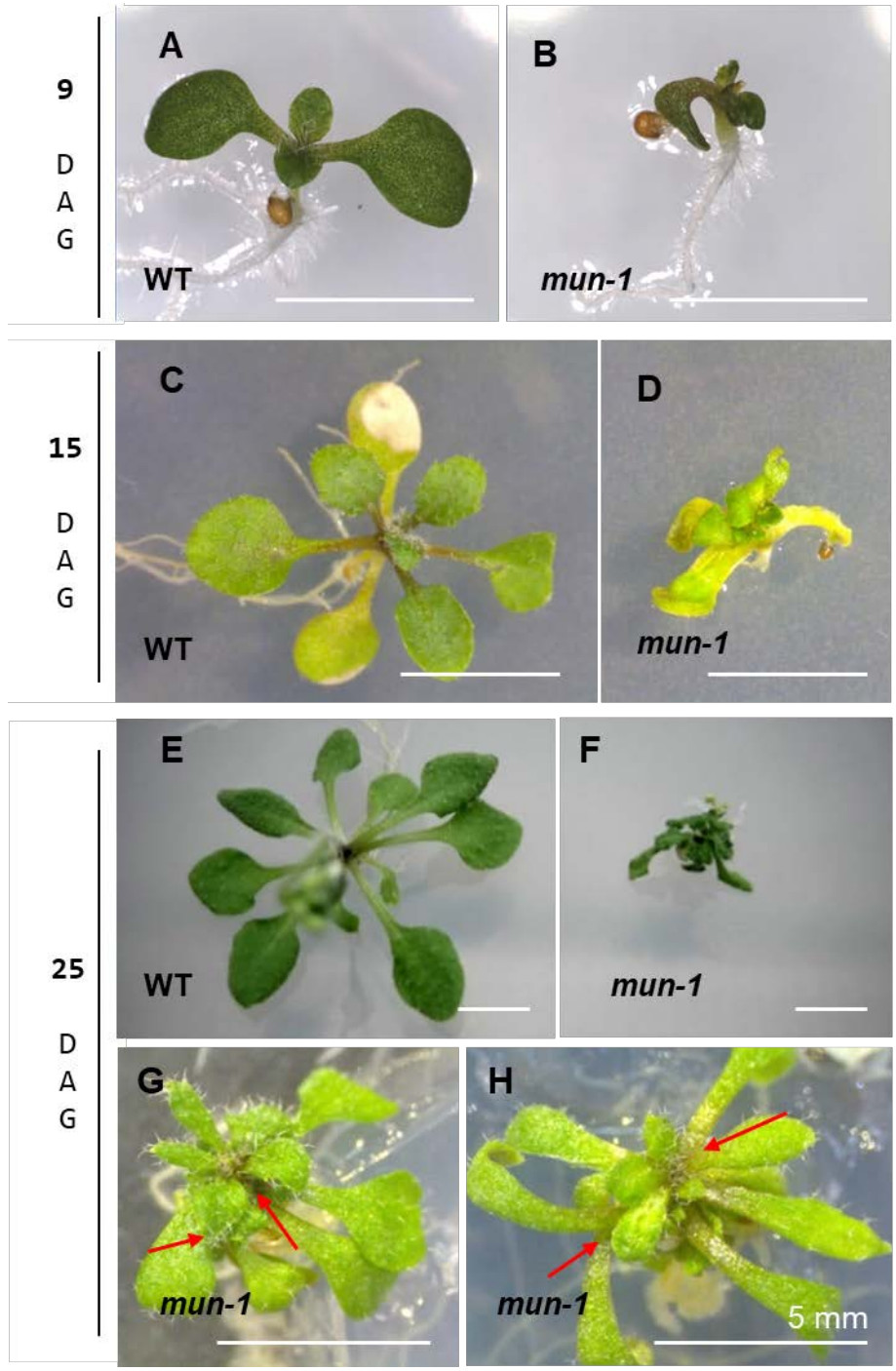
9
DAG
A
WT
B
mun-1
15
DAG
C
WT
D
mun-1
25
DAG
E
WT
F
mun-1
G
mun-1
H
mun-1
5 mm

Figure 1. Morphology of *mun-1* compared to Col-0 (WT).

The mutant shows growth retardation and multiple shoots. (**A, C, E**) WT; (**B, D, F-H**) *mun-1*. (**A, B**) 9 days after germination (DAG); (**C-D**) 15 DAG; (**E-H**) 25 DAG. Red arrows indicate multiple shoots generated before flowering. White bar = 5 mm.

Figure 2

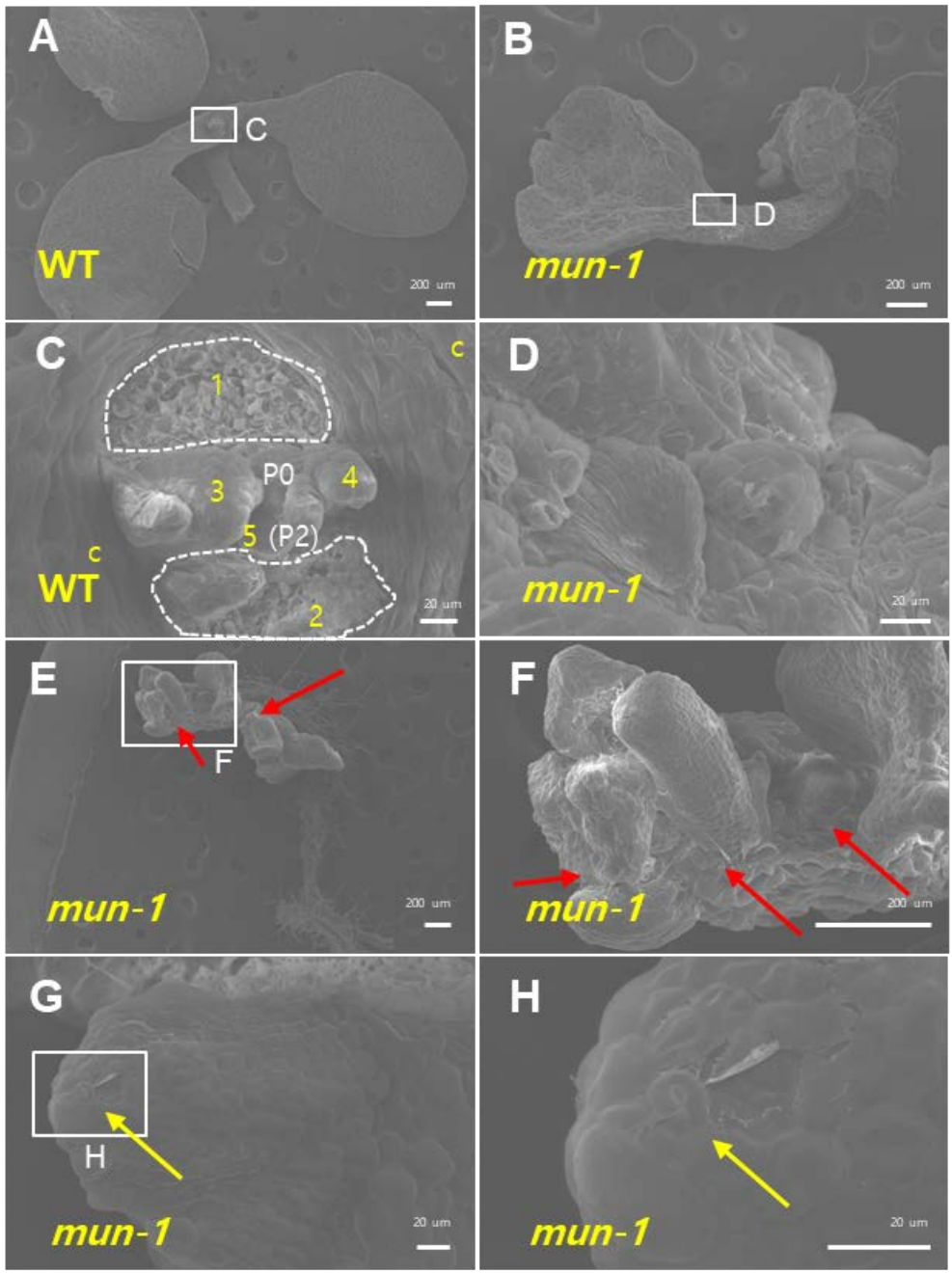
A
C
WT
200 um
B
D
mun-1
200 um
C
c
1
P0
3
4
5 (P2)
c
WT
2
20 um
D
mun-1
20 um
E
F
mun-1
200 um
F
mun-1
200 um
G
H
mun-1
20 um
H
mun-1
20 um

Figure 2. Images of SAM of WT and *mun-1* from a scanning electron microscope (SEM).

The images show seedlings 5 DAG. (**A, C**) WT; (**B, D-H**) *mun-1*. (**D**) and (**F**) are enlarged images of insets in (**B**) and (**E**), respectively, which lack regular dome-shaped SAM in *mun-1*. (**B, D**) show *mun-1* seedlings with single cotyledon. (**E, F**) show multiple SAMs generated at random locations (red arrows). (**G, H**) show ectopic protrusion of stem cell niche from differentiated leaf tissues with stomata (yellow arrows). (**C**) and (**H**) are enlarged images of insets in (**A**) and (**G**), respectively. Numbers in (**C**) indicate the order of leaf generation in; c indicates cotyledons. White bar in (**A, B, E, F**) = 200 μm, in (**C, D, G, H**) = 20 μm.

Table 1. Segregation ratio of seeds obtained from the self-cross of *mun-1*/+ for antibiotic resistance.

Approximately 12% progenies obtained from the self-cross of the heterozygotes (*mun-1*/+) were homozygotes *mun-1/mun-1*.

	Ba sensitive	**Ba resistant, WT phenotype**	**Ba resistant, *mun-1* phenotype**	**Total**
***mun-1*/+**	227 (29.6 %)	451 (58.8 %)	89 (11.6 %)	767 (100.0 %)

Eventually, the homozygotes of *mun-1* produced flowers, but failed to produce fertile seeds. In contrast, in the heterozygotes *mun-1*/+, no discernible phenotypes were observed in comparison with WT. I observed developing seeds in the siliques of *mun-1/+* after clearing. Less than a quarter of the progenies showed defects in embryo development (approximately 20–30 seeds among 240 seeds obtained from six siliques exhibited defects in the embryo). Some of them produced only a single cotyledon (**Figure 2**B). Some embryos exhibited reduced cell division, and embryogenesis was arrested as early as the globular stage as seen in **Figure 3**D, whereas others developed into later stages, such as the heart and torpedo stages (**Figure 3**E). Such embryos arrested at variable developmental stages and appeared to produce aborted seeds in siliques of *mun-1*/+ (**Figure 26**A). In addition, some seeds developed from relatively normal or mildly defective embryos (**Figure 3**F) and produced *mun-1* homozygote plants after germination.

I cloned the *MUN* gene by TAIL-PCR and confirmed it by molecular marker-assisted mapping (**Figure 4**A, B). T-DNA was inserted at the 5′-UTR region of the AT3G08880 gene in *mun-1*, which reduced gene expression in 25% of the WT plants (**Figure 4**A, C). Phenotypes of *mun-1* were complemented by the introduction of a 3.4 kb genomic fragment containing the 2 kb promoter and 1.4 kb gene sequence of AT3G08880 (**Figure 4**A, E). In contrast, although the adjacent gene, AT3G08870, showed 2.5 times higher expression in *mun-1* (**Figure 4**D), none of *35S::AT3G08870* transgenic lines

among the 35 T1 plants showed an abnormal phenotype like *mun-1*.

The analysis of seeds produced in the siliques of *mun-1/+* plants showed that approximately 11.7%, less than a quarter, exhibited a seed abortion phenotype, and 11.6% of germinated progenies had abnormal plant morphology (**Figure 26**A, **Table 1** and **Table 2**). Such results indicated that *mun-1* is a weak allele showing incomplete penetrance, which explains the relatively random arrest at various stages of embryonic development.

Figure 3

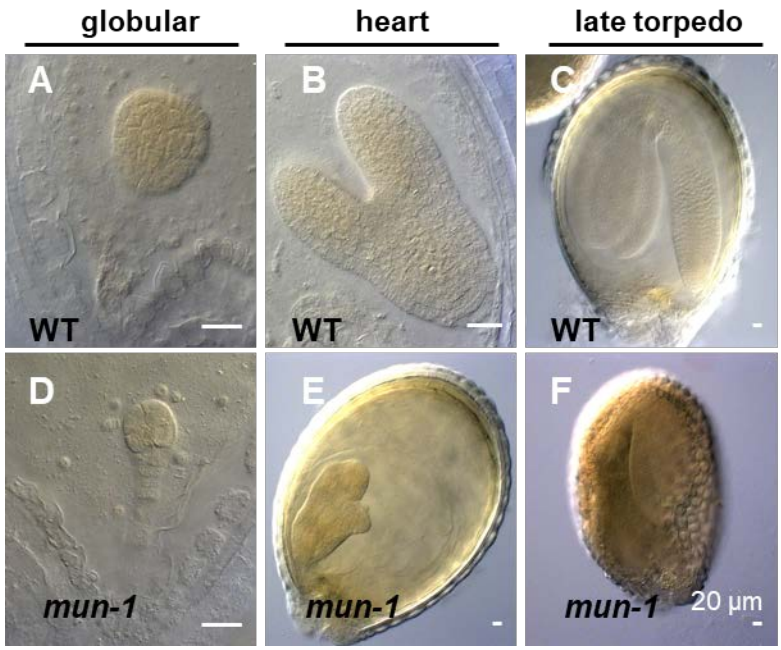

Figure 3. Defects of embryo development in *mun-1*.

Arrested embryos developed from the siliques of heterozygote, *mun-1/+*. (**A-C**) WT, (**D-F**) *mun-1*. (**A, D**) globular stage, (**B, E**) heart stage, (**C, F**) late torpedo stage. White bar = 20 μm.

Figure 4

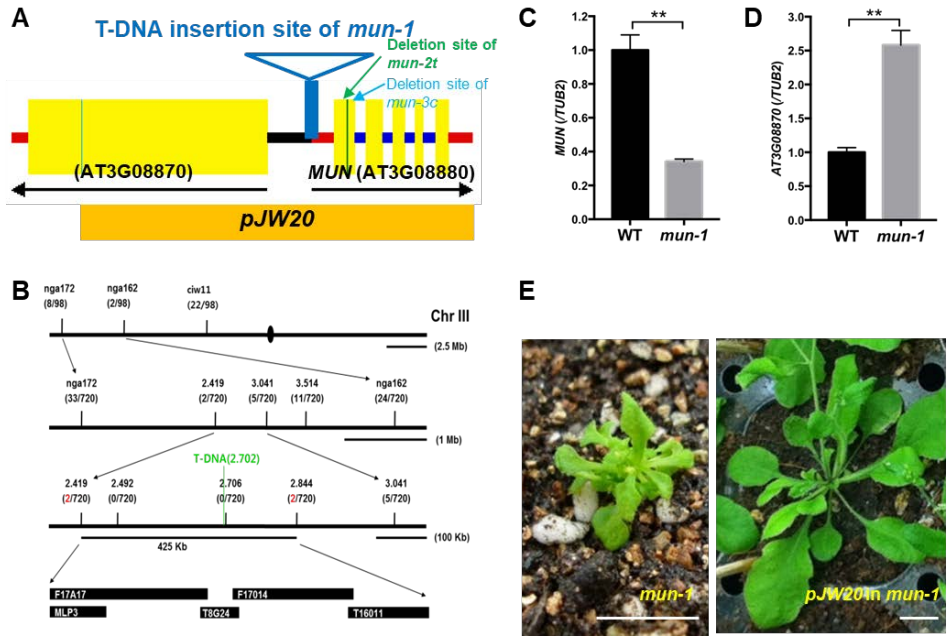

Figure 4. Cloning of *MUN*.

(**A**) Location of T-DNA insertion in the *mun-1* (blue box and triangle). T-DNA insertion locus was identified by TAIL-PCR in *mun-1*. The *mun-1* allele has a 37 bp deletion in the 5′ UTR of AT3G08880. Green arrow indicates the site of a 7 bp deletion at the first exon in *mun-2t*, the null allele. The sky-blue arrow indicates the site of a 4 bp deletion at the first exon in *mun-3c*, the null allele. Yellow box = exon, blue line = intron, red line = UTR, black line = intergenic region, orange box below = genomic DNA fragment used for complementation of *mun-1* in E.

(**B**) Marker map surrounding *MUN* locus on chromosome 3. The genetic distances among molecular markers and the regions covering BAC clones are

presented. The numbers in parenthesis are the numbers of recombinants among the 720 chromatids analyzed.

(**C**) Expression of *MUN* in WT and *mun-1* analyzed by RT-qPCR. The transcript level in *mun-1* is approximately 25% of that in WT, indicating that *mun-1* is a weak allele. Means ± SD based on three replicates are presented. Student's *t*-test (**$p < 0.002$).

(**D**) Expression of *AT3G08870* in the WT and *mun-1* analyzed by RT-qPCR. The mutant *mun-1* showed 2.5 times higher expression than did the WT plants. Means ± SD from three replicates are presented. Student's *t*-test (**$p < 0.002$).

(**E**) Mutant phenotype of *mun-1* is rescued by the introduction of *pJW20* (3.4 kb genomic DNA fragment). T1 plants show complete complementation. White bar = 1 cm.

Table 2. Phenotypic segregation of seeds from the siliques of *mun-1*/+, *mun-2t*/+, and *nuf2-1*/+.

The ratio of seed abortion (dried and dead seeds after fertilization) and ovule abortion (aborted ovule before fertilization) in *mun-1*/+, *mun-2t*/+, and *nuf2-1*/+. The ratio of seed abortion in null allele (*mun-2t*/+ and *nuf2-1*/+) is approximately 25%, which indicates zygotic lethal phenotype. The ratio of seed abortion in *mun-1*/+, a weak allele, is approximately half of 25%, indicating incomplete penetrance in *mun-1*. Ovule abortions (aborted ovule before fertilization) are not observed in *mun-1* and *mun-2t*. $n = 8$ (siliques).

	Normal	Seed Abortion	Ovule Abortion	Total
WT	403 (97.8%)	3 (0.7%)	6 (1.5%)	412 (100.0%)
***mun-1*/+**	324 (88.3%)	43 (11.7%)	0 (0.0%)	367 (100.0%)
***mun-2t*/+**	343 (73.6%)	123 (26.4%)	0 (0.0%)	466 (100.0%)
***nuf2-1*/+**	233 (69.3%)	84 (25.0%)	19 (5.7%)	336 (100.0%)

4.2. Spontaneous *de novo* shoot organogenesis (DNSO) in *mun-1* occurs without hormone treatment

In *mun-1*, ectopic protrusions developed into SAMs that produced a few leaves (**Figure 1**G, H, **Figure 2**E, F, red arrows). Undifferentiated cell colonies randomly protruded from normally differentiated tissues, such as leaf epidermis, in *mun-1* without any hormone treatment. It is known that ectopic expression of *WUSCHEL (WUS)*, a well-known marker for stem cell niche and is sufficient to lead *de novo* shoot organogenesis (DNSO) (Gallois *et al.*, 2004; Duclercq *et al.*, 2011; Zhang *et al.*, 2017). Therefore I checked the expression levels of *WUS* in *mun-1* plants (**Figure 5**D). I found that *WUS* was overexpressed in both shoot apices and whole seedlings of *mun-1*. Interestingly, *WUS* was strongly overexpressed more often in the whole seedlings than in the shoot apices, suggesting that ectopic *WUS* expression occurred in tissues other than the normal SAM area as well. Consistently, the GUS-stained signals of *pWUS::WUS-GUS* in the *mun-1* were detected in various tissues, such as the shoot apex, leaf epidermis, and roots (**Figure 5**B, C, red arrows) in contrast with the case of WT. Only one GUS spot was detected in the SAM area of WT (**Figure 5**A). It indicates that ectopic stem cell niches were established at various tissues in *mun-1*.

In addition, another stem-cell specific marker, *CLV3*, and somatic embryogenesis-related genes such as *STM*, *ABI3*, *FUS3*, *WOX2*, *KNAT2*, and *MP* were also upregulated in *mun-1* (**Figure 6**). Such an expression profile

seems to be the result of somatic embryogenesis or *de novo* shoot organogenesis in *mun-1* without hormone treatment.

Figure 5

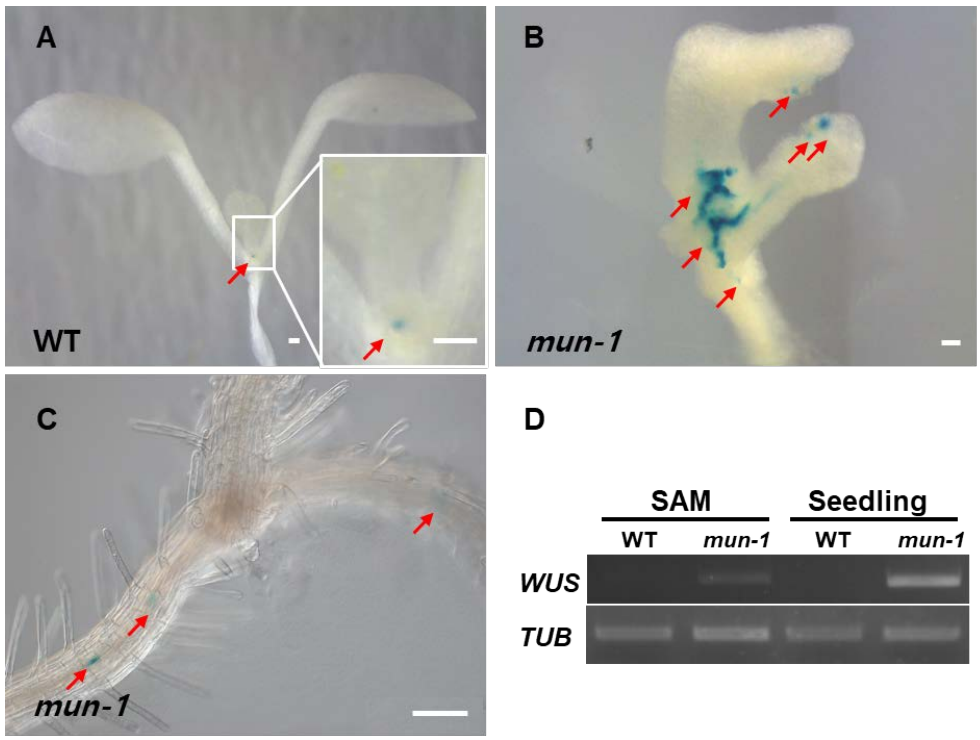

Figure 5. Ectopic expression of *WUS* in *mun-1*.

(**A-C**) GUS staining results using *pWUS::WUS-GUS* in the (**A**) WT and (**B, C**) *mun-1* plant in. seedlings 7 DAG. GUS stain is marked by red arrows. Inset in (**A**) is an enlarged image of SAM of WT plants. Only one GUS spot was detected in the SAM area of WT plants, whereas ectopic GUS spots (marked with red arrows) were detected outside the SAM in *mun-1*. (**C**) Root of *mun-1*. White bar = 100 μm.

(**D**) Expression of *WUS* by RT-PCR in SAM and whole seedlings of WT and *mun-1*.

Figure 6

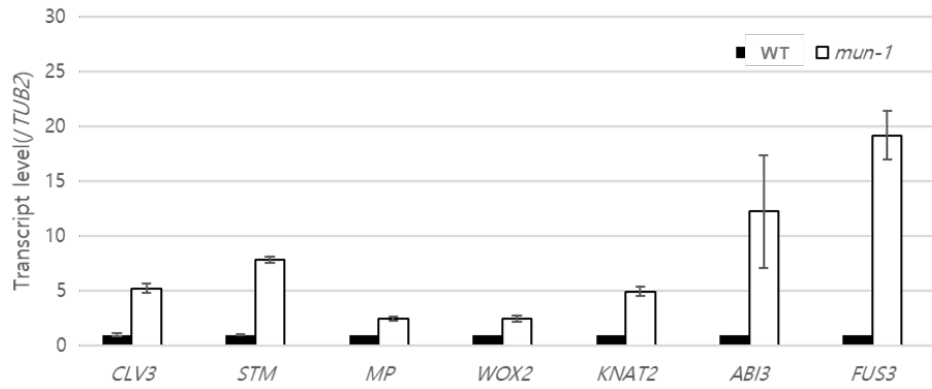

Figure 6. Expression of the genes regulating SAM and embryogenesis markers by RT-qPCR.

Each transcript level of target genes in WT is set at a relative value of one. The whole seedling 10 DAG was used for RNA extraction. Means ± SD based on three replicates are presented.

4.3. Abnormal regulations of hormones in *mun-1*

I studied the auxin regulation in *mun-1* plants by observing the GUS signal of *DR5::GUS* in *mun-1* (**Figure 7**A-a). The *mun-1* plants showed relatively random locations of auxin maxima than those of the WT plants. It appeared that protrusions of primordia were guided by auxin maxima. Exogeneous application of auxin (IAA) could not rescue the phenotype of *mun-1* (**Figure 7**A-b), indicating the defect of auxin biosynthesis is not the cause for the phenotype of *mun-1* plants. In addition, the *mun-1* plants showed normal gravitropic responses, as did the WT plants (**Figure 7**A-c). It is well known that somatic embryogenesis is controlled by the coordination between auxin and cytokinin regulation (Su *et al.*, 2014). Further studies of cytokinin signaling and response would be important for understanding the mechanisms of ectopic stem cell generation in *mun-1* plants. In addition, the levels of other phytohormones, e.g., salicylic acid (SA), abscisic acid (ABA), and jasmonic acid (JA), decreased approximately two-fold in *mun-1 plants* (**Figure 7**B). Even though the cause and effect remain unclear, *mun-1* exhibits unusual flow and abnormal amount of phytohormones.

Figure 7

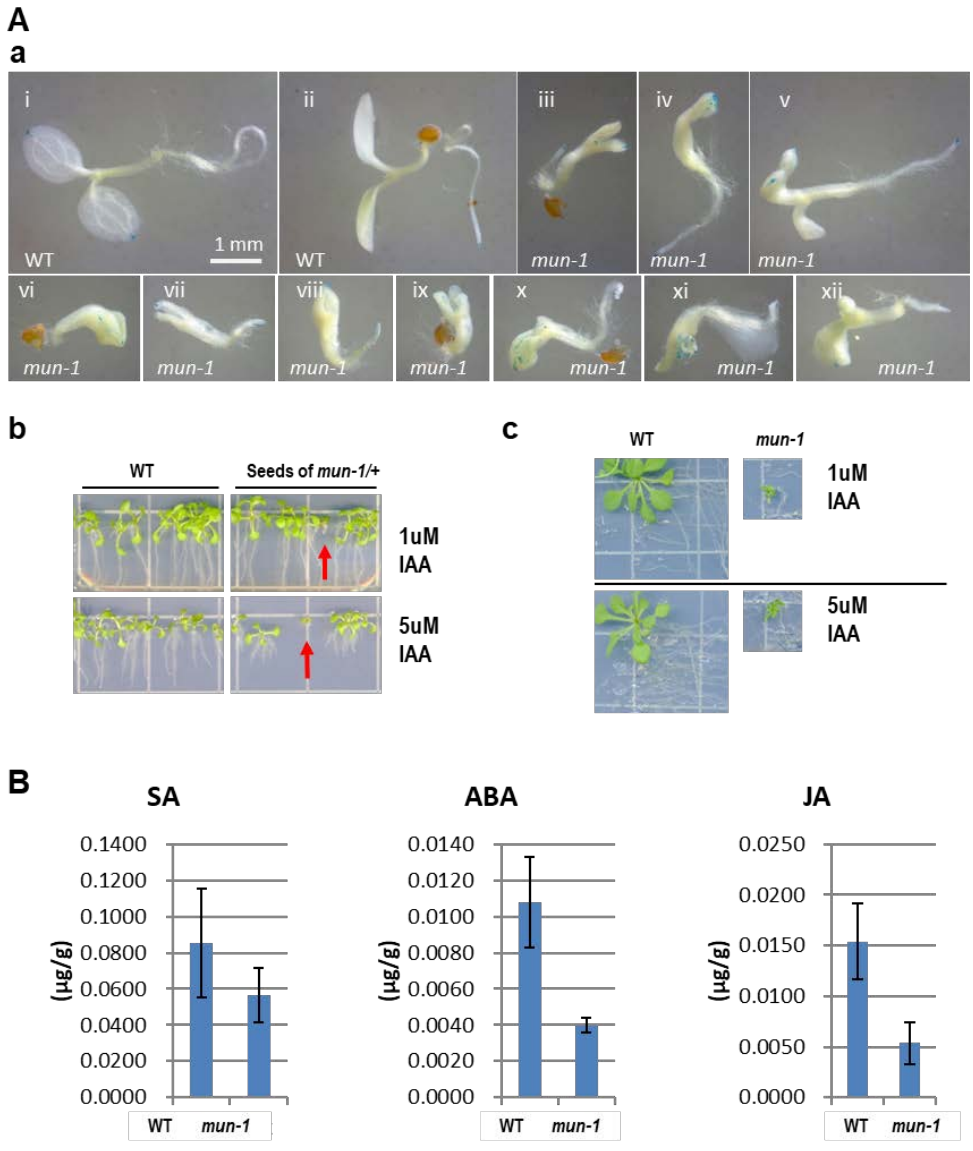
A
a
i
ii
iii
iv
v
WT
1 mm
WT
mun-1
mun-1
mun-1
vi
vii
viii
ix
x
xi
xii
mun-1
mun-1
mun-1
mun-1
mun-1
mun-1
mun-1
b
WT
Seeds of mun-1/+
1uM IAA
5uM IAA
c
WT
mun-1
1uM IAA
5uM IAA
B
SA
ABA
JA
(μg/g)
0.1400
0.1200
0.1000
0.0800
0.0600
0.0400
0.0200
0.0000
0.0140
0.0120
0.0100
0.0080
0.0060
0.0040
0.0020
0.0000
0.0250
0.0200
0.0150
0.0100
0.0050
0.0000
WT
mun-1

Figure 7. Abnormal regulations of hormones in *mun-1* plants.

(**A**) (**a**) GUS staining results of *DR5::GUS* in *mun-1* 5 DAG. White bar = 1 mm; all the pictures were represented same scale. (i, ii) WT (iii)-(xii) *mun-1*. WT plants showed auxin maxima at the tip of cotyledon, SAM, root apical meristem (RAM), lateral root initiation (LRI); however, *mun-1* showed relatively random locations of auxin maxima. It appeared that protrusions of primordia were guided by auxin maxima. (**b**) Exogeneous application of auxin could not rescue the phenotype of *mun-1*. Red arrows indicated homo mutant of *mun-1*. At 9 DAG, (**c**) *mun-1* showed normal gravitropic responses, as did the WT plants. 27 DAG (90˚ turned at 13 DAG).

(**B**) Endogeneous hormone levels measured by LC/TOF-MS. SA, ABA, and JA decreased in *mun-1* plants.

4.4. Defects in cell division and chromosome segregation, and aneuploidy, in *mun-1* plants

Roots of *mun-1* grew much slower than those of the WT plants (**Figure 8**). In addition, *mun-1* plants produced shorter roots because both the meristematic zone and elongation zone were shorter than that of the WT plants (**Figure 9**B). Yellow arrows mark the starting point of the elongation zone, and blue arrows mark the starting point of differentiation zone. The cell proliferation assay using Edu to detect actively dividing cells in the S phase in the meristematic zone showed considerably fewer Edu-stained cells in the mutants than in the WT plants, indicating lower RAM activity in *mun-1* (**Figure 9**B, D). It also suggests that the cells of *mun-1* are dividing at a slower rate than those of the WT plants.

Moreover, I compared the number of root cells undergoing M phase in the meristematic zone (**Figure 9**A, red arrows, C) in the mutant and WT plants, which was counted using *pUBQ14::GFP-TUA6* and a marker line detecting spindle fiber and phragmoplast formation (Oh *et al.*, 2010). The *mun-1* line had substantially fewer cells in M phase than the WT. Thereafter, I compared the *mun-1* and WT plants for cell sizes in leaf epidermis and mesophyll tissues (**Figure 10**). Although the overall leaf size was quite dissimilar, the sizes of cells from the leaf epidermis and mesophyll were approximately the same. Taken together, my results demonstrated that the cell division rate of *mun-1* was much lower than that of the WT.

Figure 8

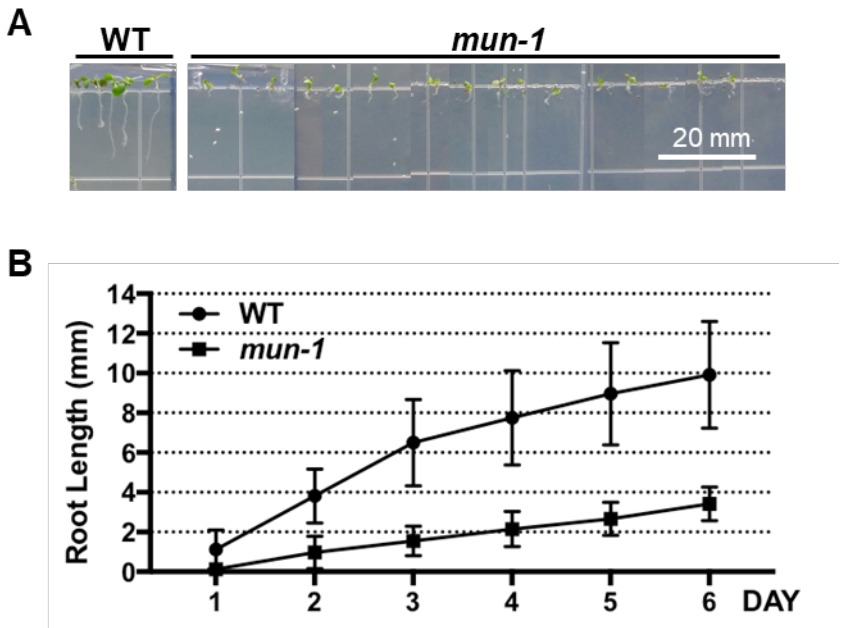

Figure 8. The *mun-1* plants show a short root phenotype.

(**A**) Roots of WT and *mun-1* plants 6 DAG. White bar = 20 mm.

(**B**) Time course measurements of root lengths in the WT and *mun-1* plants.

Means ± SD are presented, $n = 12$.

Figure 9

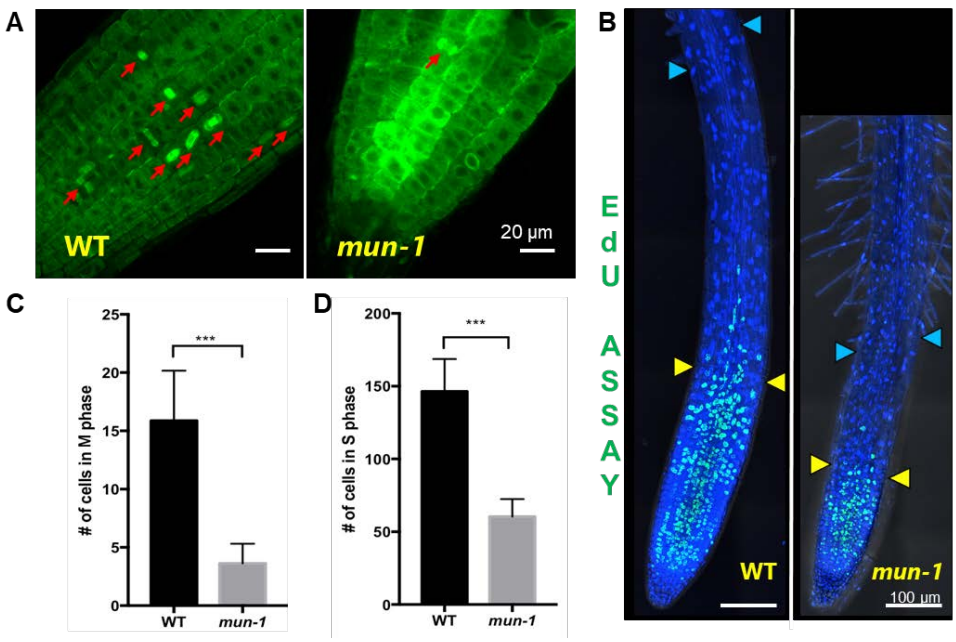

Figure 9. Reduced cell division rate in *mun-1* plants.

(**A**) CLSM images of M-phase cells (red arrows) in root meristematic zone of WT and *mun-1* plants observed in *pUBQ14::GFP-TUA6*, a microtubule-reporter transgenic line. White bar = 20 µm.

(**B**) Maximum intensity projection images of CLSM after 5-ethynyl-2′-deoxyuridine (Edu) staining. Green spots are nuclei in the S-phase stained with Alexa Fluor® 488-conjugated Edu. Nuclei were stained with 4',6-diamidino-2-phenylindole (DAPI) (blue signals). 5 DAG seedlings. Yellow arrows mark elongation zone and blue arrows mark differentiation zone. White bar = 100 µm.

(**C**) Number of M phase cells in the meristematic zone. Student's *t*-test, $n = 8$ (***$p < 0.001$).

(**D**) Number of S-phase cells in the meristematic zone. Student's *t*-test, $n = 8$ (***$p < 0.001$).

Figure 10

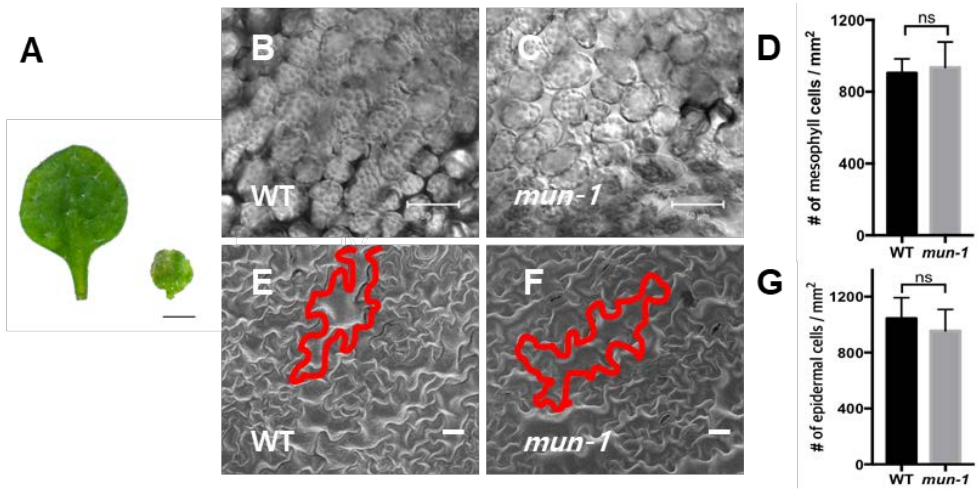

Figure 10. Cells of WT and *mun-1* have similar sizes.

Size comparison of epidermal and mesophyll cells between the WT and *mun-1* plants.

(**A**) Photo of second true leaves 12 DAG, WT (left) and *mun-1* (right). Black bar = 1 mm.

(**B, C**) Differential interference contrast (DIC) images of mesophyll cells from WT and *mun-1* plants. White bar = 50 μm.

(**D**) Number of mesophyll cells per unit area. Differences between the WT and *mun-1* plants were compared using Student's *t*-test, $n = 8$.

(**E, F**) SEM images of epidermal cells of rosette leaves from the WT and *mun-1* plants. The red lines highlight single cells. White bar = 20 μm.

(**G**) Number of epidermal cells per unit area. Differences between the WT and *mun-1* plants were compared using Student's *t*-test, $n = 8$.

Flow cytometric analysis measuring DNA content after propidium iodide (PI) staining revealed a higher frequency of cells with DNA aneuploidy in *mun-1* than in the WT plants (**Figure 11**A). No significant shift in the peak was observed in the histogram data, but the width of the peak differed in *mun-1* as compared to that of the WT plants. The peaks of *mun-1* were lower and broader at all peak points in DNA histograms, suggesting the presence of nuclei with abnormal quantities of DNA. Aneuploid cells were measured indirectly as the coefficient of variation (CV, %) of each peak (**Figure 11**B). The value of each peak was 10–20% higher in *mun-1* than in the WT plants, indicating that *mun-1* had more aneuploid cells than WT had. However, endoreduplication status of leaf cells was relatively normal in *mun-1* (**Figure 11**C). Aneuploidy, a typical error in cell division, is an outcome of chromosome mis-segregation. Aneuploidy detected in the present study indicates that *MUN* could regulate the general cell division process by controlling the chromosome segregation process. Thereafter, I directly observed defects of chromosome segregation in *mun-1*, such as micronuclei formation, and chromosome lagging during anaphase (**Figure 12**). These data suggest that *MUN* affects the process of cell division by managing the proper chromosome segregation.

Figure 11

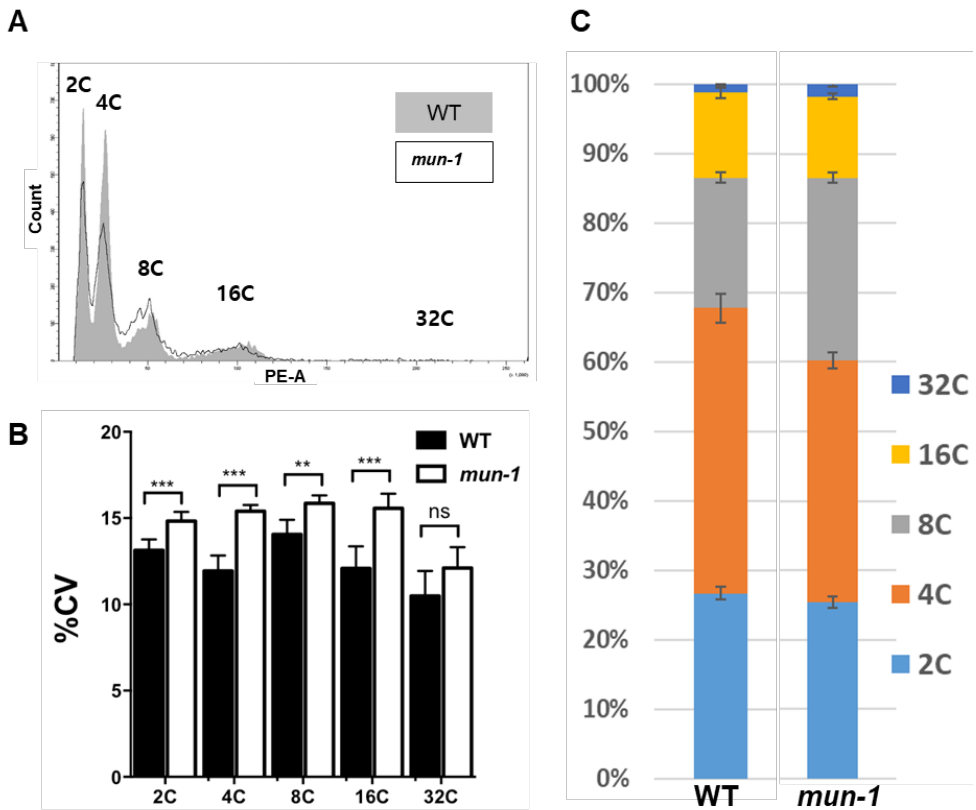

Figure 11. DNA aneuploidy in *mun-1*.

(**A**) Flow cytometry analysis. Rosette leaves of seedlings 7 DAG were used and 10,000 nuclei were counted for each sample.

(**B**) CV (%) chart of 2C, 4C, 8C, 16C, and 32C peaks in WT and *mun-1* plants, which were calculated from the analysis of 6 DNA histograms. Two-tailed *t*-test was used (ns: $p > 0.12$, *: $p < 0.033$, **p: < 0.002, ***: $p < 0.001$).

(**C**) Analysis of nuclear DNA ploidy by flow cytometry shows endoreduplication status of WT and *mun-1* plants.

Figure 12

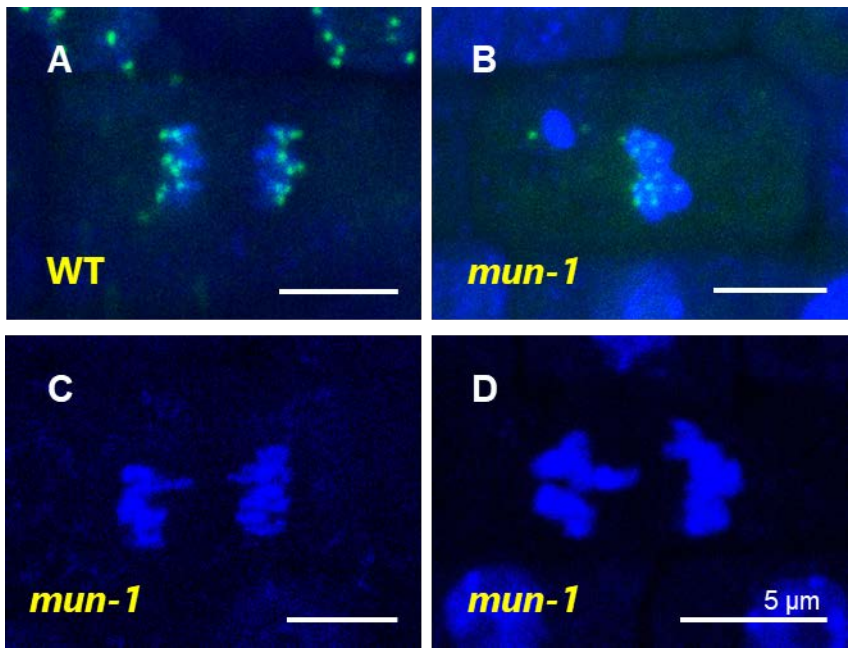

Figure 12. Defects in chromosome segregation of *mun-1*.

(**A**) Chromosome segregation of WT plants. (**B**) Micronuclei formation in *mun-1* plants. (**A, B**) Green spots are HTR12/CENH3-GFP and DAPI-stained chromosomes are blue. The figure show maximum intensity projection images. White bar = 5 µm.

(**C, D**) Lagging chromosomes of *mun-1*. DAPI-stained chromosomes are blue. Among 16 anaphases of the WT plants and 20 anaphases of *mun-1* plants, 6.3% and 35% showed lagging chromosomes, respectively. White bar = 5 µm.

4.5. *MUN* encodes a SPC24 homolog, a member of the NDC80 kinetochore complex

Predicted MUN protein has a coiled-coil region and a globular domain at the end, which are typical structural features found in all four components of the NDC80 kinetochore complex (**Figure 13**A and **Figure 16**A). Although MUN and AT3G08880 have been annotated as an unknown proteins in the from The Arabidopsis Information Resource (TAIR) 10 database (https://www.arabidopsis.org), comparative genomic analysis using the Phytozome (v11.0) database (https://phytozome.jgi.doe.gov/pz/portal.html) indicated that it is homozygous to SPC24, a member of the NDC80 kinetochore complex in several species (**Figure 13**B, C). Protein homologs of AT3G08880 in *Boechera stricta*, *Capsella rubella*, and *Capsella grandiflora* were predicted to be homologs of the SPC24 subunit of the NDC80 (Pfam family, PF08286) complex. All of these had approximately 80% similarity with MUN; thus, I inferred that MUN is a strong candidate for a SPC24 ortholog.

Using the C-terminal region of MUN (129-201, 73aa) as a query in RAPTOR-X software, I obtained a hypothetical 3D structure homologous to the structure of chicken (*Gallus gallus*) Spc24 (3vza:C) (**Figure 16**A) (Källberg *et al.*, 2012; Nishino *et al.*, 2013). The predicted Rank#1 template was the Spc24 chain located in the Spc24_Spc25_CENP-T complex of chicken. All of the SPC24s have a conserved globular domain at the C-

terminus, which is known as the “RING finger, WD repeat, DEAD-like helicases (RWD)” domain consisting of two α-helices with a β-pleated sheet in between (Schmitzberger and Harrison, 2012; Petrovic *et al.*, 2014; Petrovic *et al.*, 2016). The RWD domain was reported within a superfamily of ubiquitin (Ub)-conjugating (E2) enzymes (UBC) lacking the catalytic machinery required for covalent Ub binding. This domain is usually involved in protein-protein interactions (Burroughs *et al.*, 2008). In particular, RWD domains are important recurring scaffolds in kinetochores (Schmitzberger *et al.*, 2017). In addition, MUN has a RWD domain in the predicted 3D structure (**Figure 14**A, B, and **Figure 16**A). Multiple alignments using amino-acid sequences of C-terminal regions in SPC24s from diverse species revealed that the RWD domain is also conserved in MUN/AtSPC24 (**Figure 14**A, C). However, MUN/AtSPC24 could not complement the SPC24 of *Saccharomyces cerevisiae* (**Figure 15**). Despite the differences in overall amino acid sequences, the polarity of the C-terminus has been relatively well conserved (**Figure 14**B). In particular, tryptophan residue in the last α-helix of SPC24 is highly conserved in various organisms (**Figure 14**A, B and **Figure 16**A). In chickens, the W188 residue forms hydrophobic interactions with V191 of GgSPC24 and L149 of GgSPC25, and is critical for the α-helix formation (**Figure 16**B). Therefore, W188 is a key residue for proper folding of GgSpc24 and heterodimerization with SPC25. A tryptophan residue is generally located inside a protein owing to it hydrophobicity. It appeared that

this tryptophan residue would be not the regulatory element for modification, but the key component of a structure that is maintained for interacting with SPC25 and other kinetochore components. This critical residue is also conserved in MUN (W195 in *Arabidopsis thaliana*), supporting the view that MUN has structural similarity to GgSPC24. Taken together, the *in silico* analyses strongly suggested that MUN is an ortholog of SPC24, a member of the NDC80 kinetochore complex.

Figure 13

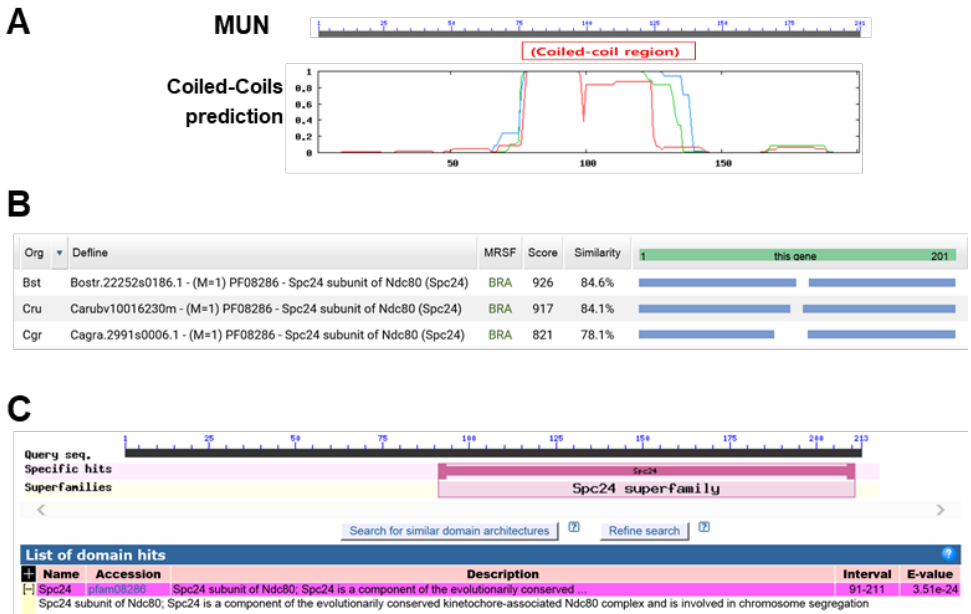

Figure 13. MUN, which has a coiled-coils domain, shows the similarity to SPC24 superfamily.

(**A**) MUN has a coiled-coil domain predicted by using "Coiled-Coils prediction" software powered by Pole Bioinformatique Lyonnais (PBIL). Number refers to amino acid positions in MUN.

(**B**) MUN homologs searched in Phytozome, v11.0 database. The MUN homologs from *Boechera stricta*, *Capsella rubella*, and *Capsella grandiflora* are predicted as SPC24 subunit of the Ndc80 complex (Pfam family, PF08286).

(**C**) General structure of SPC24 superfamily genes from NCBI database (Pfam family, PF08286).

Figure 14

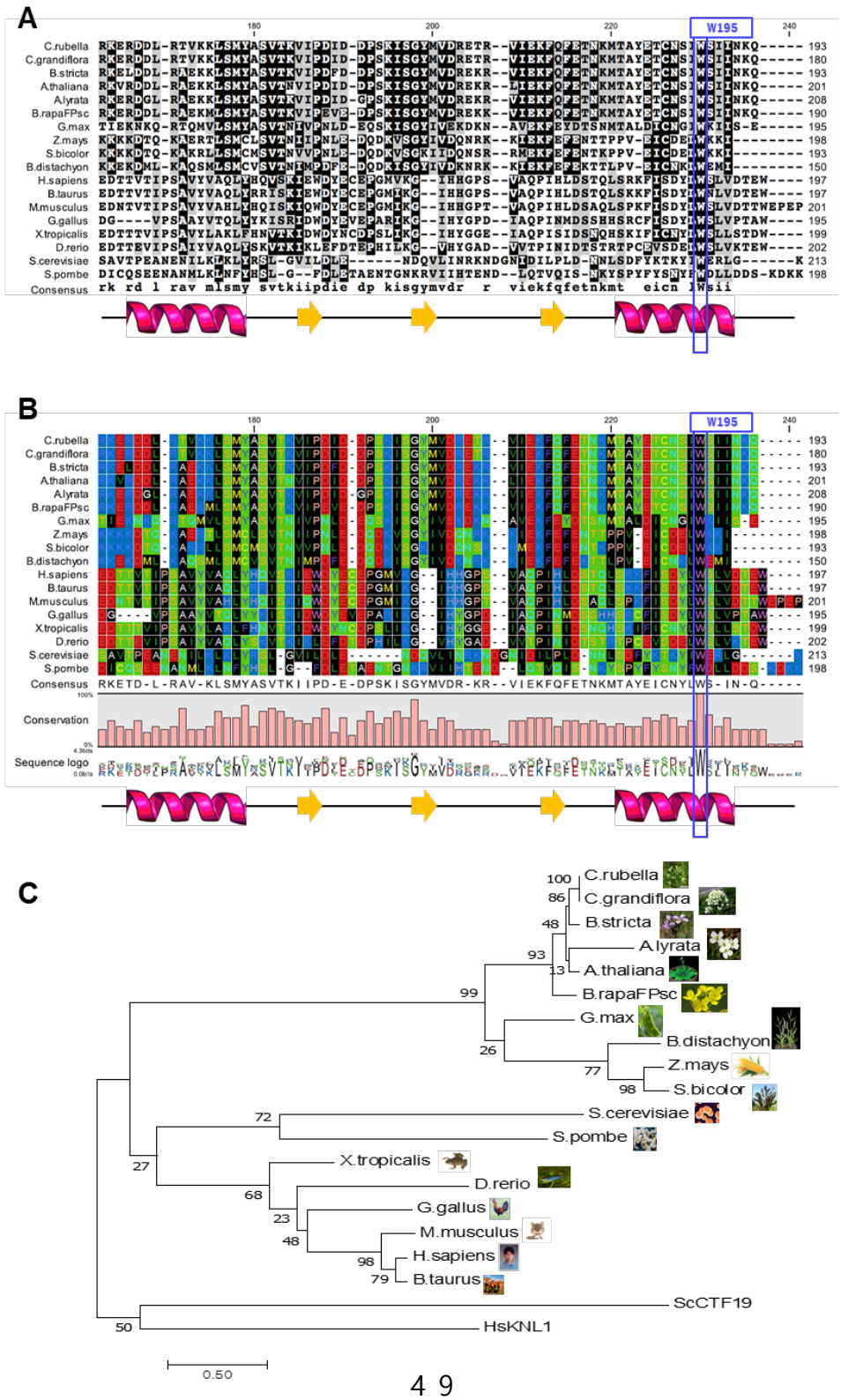
A
W195
C.rubella
C.grandiflora
B.stricta
A.thaliana
A.lyrata
B.rapaFPsc
G.max
Z.mays
S.bicolor
B.distachyon
H.sapiens
B.taurus
M.musculus
G.gallus
X.tropicalis
D.rerio
S.cerevisiae
S.pombe
Consensus
B
W195
Conservation
Sequence logo
C
C.rubella
C.grandiflora
B.stricta
A.lyrata
A.thaliana
B.rapaFPsc
G.max
B.distachyon
Z.mays
S.bicolor
S.cerevisiae
S.pombe
X.tropicalis
D.rerio
G.gallus
M.musculus
H.sapiens
B.taurus
ScCTF19
HsKNL1
0.50

Figure 14. MUN is evolutionarily conserved SPC24 ortholog in *Arabidopsis thaliana*.

(**A**) Multiple alignments of amino-acid sequences of the C-terminal regions of SPC24s from 18 species were obtained using CLC Main Workbench software, version 7.7.3. The secondary structures generated by RaptorX software have been shown at the bottom; pink ribbon: α-helix, and yellow arrow: β-sheet. A well-conserved tryptophan residue (W195 in *Arabidopsis thaliana*) is shown.

(**B**) Multiple alignments of amino-acid sequences using the C-terminal regions of SPC24s from 18 species were obtained by CLC Main Workbench software, version 7.7.3. Background colors for each residue were given according to the following four categories. Green: neutral and polar, Black: neutral and nonpolar, Red: acidic and polar, Blue: basic and polar. Conservation ratios are indicated in the bar graph. The secondary structure generated by RaptorX Structure prediction software has been shown at the bottom. Pink ribbon: α-helix, and yellow arrow: β-sheet. The highly conserved 195th tryptophan residue (W195) in *Arabidopsis thaliana* protein is marked.

(**C**) A phylogenetic tree of SPC24s from 18 species rooted by outgroup (yeast CTF19 and human KNL1) is shown. Evolutionary analyses were conducted using MEGA7. Numbers indicate bootstrap values based on 1000 trials.

Figure 15

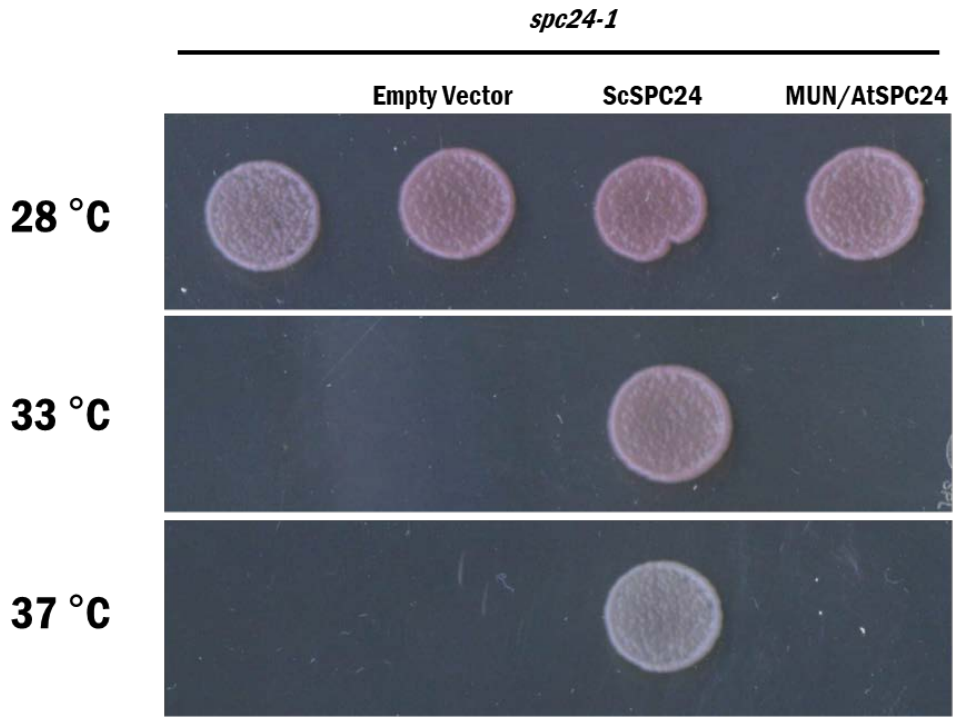

Figure 15. MUN/AtSPC24 cannot complement the yeast SPC24.

Complementation of the temperature-sensitive mutant, *spc24-1*, in the yeast *Saccharomyces cerevisiae* K699 strain by *MUN/AtSPC24*. Yeast cells were spotted on the YPD plates.

Figure 16

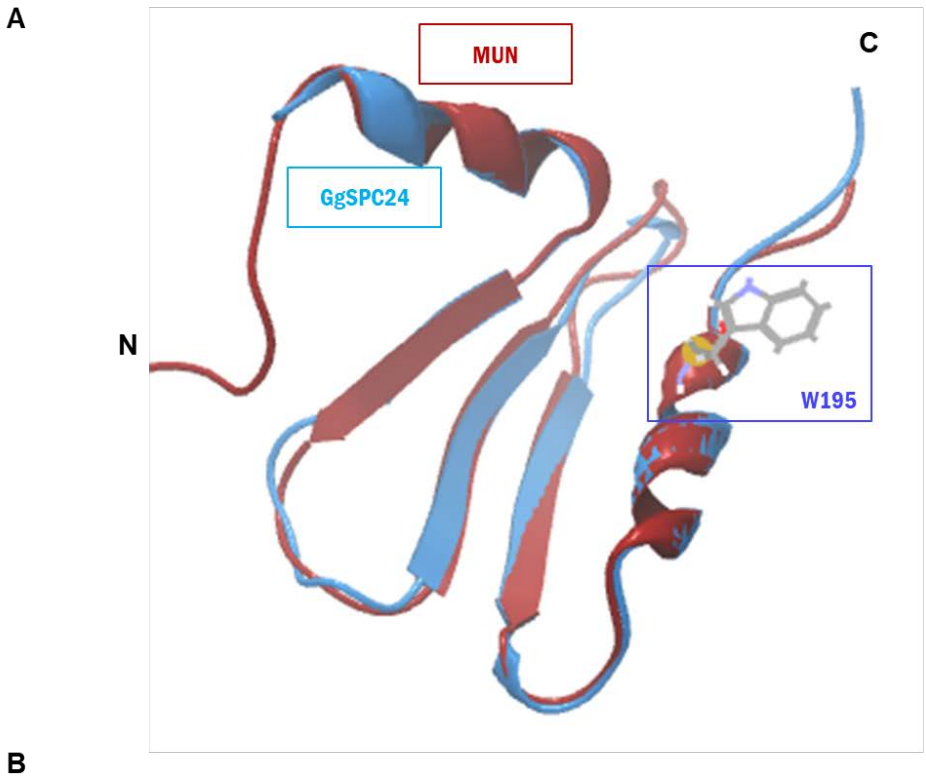

Figure 16. Predicted protein structure of MUN, a SPC24 homolog.

(**A**) Three-dimensional structure of the C-terminal region (73 aa, wine color) of MUN predicted by Raptor-X software. Rank#1 template is the Spc24 chain in the Spc24_Spc25_CENP-T complex (3vza:C, 61 aa, sky color) of chicken (*G. gallus*). Alignment of protein structure images were generated by CLC Main Workbench software version 7.7.3. W195 is buried in C-terminal α-helices.

(**B**) Amino acids interacting with W188 (=W195 in *Arabidopsis thaliana*) in Spc24_Spc25_CENP-T complex (3vza). W188 residue forms hydrophobic interactions with V191 of GgSPC24 and L149 of GgSPC25, and plays a critical role in α-helix formation. The structures were generated in Discovery studio 4.1 visualizer.

4.6. *MUN* is predominantly expressed in actively dividing tissues and the protein is co-localized at the centromere with HTR12/CENH3

To analyze the expression pattern of *MUN*, I generated *pMUN::MUN-GUS* transgenic lines containing 3.4 kb genomic sequences of *MUN*, comprising the promoter and the whole coding sequence, fused with *β-glucuronidase* (GUS) reporter gene as translational fusion (**Figure 17**). The histochemical GUS staining revealed that *MUN-GUS* is highly expressed in actively dividing tissues, such as SAM, RAM, vasculature, and newly emerging leaves. *MUN* is expressed not only in meristematic tissues but also in whole plant of very young (2-day-old) seedling. GUS signals in cotyledons and expanded true leaves weaken with time; however, primordia in new emerging true leaves and bolting stem tissues show strong GUS signals. After flowering, GUS staining was detected in the inflorescence shoots, indicating that the expression of *MUN* is associated with cell division. Interestingly, in plants containing *pMUN::MUN-eGFP* that rescued the morphological phenotype of *mun-1*, *MUN-eGFP* is expressed not only in vegetative tissues (roots and leaf epidermis), but also in reproductive tissues (petals, pollen, and ovules) (**Figure 18**). GFP spots were located in the nuclei. In general, up to 10 spots per cell in sporophytic tissues (roots, leaf epidermis, petals, and integuments of ovules) and <5 spots per cell from gametophytic tissues, such as sperm cells in mature pollen, were observed. In some cells of RAM, MUN-eGFP was occasionally detected in the metaphase plate (**Figure 18**, white arrow)

and appeared as a pair of dots, which is very likely to be a pair of sister centromeres formed at the G2 phase (**Figure 18**, yellow arrow). Such a localization pattern of MUN-eGFP suggests that MUN is a structural protein in the chromosomes. In particular, the MUN localization pattern was very similar to that of HTR12/CENH3-GFP, a main component of the inner kinetochore complex (Ingouff *et al.*, 2007; De Storme *et al.*, 2016). Therefore, I determined whether MUN and CENH3 were co-localized at the kinetochore complex using lines containing *pMUN::MUN-mRFP1* and *HTR12/CENH3-GFP* transgenes. As expected, the RFP and GFP signals were largely overlapping, indicating that the two proteins were co-localized in the same region, at the centromere (**Figure 19**).

Thereafter, I determined if the localization of HTR12/CENH3-GFP was affected by the *mun-1* mutation (**Figure 12**B, **Figure 20**). Both the signal strength and spotting patterns of HTR12/CENH3-GFP in *mun-1* plants did not differ from those detected in the WT plants, indicating that MUN is not necessary for the recruitment of HTR12/CENH3 to the centromere. This result is different from the case of *knl2* in that the immunogold signals of cenH3 antibody at chromocenters of *knl2* nuclei were strongly reduced as compared with those of WT nuclei (Lermontova *et al.*, 2013). Thus, the results suggested that the assembly of MUN into the kinetochore occurred independently of HTR12/CENH3 loading, and that MUN is assembled into kinetochore after the loading of inner kinetochore components as typical outer

kinetochore components.

Figure 17

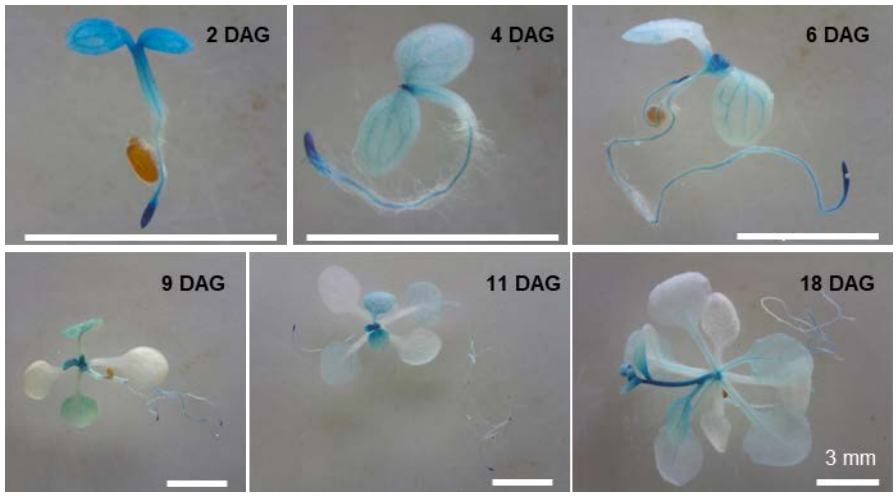

Figure 17. Expression of *MUN*.

GUS staining of *pMUN::MUN-GUS*. GUS is mainly expressed in the actively dividing young tissues. White bar = 3 mm.

Figure 18

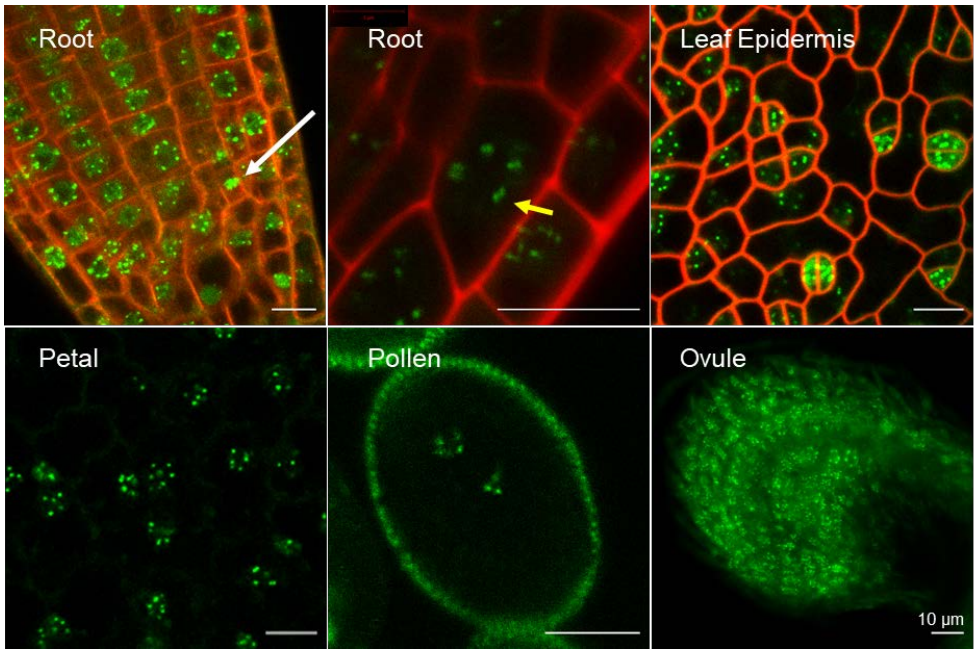

Figure 18. Cellular localization of *MUN*.

CLSM images of *pMUN::MUN-GFP* from various tissues. MUN is detected in nucleus as small spots. White arrow denotes the chromosome appeared at the metaphase plate during mitosis. Yellow arrow denotes the duplicated sister centromere at the G2 phase. The sperm cells in mature pollen show approximately five spots of MUN-GFP. White bar = 10 μm.

Figure 19

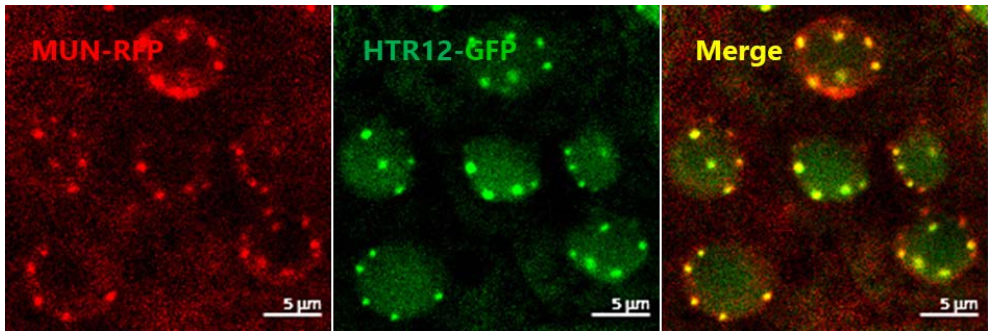

Figure 19. Co-localization of MUN and HTR12 at centromeres in root cells.

Root cells from *pMUN::MUN-mRFP1 pHTR12::HTR12-GFP* double transgenic plants were examined by CLSM. White bar = 5 µm.

Figure 20

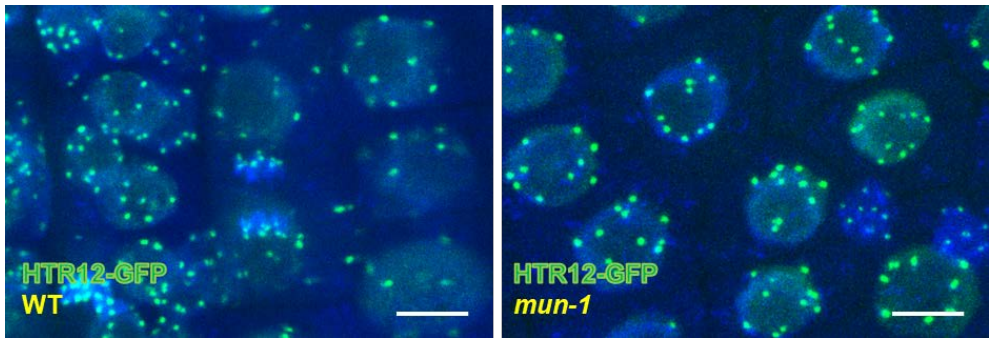

Figure 20. Localization of HTR12/CENH3-GFP in root of WT and *mun-1*.

Localization of HTR12/CENH3-GFP in root is not affected by *mun-1*. The green spots are HTR12/CENH3-GFP, DAPI-stained chromosomes are shown are blue. The figure shows maximum intensity projection images. White bar = 5 μm.

4.7. MUN interacts with components of the NDC80 complex

I checked if the components of the NDC80 complex localized at the same region. The subcellular localization patterns of eGFP proteins in the root meristems of *pNDC80::NDC80-eGFP*, *pNUF2::NUF2-eGFP*, and *pSPC25::SPC25-eGFP* transgenic lines confirmed that they had similar patterns with those of MUN-eGFP and HTR12/CENH3-GFP, specifically as dots in the nuclei throughout the cell cycle (**Figure 21**).

To confirm that MUN is a component of the NDC80 complex in *Arabidopsis thaliana*, I evaluated the protein-protein interactions between MUN and the other components of the NDC80 complex using the yeast two-hybrid assay and *in planta* co-immunoprecipitation (Co-IP) analysis (**Figure 22** and **Figure 23**). From the yeast two-hybrid assay, I found that MUN interacts with SPC25, and SPC25 interacts with NDC80 and NUF2 when SPC25 is used as a prey (SPC25 fused with activation domain). Additionally, NDC80, NUF2, and SPC25 underwent homodimerization in the yeast two-hybrid assay; however, the homodimerization of MUN has not been confirmed because MUN shows strong auto-activation activity when fused with the DNA-binding domain. In addition to confirming these interactions *in planta*, I performed Co-IP analysis of the components of the NDC80 complex in *Arabidopsis thaliana* seedlings. Each construct, namely, *pNDC80::NDC80-eGFP*, *pNUF2::NUF2-eGFP*, and *pSPC25::SPC25-eGFP*, was transformed into both the WT and *pMUN::MUN-FLAG* plants to

generate double transgenic lines for Co-IP analysis. Proteins from each sample were immunoprecipitated by beads linked to anti-GFP antibody, and immunoblotted using anti-GFP or anti-FLAG antibodies. The Co-IP analysis showed that MUN/SPC24 immunoprecipitated with NDC80, NUF2, and SPC25 in *Arabidopsis thaliana*. Thus, I inferred that even though MUN interacts with neither NDC80 nor NUF2 in the yeast two-hybrid assay, a NDC80 complex is formed *in planta* through SPC25 as a core molecule.

Consistently, the *in silico* analysis of the expression of each component of the NDC80 complex from 113 samples of RNA-Seq expression in Araport DB (https://www.araport.org/rna-seq-read-datasets-used-araport11) (**Figure 24**) showed that the expression patterns and levels of *NUF2*, *SPC25*, and *SPC24* were largely correlated. Overall, my results strongly support the supposition that MUN is an ortholog of SPC24, a component of the NDC80 complex in *Arabidopsis thaliana*. Thus, I concluded that all the components of the NDC80 complex in *Arabidopsis thaliana* exist and interact with each other. Therefore, I planned the phenotypic comparison among the mutants of NDC80 complex components.

Figure 21

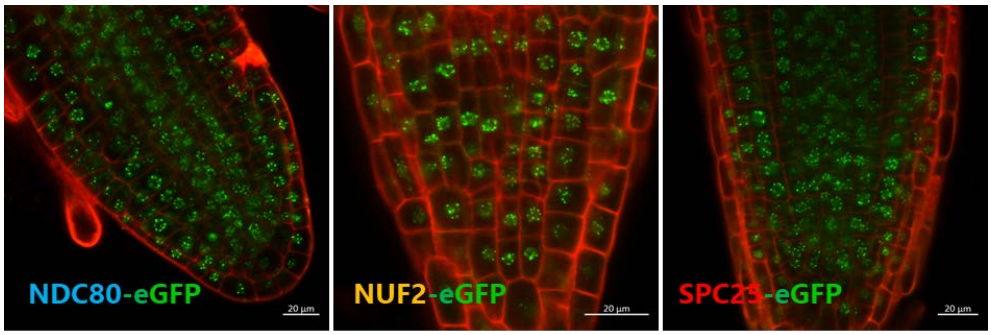

Figure 21. Subcellular localizations of the components of the NDC80 complex.

Subcellular localization patterns of eGFP in the roots of *pNDC80::NDC80-eGFP*, *pNUF2::NUF2-eGFP*, and *pSPC25::SPC25-eGFP* transgenic plants. All of the constructs were made by the fusion of 2 kb promoter and genomic region covering coding sequences with *eGFP*. All the components of NDC80 complex showed localization in the nuclei with dot patterns throughout the cell cycle, similar to HTR12-GFP and MUN-eGFP. White bar = 20 μm.

Figure 22

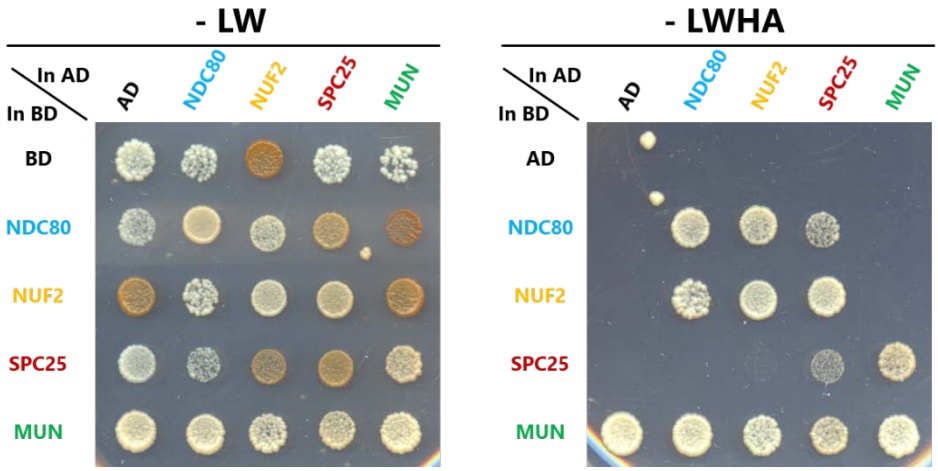

Figure 22. *In vitro* interactions of the components of the NDC80 complex with MUN.

Yeast two-hybrid assays among the components of the NDC80 complex, NDC80, NUF2, SPC25, and MUN/SPC24 of *Arabidopsis thaliana*. - LW: selection plates containing SD medium lacking Leu and Trp. - LWHA: selection plates containing SD medium lacking Leu, Trp, His, and Ade.

Figure 23

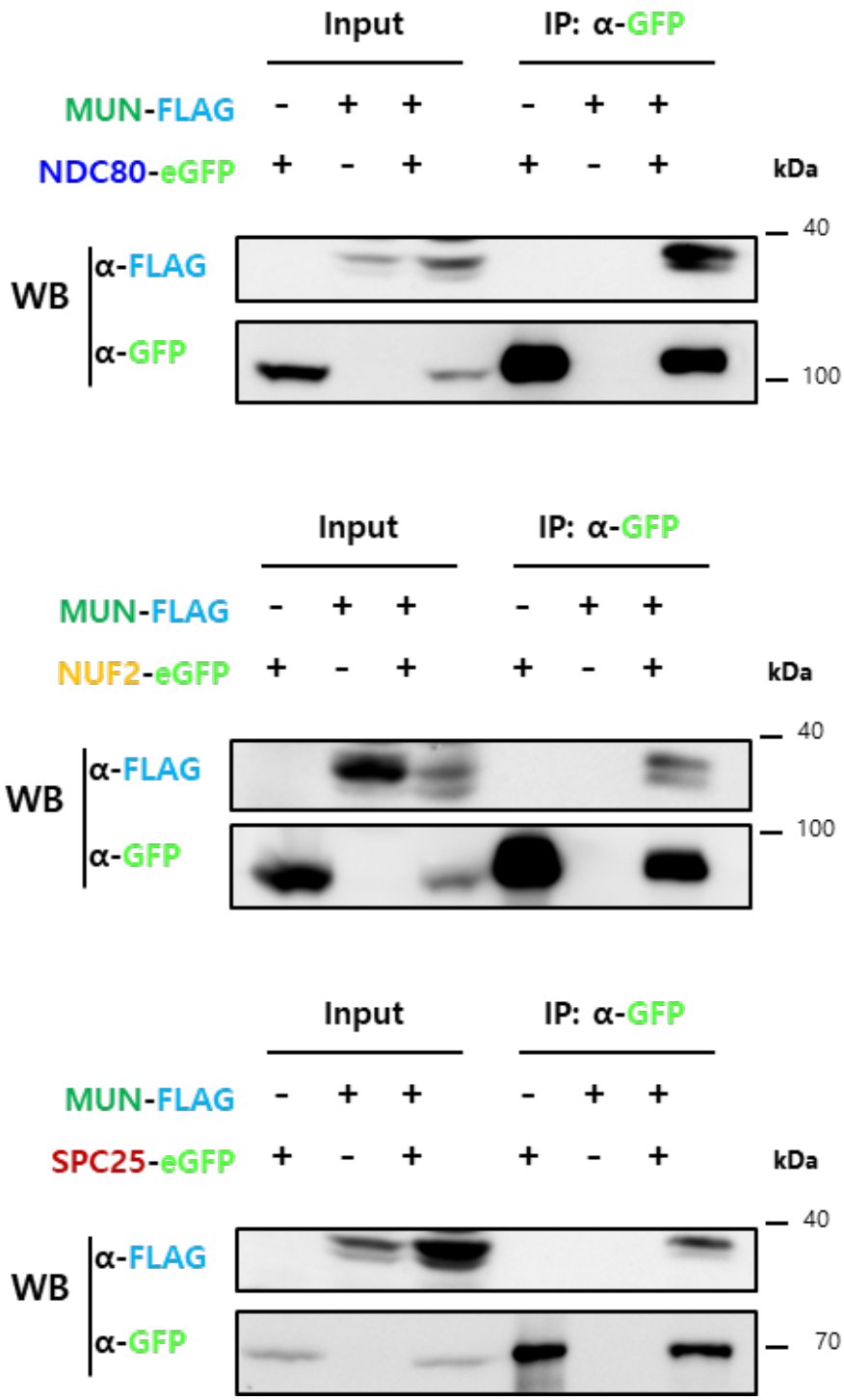
Input
IP: α-GFP
MUN-FLAG - + + - + +
NDC80-eGFP + - + + - +
kDa
40
WB
α-FLAG
α-GFP
100
Input
IP: α-GFP
MUN-FLAG - + + - + +
NUF2-eGFP + - + + - +
kDa
40
WB
α-FLAG
α-GFP
100
Input
IP: α-GFP
MUN-FLAG - + + - + +
SPC25-eGFP + - + + - +
kDa
40
WB
α-FLAG
α-GFP
70

Figure 23. *In vivo* interactions of the components of the NDC80 complex with MUN.

Co-IP analysis among the components of the NDC80 complex in seedlings of *Arabidopsis thaliana*. Constructs of *pNDC80::NDC80-eGFP*, *pNUF2::NUF2-eGFP*, and *pSPC25::SPC25-eGFP* were transformed to WT and *pMUN::MUN-FLAG* transgenic lines, respectively. T2 seedlings obtained after antibiotic selection were used for Co-IP analysis. MUN/SPC24 shows *in vivo* co-immunoprecipitation with NDC80, NUF2, and SPC25 in *Arabidopsis thaliana*. Epitope-tagged proteins were detected using FLAG and GFP antibodies. The molecular weight (kDa) is indicated on the right side of the blot. IP: immunoprecipitation.

Figure 24

NDC80-AT3G54630

NUF2-AT1G61000

SPC25-AT3G48210

MUN/SPC24-AT3G08880

Figure 24. Expression profiles of the four components of the NDC80 complex obtained from the analysis of RNA-Seq expression data for 113 different samples in Araport DB.

Expressions of *NDC80*, *NUF2*, *SPC25*, and *MUN/SPC24* from 113 samples for RNA-Seq expression analysis are presented. The red boxes denote high expression and green boxes denote low expression. *NUF2*, *SPC25*, and *SPC24* exhibited rough correlations in the expression pattern and the level in many plant tissues. *NDC80* showed lower expression, which is in general, a slightly different expression.

4.8. Null mutation in *MUN* causes zygotic embryonic lethal phenotype

Because 5′ UTR is disrupted by the insertion of T-DNA, *mun-1* is a weak allele producing reduced transcript levels (**Figure 4**). Thus, I generated null mutants using the targeted gene knockout techniques, TALEN and CRISPR/Cas9, for confirming more severe phenotypes than *mun-1*, and labeled as *mun-2t* (t stands for TALEN) and *mun-3c* (c stands for CRISPR/Cas9), respectively (**Figure 25**). Because *mun-2t* and *mun-3c* showed similar phenotypes, I described *mun-2t* as a representative null allele, hereafter. In the null mutant *mun-2t*, a premature stop codon was introduced because of a frameshift mutation caused by a 7 bp deletion in the first exon (**Figure 25**B). Thus, it generated short, truncated, and non-functional proteins. It was not possible to obtain seeds with the *mun-2t* homozygous genotype, and the seed abortion ratio observed in the siliques of heterozygotes, *mun-2t*/+, was approximately 26.4% (n = 466), suggesting that the null allele of *MUN* causes zygotic lethality (**Table 2**). Some embryos developed in the siliques showed irregular cell division patterns after formation of the apical cell (embryo proper), which resulted in embryo arrest at a very early stage (**Figure 26**B). The arrested stage of embryos in the *mun-2t* mutant generally occurred earlier than that in *mun-1* (**Figure 3**, **Figure 26**A, B). The seed abortion ratio in *mun-1*/+ was approximately half of 25%, indicating incomplete penetrance. Abnormal embryos at the heart or torpedo stage were frequently observed in the weak allele, *mun-1*; however, almost all embryos

in the null allele, *mun-2t*, were arrested before the globular stage. It is noteworthy that the *cenh3* mutant in *Arabidopsis thaliana* showed embryo arrest at the globular stage (Ravi *et al.*, 2010).

4.9. K/O alleles of *MUN* and *NUF2* shows same zygotic embryo lethal phenotype

Among the four components of the NDC80 complex, only the null allele of *NUF2* was available for research. Thus, I analyzed the heterozygotes of the *nuf2* null allele, *nuf2-1*/+ (SALK_087432) and a T-DNA insertion line. The mutant *nuf2-1* exhibited a zygotic lethal phenotype similar to *mun-2t* (**Figure 26**A, B). The seeds with the homozygous genotype of *nuf2-1* were not obtained, and approximately 25% of the seeds (n = 336) from the siliques of *nuf2-1*/+ were aborted, similar to *mun-2t* (**Table 2**). The embryos of *nuf2-1* were found to be arrested at a similar stage (before the globular stage) and showed abnormal cell division patterns similar to that of *mun-2t* (**Figure 26**B, red arrows).

4.10. *mun-2T* and *nuf2-1* did not show the phenotypes in gamete development

I determined whether mutation in *MUN* leads to any defects in gamete development. I performed Alexander staining to observe the pollen defects in the heterozygotes, *mun-1*/+ and *mun-2t*/+ (**Figure 27**). The *mun-2t*/+, as well

as *mun-1/+*, had normal pollen viability. In addition, no ovule abortion (aborted ovule before fertilization) was observed in both *mun-1/+* and *mun-2t/+* (**Table 2**). In addition, defective pollen and ovule abortion in *nuf2-1* were rarely detected (**Figure 27** and **Table 2**), indicating that *nuf2-1* also causes an embryonic zygotic lethal phenotype similar to that of *mun-2t*. Therefore, the gametophytic development in the null mutants *mun* and *nuf2* in heterozygous plants was normal, indicating that *MUN and NUF2* may not play a major role in gametophytic development. However, the *nuf2-1* mutant exhibited a weak ovule abortion phenotype (**Figure 26**A, yellow arrow and **Table 3**), indicating that *NUF2* may function partially in ovule development.

Figure 25

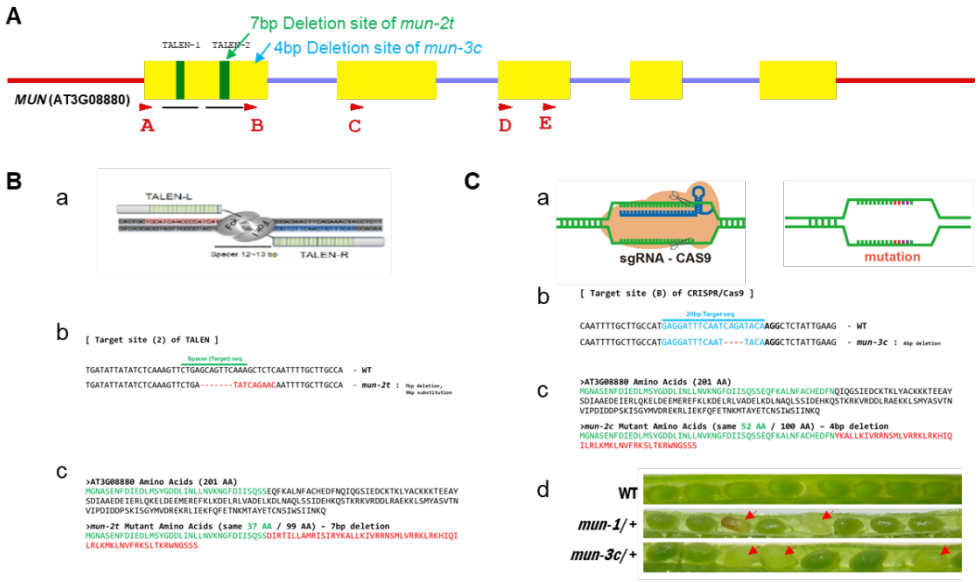
A
7bp Deletion site of mun-2t
4bp Deletion site of mun-3c
TALEN-1
TALEN-2
MUN (AT3G08880)
A
B
C
D
E
B
a
TALEN-L
Spacer 12~13 bp
TALEN-R
b
[Target site (2) of TALEN]
Spacer (Target) seq.
TGATATTATATCTCAAAGTTCTGAGCAGTTCAAAGCTCTCAATTTTGCTTGCCA - WT
TGATATTATATCTCAAAGTTCTGA-------TATCAGAACAATTTTGCTTGCCA - mun-2t : 7bp deletion, 9bp substitution
c
>AT3G08880 Amino Acids (201 AA)
MGNASENFDIEDLMSYGDDLINLLNVKNGFDIISQSSEQFKALNFACHEDFNQIQGSIEDCKTKLYACKKKTEEAY
SDIAAEDEIERLQKELDEEMEREFKLKDELRLVADELKDLNAQLSSIDEHKQSTKRKVRDDLRAEKKLSMYASVTN
VIPDIDDPSKISGYMVDREKRLIEKFQFETNKMTAYETCNSIWSIINKQ
>mun-2t Mutant Amino Acids (same 37 AA / 99 AA) - 7bp deletion
MGNASENFDIEDLMSYGDDLINLLNVKNGFDIISQSSDIRTILLAMRISIRYKALLKIVRRNSMLVRRKLRKHIQI
LRLKMKLNVFRKSLTKRWNGSSS
C
a
sgRNA - CAS9
mutation
b
[Target site (B) of CRISPR/Cas9]
20bp Target seq
CAATTTTGCTTGCCATGAGGATTTCAATCAGATACTAGGCTCTATTGAAG - WT
CAATTTTGCTTGCCATGAGGATTTCAAT----TACAAGGCTCTATTGAAG - mun-3c : 4bp deletion
c
>AT3G08880 Amino Acids (201 AA)
MGNASENFDIEDLMSYGDDLINLLNVKNGFDIISQSSEQFKALNFACHEDFNQIQGSIEDCKTKLYACKKKTEEAY
SDIAAEDEIERLQKELDEEMEREFKLKDELRLVADELKDLNAQLSSIDEHKQSTKRKVRDDLRAEKKLSMYASVTN
VIPDIDDPSKISGYMVDREKRLIEKFQFETNKMTAYETCNSIWSIINKQ
>mun-2c Mutant Amino Acids (same 52 AA / 100 AA) - 4bp deletion
MGNASENFDIEDLMSYGDDLINLLNVKNGFDIISQSSEQFKALNFACHEDFNYKALLKIVRRNSMLVRRKLRKHIQ
ILRLKMKLNVFRKSLTKRWNGSSS
d
WT
mun-1/+
mun-3c/+

Figure 25. Generation of null alleles of *MUN* by targeted gene knockout techniques.

(**A**) Map of the targeted site in the *MUN* gene for TALEN (green bar) and CRISPR/Cas9 (red arrows). Yellow box: exon, violet line: intron, and red line: UTR. Deleted sites in *mun-2t* and *mun-3c* are depicted by green and sky-blue bars, respectively.

(**B**) Generation of null allele of *MUN* by TALEN (*mun-2t* allele). (**a**) Scheme of mutation generated by TALEN. FokI nucleases break the spacer (target) DNAs between the recognition sites of TALEN-L and TALEN-R pairs of exon 1. (**b**) DNA sequence of the mutation site in *mun-2t* allele; 7 bp deletion and 9 bp substitution were generated around the spacer sequence. (**c**) Prediction of truncated protein translated from *mun-2t* allele by frameshift mutation is presented. Green and black: MUN sequences, and red: mutated sequences.

(**C**) Generation of null allele of *MUN* by CRISPR/Cas9 (*mun-3c* allele). (**a**) Scheme of mutation generated by CRISPR/Cas9. The target sequence is nicked by Cas9 nuclease with sgRNA. (**b**) DNA sequence of the deletion site in the *mun-3c* allele; 4 bp deletions occurred at target B sequence in exon 1. (**c**) Prediction of truncated protein translated from *mun-3c* allele by frameshift mutation is presented. Green and black: MUN sequences, and red: mutated sequences. (**d**) Photographs of siliques from *mun-1*/+ and *mun-3c*/+. Approximately 25% of the seeds were aborted. Red arrows indicate empty seeds caused by embryo arrest.

Figure 26

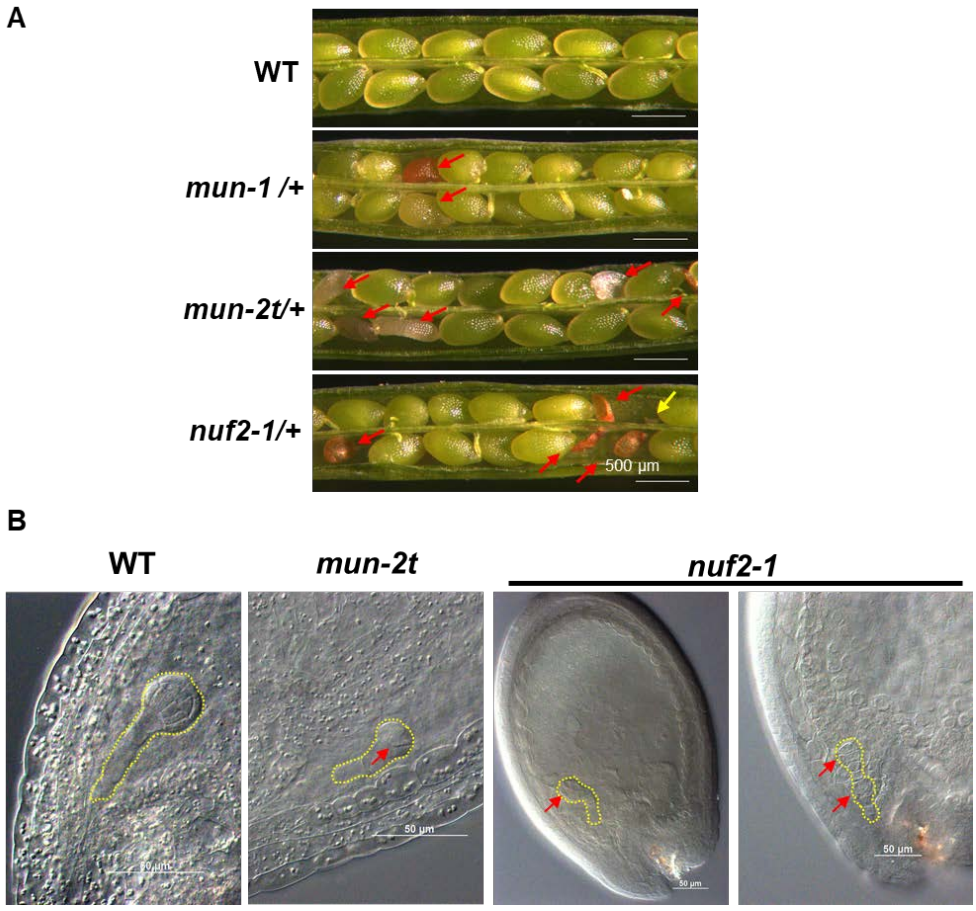
A
WT
mun-1 /+
mun-2t/+
nuf2-1/+
500 µm
B
WT
mun-2t
nuf2-1
50 µm
50 µm
50 µm
50 µm

Figure 26. Null allele, *mun-2t,* and *nuf2-1* show similar zygotic lethal phenotype.

(**A**) Seed abortion phenotypes observed in the siliques of WT, *mun-1*/+, *mun-2t*/+, and *nuf2-1*/+. Red arrows indicate seed abortion and yellow arrow indicate ovule abortion observed in *nuf2-1*/+. Approximately 25% of the seeds show defects in null alleles of *MUN* and *NUF2*. White bar = 500 μm.

(**B**) Phenotype of *mun-2t*/+ and *nuf2-1*/+ showing defects in embryo development. It seems to lead embryo arrest during seed development. Red arrows show embryo cells with abnormal cell division pattern before early globular stage. Yellow dotted lines highlight the embryos. White bar = 50 μm.

Figure 27

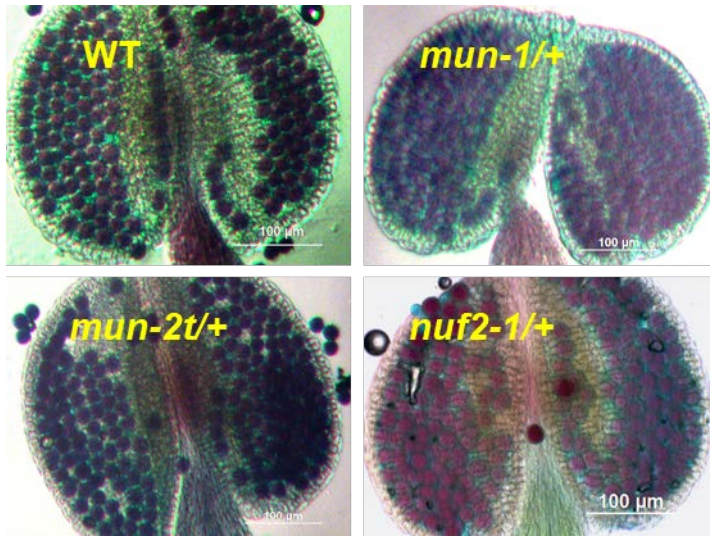

Figure 27. Normal pollen development in *mun-1* plants.

Comparison of pollen vitality by Alexander staining of WT, *mun-1*/+, *mun-2t*/+, and *nuf2-1*/+. All of the pollens are normal. White bar = 100 μm.

Table 3. Aborted seeds in siliques of *nuf2-1* (+/-).

Approximately 30% of aborted seeds in *nuf2-1* are very small, regarded as "early" abortion. Ab. = abortion.

Silique#	Total Seeds	Ovule Ab.	Sum of Seed Ab.	Normal Ab.	Early Ab.	Ratio of Early Ab.
1	51	6	12	9	3	25%
2	44	0	11	8	3	27%
3	36	3	6	5	1	17%
4	39	7	9	8	1	11%
5	39	1	9	5	4	44%
6	41	1	12	8	4	33%
7	37	1	11	8	3	27%
8	49	0	14	9	5	36%
Total	336	19	84	60	24	29%

4.11. MUN might have a role in cell cycle regulation with RBR

I found that the RETINOBLASTOMA-RELATED (RBR) protein interacts with MUN by using the interactome database, STRING (https://string-db.org) (Arabidopsis Interactome Mapping, 2011). I confirmed the interaction by using yeast two-hybrid assay of MUN and RBR of *Arabidopsis thaliana* (**Figure 28**). By using domain deletion constructs of MUN, I found that the N-terminal and middle region of MUN can interact with RBR. RBR protein is a plant homolog of the well-known human tumor suppressor pRB (Borghi *et al.*, 2010). It generally acts as a transcription repressor of the E2F target genes, negatively regulates the transition from G1 to S phase of the cell cycle (Hirano *et al.*, 2008). And RBR negatively regulates many genes of the polycomb repressive complex 2 (PRC2) (Gutzat *et al.*, 2012). Thus, I checked the expression of the genes of RBR targets and PRC2 targets (**Figure 29**). Many of target genes are derepressed in *mun-1* plants. In addition, I checked the expression of the cell cycle-related genes in *mun-1* (**Figure 30**). Interestingly, cyclin-dependent protein kinase *CYCB1;1* is upregulated in *mun-1*. *CYCB1;1* functions as an effector of growth control at G2/M phase transition (Li *et al.*, 2005), and is specifically activated after DNA damage (Weimer *et al.*, 2016). These relationships between MUN and cell cycle genes indicate that MUN might have a novel role in the regulation of cell cycle in plants.

Figure 28

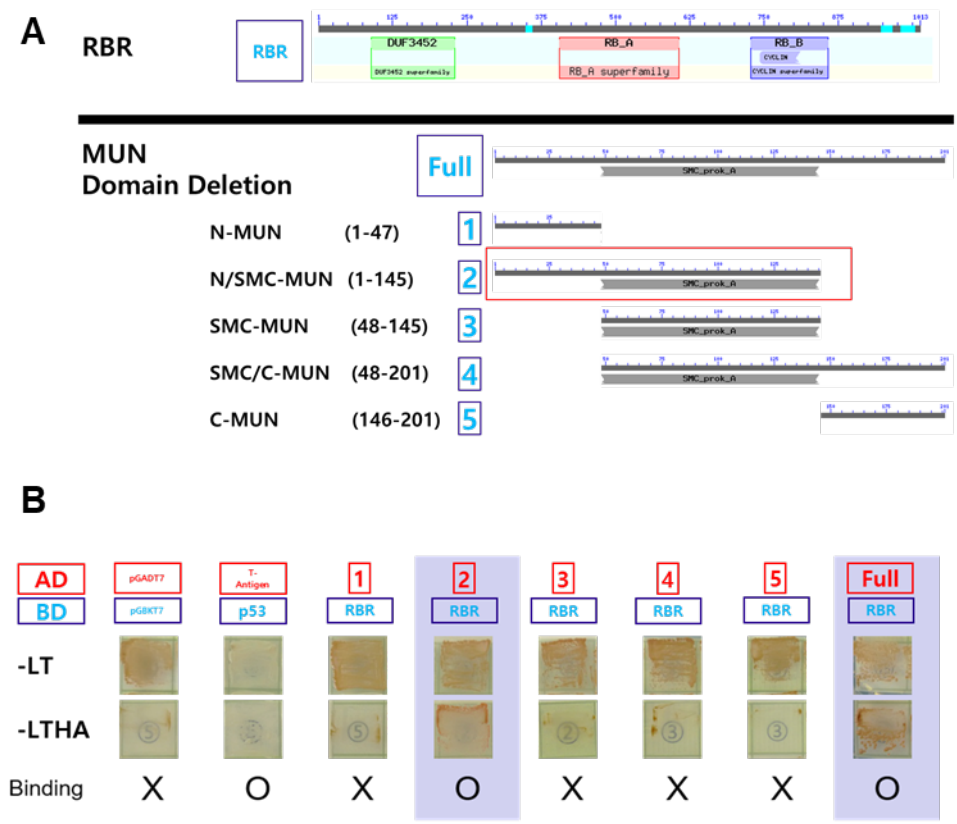

Figure 28. MUN interacts with RBR.

Yeast two-hybrid assay of MUN and RBR of *Arabidopsis thaliana*. -LW: selection plates containing SD medium lacking Leu and Trp. -LWHA: selection plates containing SD medium lacking Leu, Trp, His, and Ade.

(**A**) Domain deletion map of MUN for yeast two-hybrid assay.

(**B**) N-terminal and middle region of MUN can interact with RBR (red box in A, domain deletion No. 2).

Figure 29

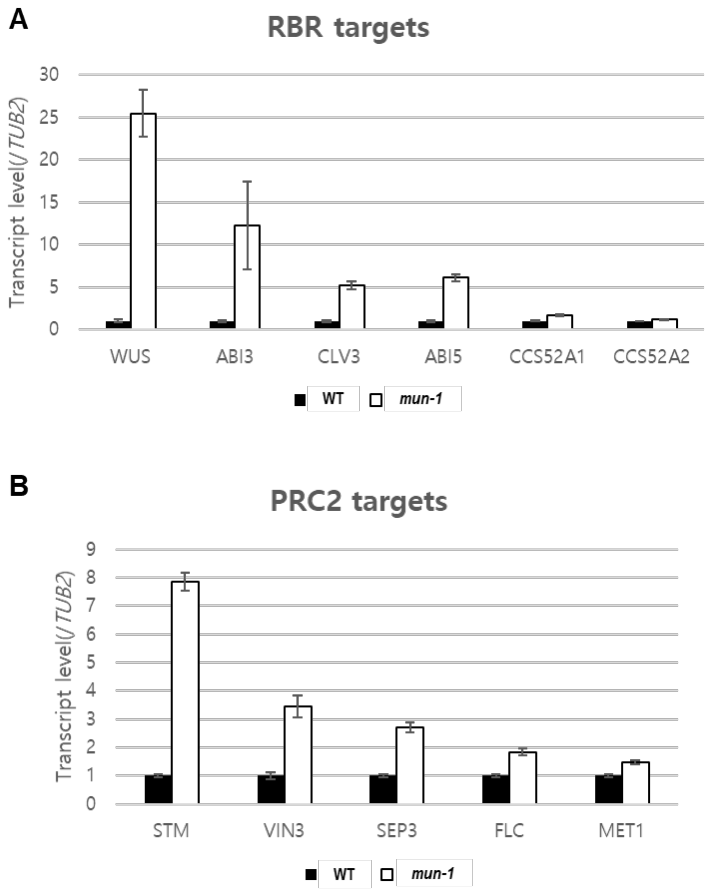

Figure 29. Expression of the genes of RBR targets.

Increased expression of several genes of (A) RBR targets and (B) PRC2 targets in *mun-1*. Each transcript level of target genes in WT plants is set at a relative value of 1. The whole seedling of 10 DAG was used for RNA extraction. Means ± SD from three replicates are presented.

Figure 30

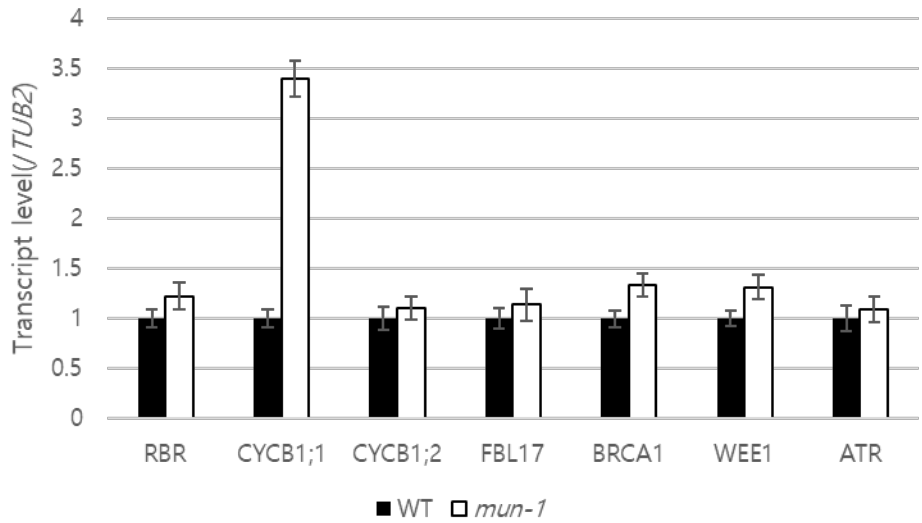

Figure 30. Expression of the cell cycle-related genes in *mun-1*.

Each transcript level of target genes in WT is set at a relative value of 1. The whole seedling, 10 DAG, was used for RNA extraction. Means ± SD from three replicates are presented.

Table 4. List of primers used in this study.

#	Primer	Sequence (5′–3′)	Remarks
1	MUN-qF	CGTTATACCGGACATTGATGATC	RT-qPCR
2	MUN-qR	CATGTCTCGTATGCCGTCAT	RT-qPCR
3	TUB2-qF	ATCGATTCCGTTCTCGATGT	RT-qPCR
4	TUB2-qR	ATCCAGTTCCTCCTCCCAAC	RT-qPCR
5	AT3G08870-qF	GTTTCATAGCACTTTTAGCATAGC	RT-qPCR
6	AT3G08870-qR	GGTAATGGGTTCACTGGTCC	RT-qPCR
7	TUB2-1	CTCAAGAGGTTCTCAGCAGTA	RT-PCR
8	TUB2-2	TCACCTTCTTCATCCGCAGTT	RT-PCR
9	WUS-LP	GTGAACAAAAGTCGAATCAAACACACATG	RT-PCR
10	WUS-RP	GCTAGTTCAGACGTAGCTCAAGAG	RT-PCR
11	WUS-qF	ACAAGCCATATCCCAGCTTCA	RT-qPCR
12	WUS-qR	CCACCGTTGATGTGATCTTCA	RT-qPCR
13	CLV3-qF	CAGATCTCACTCAAGCTCATGCT	RT-qPCR
14	CLV3-qR	CCAACCCATTCACTTTCCATTTTCA	RT-qPCR
15	STM-qF	GCCGCTTATGTCAATTGTCAGAA	RT-qPCR
16	STM-qR	GACGAGCATGCCTCCTCTAG	RT-qPCR
17	MP-qF	GATCCATGGGAAGAGTTTGTG	RT-qPCR
18	MP-qR	GTTCAAAAGCTTCATCCCTTC	RT-qPCR
19	WOX2-qF	GTTTCTCGTAGCCACCACTTG	RT-qPCR
20	WOX2-qR	GCTCAAACGTGGGTTGTGTC	RT-qPCR
21	ABI3-qF	atgtatctcctcgagaacac	RT-qPCR
22	ABI3-qR	ccctcgtatcaaatatttgcc	RT-qPCR
23	ABI5-qF	acctaatccaaacccgaacc	RT-qPCR
24	ABI5-qR	taccctcctcctcctgtcct	RT-qPCR
25	CCS52A1-qF	GACCAACTCAAGCTGGCTG	RT-qPCR
26	CCS52A1-qR	GGAACCAACATTCAACACAACCGG	RT-qPCR
27	CCS52A2-qF	CCTGATTTCGAGAATCATGTCAAGAC	RT-qPCR
28	CCS52A2-qR	CTGTGAACACGCCGCAGCAGTG	RT-qPCR
29	VIN3-qF	GTTTCAGGACAAGGTGACAAG	RT-qPCR
30	VIN3-qR	TTCCCCTGAGACGAGCATTC	RT-qPCR
31	SEP3-qF	TATGACGCCTTACAGAGAACC	RT-qPCR
32	SEP3-qR	ATACCCATCAGCTAACCTTAGTC	RT-qPCR
33	FLC-qF	GAGAATAATCATCATGTGGGAGC	RT-qPCR
34	FLC-qR	CAACCGCCGATTTAAGGTGG	RT-qPCR
35	RBR-qF	CTTGCTCAGCGGACTTCTCT	RT-qPCR
36	RBR-qR	CGACATTGTAACGCATCCAC	RT-qPCR
37	CYCB1;1-qF	TTACCCAAAGAACAACGAACC	RT-qPCR
38	CYCB1;1-qR	CAATCAACCACTCCACCAGG	RT-qPCR
39	CYCB1;2-qF	CACACCGGCTACACAGAGTC	RT-qPCR
40	CYCB1;2-qR	GAAACCATAGCAACACCTCCA	RT-qPCR
41	FBL17-qF	CTCGGGATGATCTGCGATGTC	RT-qPCR
42	FBL17-qR	GACTTGGATTCTCTACAAAGGTCG	RT-qPCR
43	BRCA1-qF	CATGTGCCTTTTGTCAGTGTTCA	RT-qPCR
44	BRCA1-qR	AAATCCGCAGAGACAGGTTCA	RT-qPCR
45	WEE1-qF	CGTAAAGCTATGATGGAAGTGCAA	RT-qPCR
46	WEE1-qR	GCTCATTTTCAAACCACGAGGA	RT-qPCR
47	ATR-qF	TGCCATTCAGATTGACCCAGA	RT-qPCR
48	ATR-qR	CCCTCATGAAGATGCCCTCA	RT-qPCR
49	KNAT2-qF	GATTCAGCGAGAGAACCATGTG	RT-qPCR
50	KNAT2-qR	CCTCGCAAGATCGGTTTTGTA	RT-qPCR
51	FUS3-qF	CGATCCTTGTTAAGTTTGTGTAAAC	RT-qPCR
52	FUS3-qR	CTACTCAAACAATTACGTTATACAAGC	RT-qPCR

V. Discussion

5.1. MUN is an ortholog of SPC24, a component of the NDC80 kinetochore complex

In this study, I characterized a mutant showing abnormal shoot apex morphology and cell division defects. While analyzing the cause of occasional shoot organogenesis in the mutant, *mun-1*, I found that *MUN* encodes an ortholog of SPC24, a component of the NDC80 complex in the kinetochore super-complex. Evidence, including genetic, cellular, and biochemical data, suggest that MUN is an ortholog of SPC24. In addition, phenotypic analysis of a weak mutation in a component of the kinetochore super-complex revealed a link between disrupted cell division and ectopic *de novo* shoot organogenesis in plants.

Although MUN is not annotated as SPC24 in the TAIR10 database, my data support the view that MUN is AtSPC24. First, *MUN* shared sequence similarity, and had coiled-coil domains and a globular RWD domain. Although overall sequence similarity was limited, the sequence from the C-terminal region in MUN is relatively well conserved with that of SPC24 across many other species during protein multiple sequence alignment (**Figure 14**). The predicted 3D protein structure also indicated that the critical residues for globular head domain in MUN are highly conserved (**Figure 16**).

Second, knockdown of *MUN* exhibited defects in chromosome segregation and cell division, a typical phenotype in various organisms with malfunction of the NDC80 complex (**Figure 12**). Third, the null allele of *MUN* exhibited a zygotic embryonic lethal phenotype similar to that of the null mutant of *NUF2*, another component of the NDC80 complex (**Figure 26**). Although there is no null allele of *NDC80* and *SPC25*, I expect them to yield the same embryo lethal phenotype. The mild growth retardation phenotypes of RNAi plant of NDC80 and SPC25 support this hypothesis (Rushing, 2008). Fourth, the spatial and cellular localization of MUN overlapped with that of NUF2, NDC80, and SPC25, which are the other known components of the NDC80 complex (**Figure 18**, **Figure 21**). Each NDC80 component showed similar localization patterns with a regular number of dots in nucleus. Additionally, CENH3, a centromere-specific histone variant, which is co-localized with NUF2 and SPC25 in *Arabidopsis thaliana* (Du and Dawe, 2007; Rushing, 2008; Ramahi, 2012), was also co-localized with MUN at the centromere (**Figure 19**). Finally, all of the components of the NDC80 complex interacted with each other in the yeast two-hybrid system and were found to co-immunoprecipitate with MUN *in planta* (**Figure 22**, **Figure 23**). Thus, I identified the NDC80 complex in *Arabidopsis thaliana*, which has not yet been disclosed.

Among the components of the NDC80 complex, *SPC24* is the only component which has not yet been annotated in the TAIR10 database. This

implies that SPC24 seems to be the rapidly evolving gene. Indeed, *MUN/AtSPC24* can not complement the yeast *SPC24* (**Figure 15**). Such rapid evolution has also been reported in other components of the kinetochore, such as DNA sequences of centromeres and CENH3 (Henikoff *et al.*, 2001; Talbert *et al.*, 2002). The rapid evolution may contribute to the establishment of post-zygotic reproductive barriers, which causes hybrid sterility after speciation (Maheshwari *et al.*, 2015). The rapid changes in the components of the kinetochore would lead to failure of chromosome movement in the hybrid offspring, thus causing hybrid sterility. Thus, MUN in *Arabidopsis thaliana*, may facilitate speciation from an evolutionary viewpoint.

5.2. Divergence of the plant NDC80 complex

Although NDC80, NUF2, SPC25, and MUN/SPC24 form a canonical tetramer complex in diverse species, each component does not seem to maintain the stoichiometric ratio in *Arabidopsis thaliana*. Thus, there is a possibility that each component has subtly different roles. The *in silico* expression analysis using 113 different plant tissues showed that the expression level of *NDC80* is in general lower than that of the other components (**Figure 24**). There is a possibility that NUF2 could form a homodimer to make a tetramer of the NDC80 complex in various tissues without expressing NDC80 in *Arabidopsis thaliana*, or this may indicate that each component of the NDC80 complex has other functions in addition to

kinetochore formation. For example, the *nuf2-1* mutant exhibited a weak ovule abortion phenotype, although the null allele of *mun-2t* did not show any ovule abortion (**Figure 26**, **Table 2**). In addition, about 30% of aborted seeds in *nuf2-1* were very small (**Table 3**), indicating NUF2 has other developmental functions such as the development of endosperm. Thus, it is possible that other functions have evolved for the many components of the NDC80 complex.

I also found that the cellular localization pattern of the NDC80 complex in *Arabidopsis thaliana* diverged from that of other species. For example, NDC80 in yeast and animals appears transiently at prophase and anaphase during the M phase as centromeric dots, whereas NDC80 in corn is stably localized at the centromere throughout the cell cycle (Chen *et al.*, 1997; Wigge and Kilmartin, 2001; Hori *et al.*, 2003; McCleland, 2003; Asakawa *et al.*, 2005; Du and Dawe, 2007). Similar to ZmNDC80 in corn, MUN and other components of the NDC80 complex in *Arabidopsis thaliana* were constitutively localized at the centromeres throughout the cell cycle (**Figure 18**, **Figure 21**). This may indicate that subtle differences in the mechanism of spindle fiber attachment to the kinetochore have evolved in plants. Studying such differences between plants and other organisms might be a challenge, especially in terms of understanding the unique features of plant cell division.

5.3. Null mutations of the NDC80 complex are fully transmissible via pollen and ovules: ‘Concentration’ or ‘Meitosis’ theory

The homozygous null mutant of *mun* from the silique of the heterozygous plant shows the zygotic embryonic lethal phenotype, but it does not exhibit any defects in gamete, pollen, and ovule development (**Table 2**, **Figure 27**). Consistently, the *nuf2-1* mutant does not show any defect in pollen development and exhibits a very weak defect in ovule development (**Figure 27**, **Table 3**). The first possible explanation for such a lack of defects in gamete development in the mutants is that there may be an adequate amount (concentration) of proteins required for multiple rounds of cell division in the megaspore or pollen mother cells produced by the heterozygote parent. For gametophyte development, only 2–3 rounds of cell division are required; thus, either the pre-made mRNA or protein in the megaspore or pollen mother cells is in excess of the threshold level, or the proteins are very stable and recycled during the multiple cell cycles for gametophyte development. Additionally, the fact that null mutations of *CENH3* are also fully transmissible via pollen and ovules from heterozygous plant supports this explanation (Ravi *et al.*, 2010).

Secondly, the main regulator components of mitosis in gametophyte (twice in pollen, 3 times in ovule) might be different from the players of mitosis in sporophytes. That is to say, MUN/AtSPC24 mainly functions in sporophytic tissues and other unknown components might be playing the

roles typical of MUN/SPC24 in gametophytic tissues. In this case, I could discriminate between ‘mitosis in gamete’ and ‘mitosis in zygote’, which were previously regarded as the same concept,. I temporarily named ‘mitosis in gamete’ as ‘meitosis’, which means the process of mitosis only in gamete. If this assumption is right, identification of the regulators of meitosis could be a big future challenge in plant gamete development.

5.4. Spontaneous *de novo* shoot organogenesis in *mun-1*

The weak allele, *mun-1,* produced shoots at random sites, which is indicative of *de novo* shoot organogenesis and formation of ectopic stem cell niche at various tissues without any hormone treatment. In general, *de novo* organ generation could be induced by hormonal manipulations in tissue culture (Skoog and Miller, 1957). Recent reports also showed that *de novo* shoot organogenesis is mediated by the coordination of auxin and cytokinin through the regulation of *WUS* (Su *et al.*, 2014; Zhang *et al.*, 2017). Indeed, *mun-1* exhibits unusual flow and abnormal amount of phytohormones (**Figure 7**). Thus, the *de novo* shoot organogenesis in the *mun-1* may be caused by the perturbation of biosynthesis or the flow of plant hormones in the mutant. In other respects, incomplete or delayed cell plate formation in the *mun-1* mutant by mis-segregation of chromosomes during the process of cell division may affect mis-localization of PIN1, which perturbs proper auxin flow. In humans, cancer cells that display aneuploid karyotypes and mis-segregate

chromosomes show a distinctive cytokinesis failure phenotype (Nicholson *et al.*, 2015). Because the growth of the cell plate is dependent upon the phragmoplast formation in plants (Higaki *et al.*, 2008) and chromosome defects generally affect phragmoplast development, I expected the defects seen in the cell walls in *mun-1*. During somatic embryogenesis, the localization of PIN1 has an important role in the initiation of stem cell niche by establishing auxin gradients (Su and Zhang, 2009; Su *et al.*, 2009). Therefore, improper localization of PIN1 by the malfunction of the phragmoplast and cell plate formation may cause the *de novo* shoot organogenesis at the inappropriate place. Currently, *de novo* activation of *WUSCHEL* by B-type ARABIDOPSIS RESPONSE REGULATORs and HD-ZIP III transcription factors are well explained (Zhang *et al.*, 2017). Therefore, further studies of cytokinin or auxin regulations are required to understand this ectopic stem cell generation in *mun-1*.

Aneuploidy in the *mun-1* mutant may also cause the *de novo* shoot organogenesis indirectly. Recent reports in mammalian studies showed that aneuploidy in the embryonic stem cells causes impaired differentiation and increased neoplastic potential (Zhang *et al.*, 2016). Similarly, aneuploid cells in the *mun-1* may have an increased totipotency via an unknown mechanism (**Figure 11**). Consistently, some aneuploid lines in *Arabidopsis thaliana* show severe morphological defects, such as curly leaves, fasciation, triple branches, and reversion to meristematic tissues (Henry *et al.*, 2005; Henry *et al.*, 2010).

Nevertheless, how aneuploidy causes such morphological defects remains to be resolved.

Lastly, this unique phenotype of weak allele, *mun-1*, indicates that there could be some relationship between cell cycle check point regulation and upregulation of the expression of DNSO marker genes. Signaling from MUN or NDC80 complex for cell cycle regulation could be working for control the generations of stem cells. NDC80 complex is not only the structural component for grabbing the microtubules and kinetochore but is also the active signaling component that regulates the spindle assembly checkpoint (SAC) by phosphorylation (Umbreit *et al.*, 2012). The Ndc80 complex is essential for the recruitment of the SAC proteins, Mad1, Mad2, and Mps1, to unattached kinetochores (Ciferri *et al.*, 2007). The N-terminal domain in the Ndc80 complex was phosphorylated by the Aurora B kinase and underwent changes in conformation to regulate the tension of microtubule-kinetochore attachment (Jia *et al.*, 2013; Kudalkar *et al.*, 2015). Hence, the NDC80 complex is tightly linked to cell cycle regulation. For example, NDC80 referred to as HEC1(Highly expressed protein in cancer 1) in human cancer cells is regarded as oncogenes for progressing the tumors (Huang *et al.*, 2014). It is really interesting that the main chromosome structural protein *MUN* has the potential to control totipotency in plant cells.

5.5. MUN might have dual functions as a cell cycle regulator.

I confirmed the physical interaction between MUN and the cell cycle regulatory protein RBR by using the yeast two-hybrid assay. RETINOBLASTOMA-RELATED (RBR) protein is a well-known cell cycle regulator and an essential protein for survival of plants (Gutzat *et al.*, 2012). Many of genes of RBR targets and PRC2 targets are derepressed in *mun-1*(**Figure 29**). Also, the cell cycle-related gene, cyclin-dependent protein kinase *CYCB1;1* is upregulated in *mun-1*(**Figure 30**). In addition, MUN with a DNA binding domain had strong auto-activation activity in the yeast two hybrid-assay (**Figure 22**); this could be indirect evidence of the transcription enhancing activity of MUN. I therefore propose that MUN could have dual functions in cell cycle regulation, beyond the structural functioning in kinetochore assembly.

In this study, I described the phenotypic effects of the mutation in SPC24 at the organism level. I characterized *mun* mutants with severe morphological defect caused by abnormal cell division and ectopic stem cell generation, and based on the results I propose the existence of a functional NDC80 complex in the cell division process of *Arabidopsis thaliana*. I confirmed that MUN is a functional homolog of SPC24 on the basis of the following aspects: sequence similarity, presence of coiled-coil and globular domains, centromere localization, defects of chromosome segregation, cell division phenotype, and physical interaction with other conserved NDC80 complexes in *Arabidopsis thaliana*. MUN is an essential gene, and is

necessary for the normal development from embryogenesis. Additionally, *MUN* could play a direct/indirect role in somatic embryogenesis and cell cycle regulation.

This study lays the foundation for kinetochore and cell division research in plants. Further analyses will be required to distinguish the different properties of the NDC80 complex between plants and animals, and to understand the mechanism underlying ectopic shoot organogenesis caused by malfunction of kinetochore components.

VI. References

Arabidopsis Interactome Mapping, C. (2011) Evidence for network evolution in an Arabidopsis interactome map. *Science (New York, N.Y.)*, **333**, 601-607.

Asakawa, H., Hayashi, A., Haraguchi, T. and Hiraoka, Y. (2005) Dissociation of the Nuf2-Ndc80 Complex Releases Centromeres from the Spindle-Pole Body during Meiotic Prophase in Fission Yeast. *Molecular biology of the cell*, **16**, 2325-2338.

Bae, S., Park, J. and Kim, J.-S. (2014) Cas-OFFinder: a fast and versatile algorithm that searches for potential off-target sites of Cas9 RNA-guided endonucleases. *Bioinformatics*, **30**, 1473-1475.

Blazquez, M.A., Soowal, L.N., Lee, I. and Weigel, D. (1997) LEAFY expression and flower initiation in Arabidopsis. *Development (Cambridge, England)*, **124**, 3835-3844.

Borghi, L., Gutzat, R., Fütterer, J., Laizet, Y.h., Hennig, L. and Gruissem, W. (2010) Arabidopsis RETINOBLASTOMA-RELATED Is Required for Stem Cell Maintenance, Cell Differentiation, and Lateral Organ Production. *The Plant cell*, **22**, 1792-1811.

Burroughs, A.M., Jaffee, M., Iyer, L.M. and Aravind, L. (2008) Anatomy of the E2 ligase fold: implications for enzymology and evolution of ubiquitin/Ub-like protein conjugation. *Journal of structural biology*, **162**, 205-218.

Chan, G.K., Liu, S.-T. and Yen, T.J. (2005) Kinetochore structure and function. *Trends in cell biology*, **15**, 589-598.

Cheeseman, I.M., Chappie, J.S., Wilson-Kubalek, E.M. and Desai, A. (2006) The conserved KMN network constitutes the core microtubule-binding site of the kinetochore. *Cell*, **127**, 983-997.

Chen, Y., Riley, D.J., Chen, P.L. and Lee, W.H. (1997) HEC, a novel nuclear protein rich in leucine heptad repeats specifically involved in mitosis. *Molecular and cellular biology*, **17**, 6049-6056.

Cho, H.-T. and Cosgrove, D.J. (2002) Regulation of Root Hair Initiation and Expansin Gene Expression in Arabidopsis. *The Plant cell*, **14**, 3237-3253.

Choi, K., Kim, S., Kim, S.Y., Kim, M., Hyun, Y., Lee, H., Choe, S., Kim, S.G.,

Michaels, S. and Lee, I. (2005) SUPPRESSOR OF FRIGIDA3 encodes a nuclear ACTIN-RELATED PROTEIN6 required for floral repression in Arabidopsis. *The Plant cell*, **17**, 2647-2660.

Choi, K., Park, C., Lee, J., Oh, M., Noh, B. and Lee, I. (2007) Arabidopsis homologs of components of the SWR1 complex regulate flowering and plant development. *Development (Cambridge, England)*, **134**, 1931-1941.

Ciferri, C., De Luca, J., Monzani, S., Ferrari, K.J., Ristic, D., Wyman, C., Stark, H., Kilmartin, J., Salmon, E.D. and Musacchio, A. (2005) Architecture of the human ndc80-hec1 complex, a critical constituent of the outer kinetochore. *The Journal of biological chemistry*, **280**, 29088-29095.

Ciferri, C., Musacchio, A. and Petrovic, A. (2007) The Ndc80 complex: Hub of kinetochore activity. *FEBS Letters*, **581**, 2862-2869.

Ciferri, C., Pasqualato, S., Screpanti, E., Varetti, G., Santaguida, S., Dos Reis, G., Maiolica, A., Polka, J., De Luca, J.G., De Wulf, P., Salek, M., Rappsilber, J., Moores, C.A., Salmon, E.D. and Musacchio, A. (2008) Implications for kinetochore-microtubule attachment from the structure of an engineered Ndc80 complex. *Cell*, **133**, 427-439.

Clough, S.J. and Bent, A.F. (1998) Floral dip: a simplified method for Agrobacterium-mediated transformation of Arabidopsis thaliana. *The Plant journal : for cell and molecular biology*, **16**.

De Rop, V., Padeganeh, A. and Maddox, P.S. (2012) CENP-A: the key player behind centromere identity, propagation, and kinetochore assembly. *Chromosoma*, **121**, 527-538.

De Storme, N., Keceli, B.N., Zamariola, L., Angenon, G. and Geelen, D. (2016) CENH3-GFP: a visual marker for gametophytic and somatic ploidy determination in Arabidopsis thaliana. *BMC plant biology*, **16**, 1.

DeLuca, J.G., Moree, B., Hickey, J.M., Kilmartin, J.V. and Salmon, E.D. (2002) hNuf2 inhibition blocks stable kinetochore–microtubule attachment and induces mitotic cell death in HeLa cells. *The Journal of cell biology*, **159**, 549-555.

Du, Y. and Dawe, R.K. (2007) Maize NDC80 is a constitutive feature of the central kinetochore. *Chromosome research : an international journal on the molecular, supramolecular and evolutionary aspects of chromosome biology*, **15**, 767-775.

Duclercq, J., Sangwan-Norreel, B., Catterou, M. and Sangwan, R.S. (2011) *De novo* shoot organogenesis: from art to science. *Trends in plant science*, **16**, 597-606.

Earnshaw, W.C. and Rothfield, N. (1985) Identification of a family of human centromere proteins using autoimmune sera from patients with scleroderma. *Chromosoma*, **91**, 313-321.

Galbraith, D.W. (2009) Simultaneous flow cytometric quantification of plant nuclear DNA contents over the full range of described angiosperm 2C values. *Cytometry. Part A : the journal of the International Society for Analytical Cytology*, **75**, 692-698.

Gallois, J.L., Nora, F.R., Mizukami, Y. and Sablowski, R. (2004) WUSCHEL induces shoot stem cell activity and developmental plasticity in the root meristem. *Genes & development*, **18**, 375-380.

Gassmann, R., Essex, A., Hu, J.S., Maddox, P.S., Motegi, F., Sugimoto, A., O'Rourke, S.M., Bowerman, B., McLeod, I., Yates, J.R., 3rd, Oegema, K., Cheeseman, I.M. and Desai, A. (2008) A new mechanism controlling kinetochore-microtubule interactions revealed by comparison of two dynein-targeting components: SPDL-1 and the Rod/Zwilch/Zw10 complex. *Genes & development*, **22**, 2385-2399.

Gutzat, R., Borghi, L. and Gruissem, W. (2012) Emerging roles of RETINOBLASTOMA-RELATED proteins in evolution and plant development. *Trends in plant science*, **17**, 139-148.

Hajdukiewicz, P., Svab, Z. and Maliga, P. (1994) The small, versatile pPZP family of Agrobacterium binary vectors for plant transformation. *Plant molecular biology*, **25**, 989-994.

Henikoff, S., Ahmad, K. and Malik, H.S. (2001) The centromere paradox: stable inheritance with rapidly evolving DNA. *Science (New York, N.Y.)*, **293**, 1098-1102.

Henry, I.M., Dilkes, B.P., Miller, E.S., Burkart-Waco, D. and Comai, L. (2010) Phenotypic consequences of aneuploidy in Arabidopsis thaliana. *Genetics*, **186**, 1231-1245.

Henry, I.M., Dilkes, B.P., Young, K., Watson, B., Wu, H. and Comai, L. (2005) Aneuploidy and genetic variation in the Arabidopsis thaliana triploid response. *Genetics*, **170**, 1979-1988.

Higaki, T., Kutsuna, N., Sano, T. and Hasezawa, S. (2008) Quantitative analysis of changes in actin microfilament contribution to cell plate development in plant cytokinesis. *BMC plant biology*, **8**, 80-80.

Hirano, H., Harashima, H., Shinmyo, A. and Sekine, M. (2008) Arabidopsis RETINOBLASTOMA-RELATED PROTEIN 1 is involved in G1 phase cell cycle arrest caused by sucrose starvation. *Plant molecular biology*, **66**, 259-275.

Hori, T., Haraguchi, T., Hiraoka, Y., Kimura, H. and Fukagawa, T. (2003) Dynamic behavior of Nuf2-Hec1 complex that localizes to the centrosome and centromere and is essential for mitotic progression in vertebrate cells. *Journal of Cell Science*, **116**, 3347-3362.

Huang, L.Y., Chang, C.-c., Lee, Y.-S., Huang, J.-J., Chuang, S.-H., Chang, J.-M., Kao, K.-J., Lau, G.M., Tsai, P.-Y., Liu, C.-w., Lin, H.-S., Gish, R.G. and Lau, J.Y. (2014) Inhibition of Hec1 as a novel approach for treatment of primary liver cancer. *Cancer Chemotherapy and Pharmacology*, **74**, 511-520.

Hyun, Y., Choi, S., Hwang, H.J., Yu, J., Nam, S.J., Ko, J., Park, J.Y., Seo, Y.S., Kim, E.Y., Ryu, S.B., Kim, W.T., Lee, Y.H., Kang, H. and Lee, I. (2008) Cooperation and functional diversification of two closely related galactolipase genes for jasmonate biosynthesis. *Developmental cell*, **14**, 183-192.

Hyun, Y., Kim, J., Cho, S.W., Choi, Y., Kim, J.-S. and Coupland, G. (2015) Site-directed mutagenesis in Arabidopsis thaliana using dividing tissue-targeted RGEN of the CRISPR/Cas system to generate heritable null alleles. *Planta*, **241**, 271-284.

Ingouff, M., Hamamura, Y., Gourgues, M., Higashiyama, T. and Berger, F. (2007) Distinct dynamics of HISTONE3 variants between the two fertilization products in plants. *Current biology : CB*, **17**, 1032-1037.

Jack, T., Fox, G.L. and Meyerowitz, E.M. (1994) Arabidopsis homeotic gene APETALA3 ectopic expression: Transcriptional and posttranscriptional regulation determine floral organ identity. *Cell*, **76**, 703-716.

Jager, S.M.d., Maughan, S., Dewitte, W., Scofield, S. and Murray, J.A.H. (2005) The developmental context of cell-cycle control in plants. *Seminars in Cell & Developmental Biology*, **16**, 385-396.

Janke, C., Ortiz, J., Lechner, J., Shevchenko, A., Shevchenko, A., Magiera, M.M., Schramm, C. and Schiebel, E. (2001) The budding yeast proteins Spc24p

and Spc25p interact with Ndc80p and Nuf2p at the kinetochore and are important for kinetochore clustering and checkpoint control. *The EMBO journal*, **20**, 777-791.

Jia, L., Kim, S. and Yu, H. (2013) Tracking spindle checkpoint signals from kinetochores to APC/C. *Trends in biochemical sciences*, **38**, 302-311.

Jones, D.T., Taylor, W.R. and Thornton, J.M. (1992) The rapid generation of mutation data matrices from protein sequences. *Computer applications in the biosciences : CABIOS*, **8**, 275-282.

Källberg, M., Wang, H., Wang, S., Peng, J., Wang, Z., Lu, H. and Xu, J. (2012) Template-based protein structure modeling using the RaptorX web server. *Nat. Protocols*, **7**, 1511-1522.

Kline-Smith, S.L., Sandall, S. and Desai, A. (2005) Kinetochore-spindle microtubule interactions during mitosis. *Curr Opin Cell Biol*, **17**, 35-46.

Kudalkar, E.M., Scarborough, E.A., Umbreit, N.T., Zelter, A., Gestaut, D.R., Riffle, M., Johnson, R.S., MacCoss, M.J., Asbury, C.L. and Davis, T.N. (2015) Regulation of outer kinetochore Ndc80 complex-based microtubule attachments by the central kinetochore Mis12/MIND complex. *Proceedings of the National Academy of Sciences of the United States of America*, **112**, E5583-E5589.

Kumar, S., Stecher, G. and Tamura, K. (2016) MEGA7: Molecular Evolutionary Genetics Analysis Version 7.0 for Bigger Datasets. *Mol Biol Evol*, **33**, 1870-1874.

Lee, H.G. and Seo, P.J. (2016) The Arabidopsis MIEL1 E3 ligase negatively regulates ABA signalling by promoting protein turnover of MYB96. *Nature communications*, **7**, 12525.

Lee, O.R., Kim, S.J., Kim, H.J., Hong, J.K., Ryu, S.B., Lee, S.H., Ganguly, A. and Cho, H.-T. (2010) Phospholipase A(2) Is Required for PIN-FORMED Protein Trafficking to the Plasma Membrane in the Arabidopsis Root. *The Plant cell*, **22**, 1812-1825.

Lermontova, I., Koroleva, O., Rutten, T., Fuchs, J., Schubert, V., Moraes, I., Koszegi, D. and Schubert, I. (2011) Knockdown of CENH3 in Arabidopsis reduces mitotic divisions and causes sterility by disturbed meiotic chromosome segregation. *The Plant journal : for cell and molecular biology*, **68**, 40-50.

Lermontova, I., Kuhlmann, M., Friedel, S., Rutten, T., Heckmann, S., Sandmann, M., Demidov, D., Schubert, V. and Schubert, I. (2013) Arabidopsis kinetochore null2 is an upstream component for centromeric histone H3 variant cenH3 deposition at centromeres. *The Plant cell*, **25**, 3389-3404.

Lermontova, I., Sandmann, M. and Demidov, D. (2014) Centromeres and kinetochores of Brassicaceae. *Chromosome research : an international journal on the molecular, supramolecular and evolutionary aspects of chromosome biology*, **22**, 135-152.

Lermontova, I., Sandmann, M., Mascher, M., Schmit, A.C. and Chaboute, M.E. (2015) Centromeric chromatin and its dynamics in plants. *The Plant journal : for cell and molecular biology*, **83**, 4-17.

Lermontova, I., Schubert, V., Fuchs, J., Klatte, S., Macas, J. and Schubert, I. (2006) Loading of Arabidopsis centromeric histone CENH3 occurs mainly during G2 and requires the presence of the histone fold domain. *The Plant cell*, **18**, 2443-2451.

Li, C., Potuschak, T., Colon-Carmona, A., Gutierrez, R.A. and Doerner, P. (2005) Arabidopsis TCP20 links regulation of growth and cell division control pathways. *Proceedings of the National Academy of Sciences of the United States of America*, **102**, 12978-12983.

Li, X. and Dawe, R.K. (2009) Fused sister kinetochores initiate the reductional division in meiosis I. *Nature cell biology*, **11**, 1103-1108.

Liu, Y.G. and Chen, Y. (2007) High-efficiency thermal asymmetric interlaced PCR for amplification of unknown flanking sequences. *BioTechniques*, **43**, 649-650, 652, 654 passim.

Liu, Y.G., Mitsukawa, N., Oosumi, T. and Whittier, R.F. (1995) Efficient isolation and mapping of Arabidopsis thaliana T-DNA insert junctions by thermal asymmetric interlaced PCR. *The Plant journal : for cell and molecular biology*, **8**, 457-463.

Maheshwari, S., Tan, E.H., West, A., Franklin, F.C., Comai, L. and Chan, S.W. (2015) Naturally occurring differences in CENH3 affect chromosome segregation in zygotic mitosis of hybrids. *PLoS genetics*, **11**, e1004970.

McCleland, M.L. (2003) The highly conserved Ndc80 complex is required for kinetochore assembly, chromosome congression, and spindle checkpoint activity. *Genes Dev.*, **17**, 101-114.

Meraldi, P., McAinsh, A.D., Rheinbay, E. and Sorger, P.K. (2006) Phylogenetic and structural analysis of centromeric DNA and kinetochore proteins. *Genome Biology*, **7**, R23-R23.

Nicholson, J.M., Macedo, J.C., Mattingly, A.J., Wangsa, D., Camps, J., Lima, V., Gomes, A.M., Dória, S., Ried, T., Logarinho, E. and Cimini, D. (2015) Chromosome mis-segregation and cytokinesis failure in trisomic human cells. *eLife*, **4**, e05068.

Nieuwland, J., Scofield, S. and Murray, J.A.H. (2009) Control of division and differentiation of plant stem cells and their derivatives. *Seminars in Cell & Developmental Biology*, **20**, 1134-1142.

Nishino, T., Rago, F., Hori, T., Tomii, K., Cheeseman, I.M. and Fukagawa, T. (2013) CENP-T provides a structural platform for outer kinetochore assembly. *The EMBO journal*, **32**, 424-436.

Ogura, Y., Shibata, F., Sato, H. and Murata, M. (2004) Characterization of a CENP-C homolog in Arabidopsis thaliana. *Genes & Genetic Systems*, **79**, 139-144.

Oh, S.A., Allen, T. and Twell, D. (2010) A ticket for the live show: Microtubules in male gametophyte development. *Plant signaling & behavior*, **5**, 614-617.

Palmer, D.K., O'Day, K., Wener, M.H., Andrews, B.S. and Margolis, R.L. (1987) A 17-kD centromere protein (CENP-A) copurifies with nucleosome core particles and with histones. *The Journal of cell biology*, **104**, 805-815.

Park, E., Diaz-Moreno, S.M., Davis, D.J., Wilkop, T.E., Bulone, V. and Drakakaki, G. (2014a) Endosidin 7 Specifically Arrests Late Cytokinesis and Inhibits Callose Biosynthesis, Revealing Distinct Trafficking Events during Cell Plate Maturation. *Plant physiology*, **165**, 1019-1034.

Park, G.T., Frost, J.M., Park, J.-S., Kim, T.H., Lee, J.S., Oh, S.A., Twell, D., Brooks, J.S., Fischer, R.L. and Choi, Y. (2014b) Nucleoporin MOS7/Nup88 is required for mitosis in gametogenesis and seed development in Arabidopsis. *Proceedings of the National Academy of Sciences*, **111**, 18393-18398.

Petrovic, A. (2010) The MIS12 complex is a protein interaction hub for outer kinetochore assembly. *J. Cell Biol.*, **190**, 835-852.

Petrovic, A., Keller, J., Liu, Y., Overlack, K., John, J., Dimitrova, Yoana N., Jenni, S., van Gerwen, S., Stege, P., Wohlgemuth, S., Rombaut, P., Herzog, F.,

Harrison, Stephen C., Vetter, Ingrid R. and Musacchio, A. (2016) Structure of the MIS12 Complex and Molecular Basis of Its Interaction with CENP-C at Human Kinetochores. *Cell*, **167**, 1028-1040.e1015.

Petrovic, A., Mosalaganti, S., Keller, J., Mattiuzzo, M., Overlack, K., Krenn, V., De Antoni, A., Wohlgemuth, S., Cecatiello, V., Pasqualato, S., Raunser, S. and Musacchio, A. (2014) Modular Assembly of RWD Domains on the Mis12 Complex Underlies Outer Kinetochore Organization. *Molecular Cell*, **53**, 591-605.

Rago, F., Gascoigne, K.E. and Cheeseman, I.M. (2015) Distinct organization and regulation of the outer kinetochore KMN network downstream of CENP-C and CENP-T. *Current biology : CB*, **25**, 671-677.

Ramahi, J.S. (2012) Quantitative Analysis of CENH3 and NDC80 Complexes in Arabidopsis Kinetochores During Mitosis and Meiosis: University of California, Davis, pp. 166.

Ravi, M., Kwong, P.N., Menorca, R.M., Valencia, J.T., Ramahi, J.S., Stewart, J.L., Tran, R.K., Sundaresan, V., Comai, L. and Chan, S.W. (2010) The rapidly evolving centromere-specific histone has stringent functional requirements in Arabidopsis thaliana. *Genetics*, **186**, 461-471.

Rushing, S. (2008) Characterization of Arabidopsis thaliana kinetochore proteins: University of Georgia, pp. 1-35.

Saitoh, H., Tomkiel, J., Cooke, C.A., Ratrie, H., 3rd, Maurer, M., Rothfield, N.F. and Earnshaw, W.C. (1992) CENP-C, an autoantigen in scleroderma, is a component of the human inner kinetochore plate. *Cell*, **70**, 115-125.

Samejima, I., Spanos, C., Alves, F.d.L., Hori, T., Perpelescu, M., Zou, J., Rappsilber, J., Fukagawa, T. and Earnshaw, W.C. (2015) Whole-proteome genetic analysis of dependencies in assembly of a vertebrate kinetochore. *The Journal of cell biology*, **211**, 1141-1156.

Sandmann, M., Talbert, P., Demidov, D., Kuhlmann, M., Rutten, T., Conrad, U. and Lermontova, I. (2017) Targeting of Arabidopsis KNL2 to Centromeres Depends on the Conserved CENPC-k Motif in Its C Terminus. *The Plant cell*, **29**, 144-155.

Sato, H., Shibata, F. and Murata, M. (2005) Characterization of a Mis12 homologue in Arabidopsis thaliana. *Chromosome research : an international journal on the molecular, supramolecular and evolutionary*

aspects of chromosome biology, **13**, 827-834.

Schleiffer, A., Maier, M., Litos, G., Lampert, F., Hornung, P., Mechtler, K. and Westermann, S. (2012) CENP-T proteins are conserved centromere receptors of the Ndc80 complex. *Nature cell biology*, **14**, 604-613.

Schmitzberger, F. and Harrison, S.C. (2012) RWD domain: a recurring module in kinetochore architecture shown by a Ctf19–Mcm21 complex structure. *EMBO reports*, **13**, 216-222.

Schmitzberger, F., Richter, M.M., Gordiyenko, Y., Robinson, C.V., Dadlez, M. and Westermann, S. (2017) Molecular basis for inner kinetochore configuration through RWD domain–peptide interactions. *The EMBO journal*.

Skoog, F. and Miller, C.O. (1957) Chemical regulation of growth and organ formation in plant tissues cultured in vitro. *Symposia of the Society for Experimental Biology*, **11**, 118-130.

Su, Y.H., Liu, Y.B., Bai, B. and Zhang, X.S. (2014) Establishment of embryonic shoot–root axis is involved in auxin and cytokinin response during Arabidopsis somatic embryogenesis. *Frontiers in plant science*, **5**, 792.

Su, Y.H. and Zhang, X.S. (2009) Auxin gradients trigger de novo formation of stem cells during somatic embryogenesis. *Plant signaling & behavior*, **4**, 574-576.

Su, Y.H., Zhao, X.Y., Liu, Y.B., Zhang, C.L., O'Neill, S.D. and Zhang, X.S. (2009) Auxin-induced WUS expression is essential for embryonic stem cell renewal during somatic embryogenesis in Arabidopsis. *The Plant Journal*, **59**, 448-460.

Sun, S.C., Lee, S.E., Xu, Y.N. and Kim, N.H. (2010) Perturbation of Spc25 expression affects meiotic spindle organization, chromosome alignment and spindle assembly checkpoint in mouse oocytes. *Cell Cycle*, **9**, 4552-4559.

Takeuchi, K., Nishino, T., Mayanagi, K., Horikoshi, N., Osakabe, A., Tachiwana, H., Hori, T., Kurumizaka, H. and Fukagawa, T. (2014) The centromeric nucleosome-like CENP-T-W-S-X complex induces positive supercoils into DNA. *Nucleic acids research*, **42**, 1644-1655.

Talbert, P.B., Masuelli, R., Tyagi, A.P., Comai, L. and Henikoff, S. (2002) Centromeric localization and adaptive evolution of an Arabidopsis histone

H3 variant. *The Plant cell*, **14**, 1053-1066.

Umbreit, N.T., Gestaut, D.R., Tien, J.F., Vollmar, B.S., Gonen, T., Asbury, C.L. and Davis, T.N. (2012) The Ndc80 kinetochore complex directly modulates microtubule dynamics. *Proceedings of the National Academy of Sciences*, **109**, 16113-16118.

Wei, R.R., Sorger, P.K. and Harrison, S.C. (2005) Molecular organization of the Ndc80 complex, an essential kinetochore component. *Proc. Natl Acad. Sci. USA*, **102**, 5363-5367.

Weimer, A.K., Biedermann, S., Harashima, H., Roodbarkelari, F., Takahashi, N., Foreman, J., Guan, Y., Pochon, G., Heese, M., Van Damme, D., Sugimoto, K., Koncz, C., Doerner, P., Umeda, M. and Schnittger, A. (2016) The plant-specific CDKB1-CYCB1 complex mediates homologous recombination repair in Arabidopsis. *The EMBO journal*.

Westermann, S. (2006) The Dam1 kinetochore ring complex moves processively on depolymerizing microtubule ends. *Nature*, **440**, 565-569.

Wigge, P.A., Jensen, O.N., Holmes, S., Soues, S., Mann, M. and Kilmartin, J.V. (1998) Analysis of the Saccharomyces spindle pole by matrix-assisted laser desorption/ionization (MALDI) mass spectrometry. *The Journal of cell biology*, **141**, 967-977.

Wigge, P.A. and Kilmartin, J.V. (2001) The Ndc80p complex from Saccharomyces cerevisiae contains conserved centromere components and has a function in chromosome segregation. *The Journal of cell biology*, **152**, 349-360.

Zhang, M., Cheng, L., Jia, Y., Liu, G., Li, C., Song, S., Bradley, A. and Huang, Y. (2016) Aneuploid embryonic stem cells exhibit impaired differentiation and increased neoplastic potential. *The EMBO journal*, **35**, 2285-2300.

Zhang, T.-Q., Lian, H., Zhou, C.-M., Xu, L., Jiao, Y. and Wang, J.-W. (2017) A Two-Step Model for de novo Activation of WUSCHEL during Plant Shoot Regeneration. *The Plant cell*.

Zhong, C.X., Marshall, J.B., Topp, C., Mroczek, R., Kato, A., Nagaki, K., Birchler, J.A., Jiang, J. and Dawe, R.K. (2002) Centromeric retroelements and satellites interact with maize kinetochore protein CENH3. *The Plant cell*, **14**, 2825-2836.

VII. Abstract in Korean

국문초록

염색체의 중심절 (centromere)에 위치하는 동원체 (kinetochore)는 세포분열동안 방추사와 염색체의 접합을 유도하여 염색체 분리 과정을 매개하는 단백질 복합체이다. NDC80, NUF2, SPC24, SPC25 4개의 단백질로 구성된 NDC80 복합체는 외부 동원체에 위치하여 방추사와 동원체를 이어준다. 다양한 생물종들에서 보존되어 있음에도 불구하고, NDC80 복합체의 단백질들은 기능상실돌연변이체의 심한 표현형 때문에 현재까지 제한적인 연구만 진행되었다. 특히 모델식물인 애기장대에서 SPC24 상동유전자는 전혀 보고되지 않았다.

본 연구를 통해 애기장대의 열성 돌연변이체인 *meristem unstructured-1* (*mun-1)* 에 대한 특성 분석을 개체 수준에서 진행하였다. *mun-1*은 *WUSCHEL* 유전자를 비롯한 분열조직 관련 유전자들의 전위적 과발현으로 인해 정단분열조직이 비구조화되어 비정상적인 형태 발생을 보인다. *mun-1*은 NCD80복합체의 SPC24 상동유전자 프로모터 부위에 T-DNA가 삽입되어 MUN유전자의 발현이 감소한, 표현형의 발현에 있어서 불완전침투성 (incomplete penetrance)을 보이는 약대립유전자 (weak allele) 돌연변이체이다. *mun-1*은 성장저해, 배발생 정지, DNA 이수성 (aneuploidy), 염색체 분리 이상, 낮은 세포분열 속도 등의 표현형을 보인다. TALEN과 CRISPR/Cas9 기반의 유전자 가위 기술을 적용하여 생성된 MUN의 비대립 유전자 (mull allele mutants) 돌연변이체들은 다른 NDC80복합체의 돌연변이체인 *nuf2-1*와 같은 배아 치사성 (zygotic embryonic lethality)을 보인다. 해당 비대립 유전자들은 화분, 밑씨를 통해서 다음세대로

성공적으로 전달된다. 효모단백질잡종법과 식물체 내 공면역침강법을 이용하여 애기장대 NDC80 복합체 단백질들간의 결합을 확인하였다. MUN은 식물체 전반에 걸쳐 주로 활발하게 분열하는 세포조직에서 발현되며 히스톤 변형체로 중심절 표지 인자인 HTR12/CENH3 단백질과 세포내 동일위치에 존재함이 규명되었다. MUN이 HTR12/CENH3의 세포내 위치에 영향을 미치지 않는 것으로 보아 MUN은 외부 동원체 단백질로서 내부 동원체 단백질들의 조립 이후 동원체에 결합 하는 것으로 추정된다.

본 연구를 통해 애기장대의 SPC24 상동유전자인 MUN의 존재와 세포분열조절기능을 규명하였다. 동물 NDC80 복합체와 달리, 애기장대의 NDC80복합체들은 세포 분열 주기 전 과정에서 동원체에 위치하고 있음을 확인하였다. 추가적으로 MUN과 세포분열조절인자 RBR간의 결합을 확인하였다. 따라서 애기장대의 MUN은 동원체의 구조적인 요소일 뿐 아니라 세포분열 조절인자로서의 기능도 가진 복합기능 단백질로 추정된다. 한편, 약대립유전자(weak allele) 돌연변이체 *mun-1*의 표현형 분석을 통해 동원체 단백질의 기능결손이 줄기세포의 이상 생성과 관련이 있다는 사실을 알 수 있었다. 본 연구를 통해 동물과 차별화되는 식물의 세포분열 및 동원체 단백질 조절 기작의 일부를 규명하였다.

주요어: SPC24, NDC80 복합체, 동원체, 중심절, 염색체 분리, 세포분열, 애기장대

학 번: 2008-20360

VIII. Appendix

종자분주기 등록특허공보 및 특허증

(19) 대한민국특허청(KR)
(12) 등록특허공보(B1)

(45) 공고일자 2012년08월24일
(11) 등록번호 10-1177171
(24) 등록일자 2012년08월20일

(51) 국제특허분류(Int. Cl.)
B01L 3/00 (2006.01)
(21) 출원번호 10-2009-0086823
(22) 출원일자 2009년09월15일
심사청구일자 2009년12월09일
(65) 공개번호 10-2011-0029238
(43) 공개일자 2011년03월23일
(56) 선행기술조사문헌
US20030005868 A1*
*는 심사관에 의하여 인용된 문헌

(73) 특허권자
서울대학교산학협력단
서울특별시 관악구 관악로 1 (신림동)
(72) 발명자
이일하
경기도 성남시 분당구 수내로 181, 308동 1103호 (분당동, 샛별마을)
신진우
서울특별시 강남구 영동대로114길 23, 월성아파트 302호 (삼성동)
(74) 대리인
박진호

전체 청구항 수 : 총 4 항 심사관 : 김지우

(54) 발명의 명칭 **종자 분주기**

(57) 요 약

본 발명은 종자분주기에 관한 것으로, 보다 상세하게는 일정량의 종자를 균일하게 꺼내어 균일하게 분주하는 것을 용이하게 하는 분주 도구에 관한 것이다.

대 표 도 - 도3

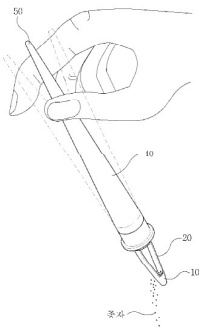

이 발명을 지원한 국가연구개발사업

과제고유번호	10543
부처명	서울특별시
연구사업명	서울시 산학연 협력사업(기술기반구축사업)
연구과제명	나노바이오 시스템 및 응용소재
주관기관	서울대학교 산학협력재단
연구기간	2005년 12월 01일~2010년 11월 30일

특허청구의 범위

청구항 1

종자를 담을 수 있는 접촉접시;

손으로 쥘 수 있는 콘 형상의 지지대;

상기 접촉접시와 지지대를 연결하는 연결기둥; 및

상기 지지대 상부로 형성되는 탄력부; 를 포함하는 것을 특징으로 하는 종자 분주기.

청구항 2

제 1항에 있어서, 상기 접촉접시는 금속재질로 이루어진 것을 특징으로하는 종자 분주기.

청구항 3

제 1항에 있어서, 상기 지지대는 탄성을 갖는 금속 또는 플라스틱 재질로 이루어진 것을 특징으로 하는 종자 분주기.

청구항 4

제 1항에 있어서, 상기 연결기둥은 2개인 것을 특징으로 하는 종자 분주기.

명 세 서

발명의 상세한 설명

기 술 분 야

[0001] 본 발명은 종자분주기에 관한 것으로, 보다 상세하게는 일정량의 종자를 균일하게 꺼내어 균일하게 분주하는 것을 용이하게 하는 분주 도구에 관한 것이다.

배 경 기 술

[0002] 실험실 등에서 종자를 통상 에펜돌프 튜브(e-tube)에 보관하여 사용한다. 이렇게 보관되어 있는 종자의 일정량을 꺼내어 분주하는 경우, 적당량을 덜어내기 어렵고, 또한 덜어낸 종자의 개수를 계수하기 어렵다. 현실적으로 에펜돌프 튜브를 기울여 적당량을 꺼내어 수작업으로 일일히 그 개수를 측정하고 필요이상의 것은 다시 집어 넣거나 오염된 경우 버리게 된다. 특히 애기장대의 종자의 경우 그 크기가 통상 1㎜ 내외로 매우 작아 손으로 다루기 어려우며, 특히 종자를 대량으로 모아 사용하고자 할 때 육안 식별 및 계수에 어려움이 많고, 분주 시간이 오래 걸려 작업의 능률성이 떨어진다.

[0003] 한편, 여러종의 종자를 꺼내어 분주하는 경우에는 오염사고가 발생할 우려가 있어서, 실험오차가 발생할 수 있고 이는 실험의 신뢰도를 떨어뜨리는 결과를 초래한다.

[0004] 종자의 개수를 계수함에 있어, 종자가 방사선이나 빛을 방해하는 성질을 이용한 광학 종자 계수기 등이 알려져 있다. 그러나 이들의 경우 광원 및 광검출기의 공간적 불균일성이 있어 왔으며, 광검출기에 의해 발생하는 신호는 광의 어느 부분을 차단하는가에 따라 결정되므로 문제가 있으며, 별도의 복잡한 조작행위가 있어야 하며 장치가 복잡하기 때문에 손쉽게 사용하기가 곤란하다.

발명의 내용

해결 하고자하는 과제

[0005] 본 발명은 종자를 신속하고 오차없이 균일하게 분주할 수 있는 종자 분주기를 제공하고자 한다. 또한 복잡한 전기적 장치의 계수기가 아닌 매우 간단하게 계수할 수 있는 종자 분주기를 제공하고자 한다.

[0006] 그리고, 통상 실험실에서 사용되는 에펜돌프 튜브와의 호환성이 좋은 구현 형태를 제공하여 작업의 능률성을

높이고, 종자의 분주시 오염사고를 줄일 수 있는 수단도 제공하고자 한다.

과제 해결수단

[0007] 이를 위한 본 발명은 종자를 담을 수 있는 접촉접시; 손으로 쥘 수 있는 콘 형상의 지지대; 상기 접촉접시와 지지대를 연결하는 연결기둥; 및 상기 지지대 상부로 형성되는 탄력부; 를 포함하는 것을 특징으로 하는 종자 분주기이다.

[0008] 또한, 상기 접촉접시는 금속재질로 이루어진 것이 바람직하며, 상기 지지대는 탄성이 높은 금속 또는 플라스틱 재질로 이루어진 것이 바람직하고, 상기 연결기둥은 2개인 것이 바람직하다.

효 과

[0009] 본 발명에 따른 종자 분주기는 신속하고 오차없이 균일하게 종자를 분주할 수 있다. 또한 그 사용방법이 간편하고, 에펜돌프 튜브와의 호환성이 좋으며, 종자의 분주시 오염사고를 줄일 수 있다.

발명의 실시를 위한 구체적인 내용

[0010] 이하, 본 발명에 따른 바람직한 실시예를 첨부된 도면을 참조하여 설명하며, 관련된 공지 기능 또는 구성에 대한 구체적인 설명은 발명의 요지를 명확하기 위하여 생략될 수 있다. 이 과정에서 도면에 도시된 선들의 두께나 구성요소의 크기 등은 설명의 명료성과 편의상 과장되게 도시되어 있을 수 있으며 하기 실시예는 본 발명의 권리범위를 한정하는 것이 아니라 단지 예시로 제시하는 것이며, 본 기술 사상을 통해 구현되는 다양한 실시예가 있을 수 있다.

[0011] 도 1은 본 발명의 일실시예에 따른 종자 분주기의 사시도이다. 접촉접시(10)는 일정량의 종자를 담을 수 있도록 어느 정도 깊이가 있는 형태를 가지는 종지형태가 바람직할 것이다. 접촉접시(10)의 용적은 원하는 종자의 개수에 따라서 부피를 계산하여 다양하게 변경이 가능함은 물론이다. 또한, 투명재질의 접촉접시(10)를 사용하는 경우라면, 접촉접시(10)에 다양한 표시선을 구비시켜 원하는 표시선 만큼의 양을 담을 수도 있을 것이다. 후술되어 있는 탄력부(50)는 원칙적으로 접촉접시(10)의 높이만큼 종자가 담기게 하는데에 사용되겠지만, 경우에 따라서는 그 아래의 표시선부까지 담기게 될 때까지 사용하여 종자의 양을 조절할 수도 있을 것이다.

[0012] 접촉접시(10)의 위쪽으로 연결기둥(20)이 형성된다. 연결기둥(20)은 필요에 따라 1 이상 구비될 수 있으며, 2개를 형성하는 것이 바람직하다. 연결기둥(20)은 접촉접시(10)와 지지대를 연결하는 역할을 할 뿐만 아니라, 연결기둥(20)들 사이로 종자가 들어가 접촉접시(10)에 종자가 안착할 수 있는 통로 역할을 한다.

[0013] 연결기둥(20) 상부로 작업자의 손으로 잡을 수 있게 지지대(40)를 구비한다. 지지대(40)는 그 상부로 탄력부(50)를 구비한다. 여기에서 지지대(40)는 탄력부(50)를 포함하는 것이며, 탄력부(40)는 지지대의 일부로 이해될 것이다. 지지대(40)의 형태는 콘 형태(또는 고깔형태)로 구현되는 것이 바람직한데, 이는 이러한 형태가 탄성을 가하기에 적당한 구조이기 때문이다. 따라서 콘 형태가 의미하는 것은 탄성을 줄 수 있는 구조를 의미한다. 보다 바람직하게는 지지대(40)는 탄성이 높은 금속이나, 플라스틱을 사용하여 성형 사출할 수 있다.

[0014] 도 2는 본 발명의 일실시예에 따른 종자 분주기의 단면도이다. 접촉접시(10) 및 연결기둥(20)을 지지대(40)에 결속하는 결속부재(30)가 구비될 수 있다. 도면에서 보는 바와 같이 끼우는 구조 형태뿐만 아니라, 양 구조체를 간단하게 테이프 등을 이용해 연결하여 사용하여도 구조의 견고성에는 문제가 되지 않을 것으로 생각된다. 즉 도면의 결속부재(30)는 예시적인 것으로 이해하여야 한다.

[0015] 접촉접시(10)는 종자가 접촉하면서 담기는 부분이기 때문에 정전기가 발생할 수 있고, 정전기가 발생하면 종자 분주 후 접촉접시(10)와 종자의 분리가 깔끔하게 일어나지 않을 수도 있다. 이는 정확한 계수에 방해가 되고, 또한, 여러 종류의 종자 분주시에는 오염 사고가 발생할 우려도 있게 된다. 따라서 정전기가 자주 발생하지 않는 소재를 사용하는 것이 바람직하다. 따라서, 상기 접촉접시(10)는 정전기 방지처리가 된 플라스틱소재나, 플라스틱 소재가 아닌 금속재질로 만들어지는 것이 보다 바람직할 것이다.

[0016] 접촉접시(10), 연결기둥(20), 및 결속부재(30)를 포함하는구조체를 공장에서 대량으로 일체로 생산하여 보다 일정하고 균일하게 제조할 수도 있다. 이렇게 제조된 구조체를 상부의 지지대(40)와 결속하여 본 발명의 종자

분주기를 간단하게 제조할 수 있다.

[0017] 도 3은 본 발명의 일실시예에 따른 종자 분주기의 사용방법을 보여주기 위한 도면이다. 종자는 연결기둥(20) 사이의 통로를 통해 접촉접시(10)에 담기게 되는데 접촉접시(10)에 담길 때에 수평부분이상으로 과도하게 담기는 것이 일반적이다. 그러나 이러한 경우, 수평부분이상의 양이 항상 달라지게 되므로 종자 개수의 균일도가 떨어지게 된다. 본 발명의 경우에는 지지대(40)상부로 탄력부(50)를 가지는데, 이를 이용해 탄성을 가하면, 접촉접시(10)에 담긴 종자가 수평상태를 유지하여 항상 일정량의 종자만이 접촉접시(10)에 담기게 되어 균일도를 유지할 수 있다.

[0018] 통상, 엄지와 약지로 지지대(40)를 쥔 상태에서, 검지로 탄력부(50)에 탄력을 주어 접촉접시(10)에 담긴 종자의 양을 균일한 양으로 조정할 수 있다.

[0019] 본 발명의 종자 분주기의 구조 형태는 통상 사용되는 에펜돌프 튜브의 규격과 호환되기 때문에 보다 효용성이 높다.

[0020] 도 4는 본 발명의 시제품(prototype)을 실험실에서 자주 사용되고 있는 PCR튜브와 옐로우팁을 사용하여 만들어, 종자가 보관된 에펜돌프 튜브에서 종자를 분주하는 과정을 보여준다. (a) 종자가 담긴 e-tube에 본 발명의 시제품을 삽입하여 종자가 접촉접시에 담기도록한다. (b) 검지를 이용하여 적당한 탄력을 주어 종자의 양을 조절한다. 일반적으로 과도하게 얹어진 종자를 제거하고 표시선 만큼의 양을 담는 목적으로사용되는 과정이다. (c) 일정량의 종자가 분주되어 꺼내는 모습이다.

[0021] <실시예>

[0022] 대다수의 분자생물학 실험실에서 빈번하게 사용되는 PCR튜브와 200㎕ 옐로우 팁(yellow tip)을 이용하여 시제품을 만들었다. PCR 튜브의 옆면을 조각하여 불필요한 부분을 잘라내고 2개의 연결기둥을 만들고, 아래부분의 공간은 작은 접시 형태로 남겨두었다. 옐로우 팁의지름이 넓은 부분을 PCR튜브의 위쪽의 원판모양의 구조부분와 테이프로 부착, 연결하여 이를 완성하였다.

[0023] 애기장대 종자가 담긴 1.5 mL e-tube에 상기 종자 분주기를 사용하여 애기장대 종자를 분주하여 보았다. 매우 편리하고 간편하면서도 시간을 매우 단축시켜 분주가 가능하였다. 그리고, 본 발명의 종자 분주기의 분주 균일성을 확인하기 위해 분주된 애기장대 종자의 개수를 직접 계수하여 이를 대비하여 보았다. 그 결과 수차례의 분주 결과 거의 동일하게 약 150여개의 애기장대 종자가 균일하게 분주되는 결과가 나왔다.

도면의 간단한 설명

[0024] 도 1은 본 발명의 일실시예에 따른 종자 분주기의 사시도이다.

[0025] 도 2는 본 발명의 일실시예에 따른 종자 분주기의 단면도이다.

[0026] 도 3은 본 발명의 일실시예에 따른 종자 분주기의 사용방법을 보여주기 위한 도면이다.

[0027] 도 4는 본 발명의 시제품(prototype)을 사용하여 에펜돌프 튜브에서 종자를 분주하는 과정을 보여준다.

[0028] <도면 부호의 설명>

[0029] 10 : 접촉접시 20 : 연결기둥

[0030] 30 : 결속부재 40 : 지지대

[0031] 50 : 탄력부

도면

도면1

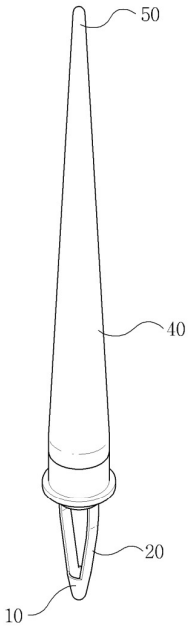

도면2

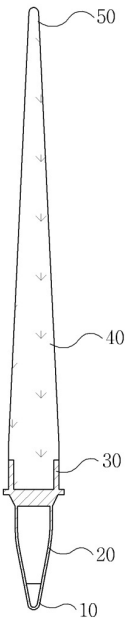

도면3

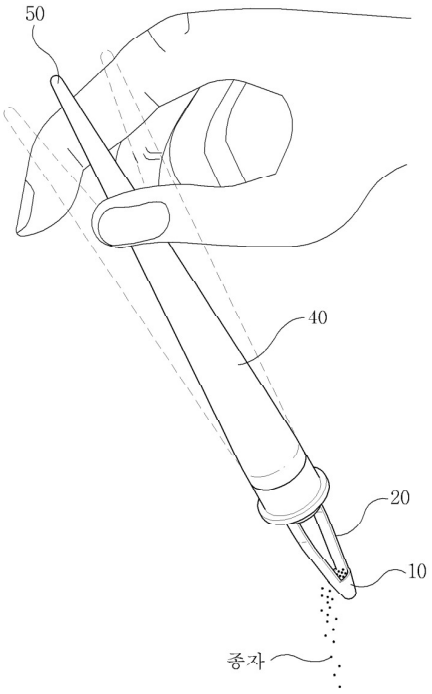

도면4

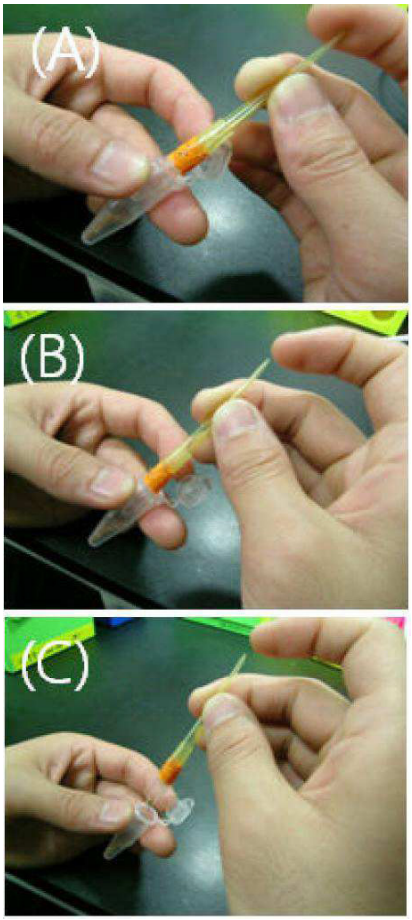

특 허 증

CERTIFICATE OF PATENT

특 허 제 10-1177171 호
(PATENT NUMBER)

출원번호 (APPLICATION NUMBER)	제 2009-0086823 호
출 원 일 (FILING DATE:YY/MM/DD)	2009년 09월 15일
등 록 일 (REGISTRATION DATE:YY/MM/DD)	2012년 08월 20일

발명의명칭 (TITLE OF THE INVENTION)
종자 분주기

특허권자 (PATENTEE)
서울대학교산학협력단(114371-0******)
서울특별시 관악구 관악로 1 (신림동)

발명자 (INVENTOR)
등록사항란에 기재

위의 발명은 「특허법」에 의하여 특허등록원부에 등록되었음을 증명합니다.

(THIS IS TO CERTIFY THAT THE PATENT IS REGISTERED ON THE REGISTER OF THE KOREAN INTELLECTUAL PROPERTY OFFICE.)

2012년 08월 20일

특 허 청 장
COMMISSIONER, THE KOREAN INTELLECTUAL PROPERTY OFFICE

연차등록료 납부일은 설정등록일 이후 4년차부터 매년 08월 20일까지이며 등록원부로 권리관계를 확인바랍니다.